SELINUS UNIVERSITY
OF SCIENCES AND LITERATURE

Nitrogen, Methane and Ethane Recovery from a Domestic Petrochemical Flare Gas by Using Pressure Swing Adsorption System

By
Ehsan Javadi Shokroo

Supervised by
Prof. Salvatore Fava Ph.D

A DISSERTATION

Presented to the Department of
Chemical Engineering
program at Selinus University

Faculty of Engineering Sciences
in fulfillment of the requirements
for the accelerated degree of
Doctor of Philosophy

31 August 2018

Table of figures

Table of tables

Table of content

Abstract

The main object of this project was to applying a pilot plant to simultaneously nitrogen, methane and ethane separation from a flare gas in a domestic industrial petrochemical unit. In order to realization of experimental section, a two-stage semi-industrial unit was set-up in FAPKCO Engineering Group of Iran with a length of 70 cm, an i.d. of 4.5 cm and also equipped with control and analysis systems of feed and product streams. To investigate the PSA unit, a 6-step cycle includes steps as: Pressurization with feed, Adsorption, Equalization to Depressurization, Blow Down, Purge and Equalization to Pressurization. The experiments are designed in a way to take into account the effect of adsorption step pressure, purge flow rate, adsorption step time, and length of the absorbent layer and also feed flow rate on process performance. The operation pressure was considered in range of 9-13 bar. In addition, the simulation of the PSA process using axially dispersed plug flow model, three-component Langmuir-freundlich adsorption isotherm model and linear driving force model was made by using MATLAB® software and Rang-Kutta Gill scheme to reach a sufficiently high study. Therefore, theoretical and empirical results are presented.

Keywords: Flare gas recovery; Nitrogen recovery; Methane recovery; Ethane recovery; Pressure swing adsorption; Pilot plant experiments

Dedicate

To my dear wife for his support

And

To my lovely and blessed son that he will come into my life for the next few days

And

To my dear father and mother that they always endured a lot of difficulties for me

God keep them always healthy and happy

Acknowledgements

I am highly indebted to my research supervisor, Dr. **Salvatore Fava** for his dedicated assistance, consistent guidance and suggestion throughout my research work.

Special thank must go to **FAPKCO Engineering Group (*PART-SHIMI Co.*)** for support in the experimental work carried out for this work. I would like to thank manager Mr. **Mehdi Baghbani**, R&D manager engineer Mr. **Mehdi Farniaei**, for their kind help and for making this project feasible.

Nomenclature

A_w	cross-sectional area of the wall (cm^2)
AD	adsorption step
BD	blow down step
Cp_g, C_{ps}, C_{pw}	gas, pellet, and wall heat capacities, respectively (cal/g.K)
D_L	axial dispersion coefficient (cm^2/s)
G	purge to feed ratio ($kg_{feed}/kg_{purge)}$
hi	internal heat-transfer coefficient ($cal/cm^2.K.s$)
ho	external heat-transfer coefficient ($cal/cm^2.K.s$)
$\Delta\bar{H}$	average heat of adsorption (cal/mol)
K_L	axial thermal conductivity (cal/cm.s.K)
L	bed length (cm)
P	total pressure (atm)
P_r	reduced pressure, dimensionless
PG	purge step
PR	pressurization step
P/F	ratio of purge flow rate to feed flow rate
P_H/P_L	ratio of operating pressures
q, q*, $\hat{q}$	amount adsorbed, equilibrium amount adsorbed, and average amount adsorbed, respectively (mol/g)
q_m	equilibrium parameter for the Langmuir model (mol/g)
R	gas constant (cal/mol.K)
R_p	radius of the pellet (cm)
R_{Bi}, R_{Bo}	inside and outside radial of the bed, respectively (cm)
T	temperature (K)
T_{atm}	temperature of the atmosphere (K)
T, T_w	pellet or bed temperature and wall temperature, respectively (K)
t	time (s)
u	interstitial velocity (cm/s)

y_i	mole fraction of species i in the gas phase
z	axial distance in the bed from the inlet (cm)

Greek Letters

α	particle porosity
β	equilibrium parameter for the Langmuir model in the form of dimensionless
ε, ε_t	voidage of the adsorbent bed and total void fraction, respectively
ρ_g, ρ_p, ρ_B, ρ_w (g/cm^3)	gas density, pellet density, bulk density, and bed wall density, respectively

Subscripts

B	bed
H	higher operating pressure
i	component i
L	lower operating pressure
p	pellet
g	gas phase
s	solid
w	wall

Author Main Resume on PSA systems from 2013 related to thesis Studies

Petroleum & Coal
ISSN 1337-7027

Available online at www.vurup.sk/petroleum-coal
Petroleum & Coal 55 (3) 216-225, 2013

COMPARISON OF TWO PRESSURE SWING ADSORPTION PROCESSES FOR AIR SEPARATION USING ZEOLITE 5A AND ZEOLITE 13X

Masoud Mofarahi[1], Ehsan Javadi Shokroo[2]

[1]*Chemical Engineering Department, School of Gas and Petrochemical Engineering, Persian Gulf University, Bushehr, Iran, Email Address: mofarahi@pgu.ac.ir*
[2]*The Parthia Chemistry Company, Knowledge Based Companies Campus, Martyr Fahmideh Talent Foundation, Shiraz, Iran, Email Address: ejavadi@nsf-partshimico.tk*

Received April 5, 2013, Accepted August 15, 2013

Abstract

The performances of two types of zeolite 5A and zeolite 13X in oxygen separation from air with a two-bed six-step pressure swing adsorption (PSA) system were investigated using mathematical modeling. The effects of feed flow rate, adsorption step pressure, adsorption step time and purge to feed ratio on oxygen purity and recovery are studied. Comparison of two types of zeolites shows that the PSA process performance (in terms of purity and recovery) was better with zeolite 13X than the zeolite 5A. Furthermore, Results of simulation indicated a very good agreement with some current literature experimentally work.

Keywords: Pressure swing adsorption; Simulation; Air separation; Oxygen production; Zeolite 5A; Zeolite 13X.

1. Introduction

Three commercial methods are available for oxygen separation from air, namely cryogenic, membrane technologies and pressure swing adsorption. Usually the PSA technique will be used for lower production scales [1]. The PSA system is well suited to rapid cycling, in contrast to other cyclic adsorption separation processes, and this has the advantage of minimizing the absorbent inventory and therefore the capital costs of the system [2].

PSA process is a wide operating unit to separation and purification of gases that operates based on capability of solids adsorption and selective separation of gases. The important operational parameter in this system is the pressure, and most industrial units operate at/or vicinity of the surrounding temperature. Today, the PSA process completely is known in a wide region of the processes, and this process was preferred in contrast to other conventional separation methods especially, for lower capacity and higher purity. The PSA process nowadays is used for separation of the different gas mixtures. In recent years, use of this method was followed by researchers as a more important separation technique in the air separation, because generally the PSA process is more economical to other separation processes. The evolution of the PSA process around the world wide was still continuous, and each day the new act is done for this important process to achieve the best economic conditions.

Use of this process to oxygen and nitrogen separation from air took for the first time in 1958 by Skarstrom. He provided his recommended PSA cycles to enrich oxygen and nitrogen in air under subject of heatless drier [3]. Therefore, Skarstrom invented a two-bed PSA cycle with equalization step for oxygen production from air using zeolite 13X adsorbent in 1966 [4]. The main reasons for the success of this technology are many reforms that achieved in this field and also is the new design and configuration for the cycles and devices [5-8].

In general, the PSA process performance strongly influenced by design parameters (such as: bed size, adsorbent physical properties, configuration and number of beds) and operational variables (such as: pressurization time, production time, purge time, feed flow rate, purge flow rate, production flow rate, temperature and/or pressure variations). So, this could be achieves maximum possible performance relate to an optimum amount of process variables. Therefore it is important that the behavior of the PSA operating variables were under take a review to knowing the optimum operating conditions. The selection of a

suitable adsorbent in designation of the PSA unit is a critical parameter. The prevalent adsorbents in oxygen production from air by PSA process are namely, zeolite 5A and zeolite 13X. In this PSA process using zeolite adsorbents, the nitrogen is adsorbed on the adsorbent and oxygen plus argon subsequently remain in the effluent gas. Zeolite is an aluminosilicate mineral which swells and evolves steam under the blowpipe. Some zeolitic crystal structures can be synthesized by hydrothermal reaction in autoclaves. A limited number of synthetic zeolites are currently used as commercial adsorbents i.e., 5A and 13X. During the progress was made on the PSA process, zeolites studies continually be looking away from the years in order to improve their quality (capacity and selectivity). For example, the improvements in this area include reduction of the inert inorganic material. [9-10]. The most important theoretical models to describe the PSA process behavior in terms of equilibrium and pore diffusion models are cited to Farooq & Ruthven [11], Farooq *et al.* [12], Hassan *et al.* [13], Ruthven & Farooq [14], Fernandez & Kenney [15], Farooq *et al.* [16], Farooq & Ruthven [17] and Knaebel & Hill [18].

In order to separation of oxygen from air by two-bed PSA process many theoretical and experimental works have been carried out by researchers separately using zeolite 5A and 13X, but to survey the effective zeolite in air separation is not yet compared the performance of zeolite 5A and 13X side to each other. These two types of zeolite are the common adsorbents in oxygen production from air by PSA process, but the question is, that have still not been solved, what kind of the zeolite is well suited to producing oxygen from air by PSA in the same fully conditions? Since the selection of a suitable adsorbent serves a significant role in the PSA performance, type of zeolite for the separation process is important question and we want answer to it here. The answer to this problem can be rose from a high efficiently study of these two types of adsorbent. Therefore, study of the performances of zeolite 5A and zeolite 13X to find the highly profitable zeolite in oxygen production from air by PSA process helps to get the high efficiently separation process. In this work, therefore, we were compared the performances of two types of zeolite adsorbent (zeolite 5A & 13X) in a two-bed PSA oxygen production system by mathematical modeling and numerical simulation. The six-step process used is as follows: (I) co-current feed pressurization (PR) of a partially pressurized bed by a previous pressurizing pressure equalization step (RP); (II) high-pressure adsorption (AD) step; (III) counter-current depressurizing pressure equalization (ED) step; (IV) counter-current blow down (BD) step; (V) counter-current purge with a light product (PG) step; (VI) co-current RP step.

2. Mathematical Model

In order to develop a mathematical model for a PSA system the main assumptions that have been applied include:

a. Gas behaves an ideal gas.
b. The flow pattern is described by the axially dispersed plug-flow model.
c. Adsorbing properties throughout the tower would remain constant and unchanged.
d. Radial gradient is to be negligible.
e. Equilibrium equations for the components of air can be expressed by three-component Langmuir-Freundlich isotherm.
f. Mass transfer rate is expressed by a linear driving force equation.
g. Thermal equilibrium between gas and solid phases is assumed.
h. Pressure drop along the bed is calculated by the Ergun's equation.

Overall and component mass balances for the bulk phase in the adsorption bed to form the following equations are written, [19]:

$$\frac{\partial C_i}{\partial t} - D_L \frac{\partial^2 C_i}{\partial z^2} + \frac{\partial (C_i.u)}{\partial z} + \rho_p . \left(\frac{1-\varepsilon}{\varepsilon} \right) . \frac{\partial \overline{q}_i}{\partial t} = 0 \quad (1)$$

$$\frac{\partial C}{\partial t} - D_L \frac{\partial^2 C}{\partial z^2} + \frac{\partial (C.u)}{\partial z} + \rho_p . \left(\frac{1-\varepsilon}{\varepsilon} \right) . \sum_{i=1}^{N} \frac{\partial \overline{q}_i}{\partial t} = 0 \quad (2)$$

When the ideal gas law ($C_i = y_i P/RT$ and $C = P/RT$) is applied to eqns. (1) and (2), the component and overall mass balances can be represented as follows, [19]:

$$-D_L\frac{\partial^2 y_i}{\partial z^2}+y_i.\frac{\partial u}{\partial z}+u.\left(\frac{\partial y_i}{\partial z}+y_i.\left(\frac{1}{P}.\frac{\partial P}{\partial z}-\frac{1}{T}.\frac{\partial T}{\partial z}\right)\right)+$$
$$\frac{\partial y_i}{\partial t}+y_i\left(\frac{1}{P}.\frac{\partial P}{\partial t}-\frac{1}{T}.\frac{\partial T}{\partial t}\right)+\left(\frac{\rho_p.R.T}{P}\right).\left(\frac{1-\varepsilon}{\varepsilon}\right).\frac{\partial \overline{q}_i}{\partial t}=0 \quad (3)$$

$$\frac{\partial P}{\partial t}+P\frac{\partial u}{\partial z}+u\frac{\partial P}{\partial z}+PT.\left(\frac{\partial}{\partial t}\left(\frac{1}{T}\right)+u\frac{\partial}{\partial z}\left(\frac{1}{T}\right)\right)-\rho_p.R.T.\left(\frac{1-\varepsilon}{\varepsilon}\right).\sum_{i=1}^{N}\frac{\partial \overline{q}_i}{\partial t}=0 \quad (4)$$

Another characteristic of adsorption process is temperature variations caused by heat of adsorption and desorption occur. In this system, energy balance for the gas phase and also heat transfer to the bed wall is included, [19]:

$$-K_l\frac{\partial^2 T}{\partial z^2}+\varepsilon.\rho_g.c_{p,g}.\left(u\frac{\partial T}{\partial z}+T\frac{\partial u}{\partial z}\right)+\left(\varepsilon_t.\rho_g.c_{p,g}+\rho_B.c_{p,s}\right).\frac{\partial T}{\partial t}-\rho_B.\sum_{i=1}^{N}\left(\frac{\partial \overline{q}_i}{\partial t}.\left(-\Delta\overline{H}_i\right)\right)+$$
$$\frac{2h_i}{R_{B,i}}\left(T-T_w\right)=0 \quad (5)$$

To evaluate heat loss through the walls and the accumulation of energy, corresponding to an energy balance has also been used, [19]:

$$\rho_w.c_{p,w}.A_w\frac{\partial T_w}{\partial t}=2\pi R_{B,i}h_i\left(T-T_w\right)-2\pi R_{B,o}h_o\left(T_w-T_{atm}\right) \quad (6)$$

where,

$$A_w=\pi\left(R_{B,o}^2-R_{B,i}^2\right) \quad (7)$$

The well-known Danckwerts boundary conditions are applied

Pressurization and production step

$$-D_l\left(\frac{\partial y_i}{\partial z}\right)\Big|_{z=0}=u.\left(y_i\big|_{z=0^-}-y_i\big|_{z=0^+}\right);\frac{\partial y_i}{\partial z}\Big|_{z=L}=0 \quad (8)$$

$$-K_l\left(\frac{\partial T}{\partial z}\right)\Big|_{z=0}=\rho_g.c_{p,g}.u.\left(T\big|_{z=0^-}-T\big|_{z=0^+}\right);\frac{\partial T}{\partial z}\Big|_{z=L}=0 \quad (9)$$

Where $y_i\big|_{z=0^-}$ means the feed composition for the component i.

Counter current purge step

$$-D_l\left(\frac{\partial y_i}{\partial z}\right)\Big|_{z=L}=u.\left(y_i\big|_{z=L^+}-y_i\big|_{z=L^-}\right);\frac{\partial y_i}{\partial z}\Big|_{z=0}=0 \quad (10)$$

$$-K_l\left(\frac{\partial T}{\partial z}\right)\Big|_{z=L}=\rho_g.c_{p,g}.u.\left(T\big|_{z=L^+}-T\big|_{z=L^-}\right);\frac{\partial T}{\partial z}\Big|_{z=0}=0 \quad (11)$$

Where $y_i\big|_{z=L^+}$ means a volume-averaged composition of the effluent stream during the adsorption step for the purge step.

Counter current blow down step

$$\frac{\partial y_i}{\partial z}\Big|_{z=0}=\frac{\partial y_i}{\partial z}\Big|_{z=L}=0 \quad (12)$$

$$\frac{\partial T}{\partial z}\Big|_{z=0}=\frac{\partial T}{\partial z}\Big|_{z=L}=0 \quad (13)$$

Boundary conditions for the interstitial velocity

Pressurization and counter current blow down step

$$u\big|_{z=L}=0 \quad (14)$$

Pressurization and production step

$$u\big|_{z=0}=u\big|_{feed} \quad (15)$$

Counter current purge step

$$u\big|_{z=L} = G.u\big|_{feed} \tag{16}$$

The initial conditions for feed flow

$$y_i(z,0) = 0; \overline{q}_i(z,0) = 0; u(z,0) = 0 \tag{17}$$

$$T(z,0) = T_{atm}; T_w(0) = T_{atm} \tag{18}$$

The pressure is assumed as a second order function of the time which is adapted to the literature [20].

$$P(t) = a.t^2 + b.t + c \tag{19}$$

In the above equation *a*, *b* and *f(t)* parameteres defined regared to duration and initial and final pressures of each step.

To consider the pressure drop effect across the bed, Ergun's equation was introduced as a momentum balance [21].

$$-\frac{dP}{dz} = a.\mu.u + b.\rho.u.|u| \tag{20}$$

$$a = \frac{150}{4R_p^2}.\frac{(1-\varepsilon)^2}{\varepsilon^2}; b = 1.75\frac{(1-\varepsilon)}{2R_p\varepsilon} \tag{21}$$

Where u is the interstitial velocity.

The multi-component adsorption equilibrium was predicted by the following Langmuir isotherm.

$$q_i = \frac{q_{m,i}.B_i.P_i}{1+\sum_{j=1}^{N} B_j.P_j} \tag{22}$$

where,

$$q_{m,i} = k_1 + k_2.T; B_i = k_3.\exp(k_4/T) \tag{23}$$

The sorption rate into an adsorbent pellet is described by the LDF model with a single lumped mass-transfer parameter [22].

$$\frac{\partial \overline{q}_i}{\partial t} = \omega_i.(\dot{q}_i - \overline{q}_i); \omega_i = \frac{15D_{ei}}{r_c^2} \tag{24}$$

where [23],

$$\frac{15D_{ei}}{r_c^2} = C_i.P_r^{0.5}.(1+B_i.P_i)^2 \tag{25}$$

The adsorption isotherm parameters and diffusion rate constant of N_2 and O_2 over zeolite 5A and zeolite 13X are shown in Table 1. In Table 2 the adsorbent characteristics for both zeolites are indicated [20]. Table 3 shows physical properties of the adsorption bed [20,24].

Table 1 Equilibrium\Rate parameters and heat of adsorption of N_2 and O_2 on zeolite 5A and 13X.

Parameters	Zeolite 5A [20]		Zeolite 13X [24]	
	N_2	O_2	N_2	O_2
$k_1 \times 10^3$ (mol/g)	6.21	7.252	12.52	6.705
$k_2 \times 10^5$ (mol/g.k)	-1.27	-1.820	-1.785	-1.435
$k_3 \times 10^4$ (1/atm)	1.986	54.19	2.154	3.253
k_4 (k)	1970	662.6	2333	1428
K_5	2.266	-1.101	1.666	-0.3169
K_6 (k)	-396.5	656.4	-245.2	387.8
Heat of adsorption, (cal/mol)	5470	3160	4390	3060
LDF constant (s^{-1})	0.05	0.15	0.197	0.62

Table 2 Characteristics of 5A and 13X adsorbents.

Characteristic	Zeolite 5A [20]	Zeolite 13X [24]
Type	Sphere	Sphere
Average pellet size, R_P (cm)	0.157	0.07
Pellet density, ρ_p (g/cm^3)	1.16	1.17
Heat capacity, C_{ps} (cal/g.k)	0.32	0.32
Particle porosity, α	0.65	0.21
Bed density, ρ_B (g/cm^3)	0.795	0.713

Table 3 Characteristics of adsorption bed

Length, L (cm), [28]	76
Inside radius, R_{Bi} (cm), [28]	2.138
Outside radius, R_{Bo} (cm), [28]	2.415
Heat capacity of the column, C_{pw} (cal/g.K), [20]	0.12
Density of column, ρ_w (g/cm^3), [20]	7.83
Internal heat-transfer coefficient, h_i (cal/cm^2.K.s) [20]	9.2×10^{-4}
External heat-transfer coefficient, h_o (cal/ cm^2.K.s) [20]	3.4×10^{-4}
Axial thermal conductivity, K_L (cal/cm.s.K) [20]	6.2×10^{-5}
Axial dispersion coefficient, D_L (cm^2/s) [20]	1×10^{-5}

3. Results and Discussion

The fourth order Rung-Kutta scheme was used to solve a mathematical model that considered of coupled partial differential equations.

In order to validate the simulation results, the results of this work first were compared with other experimental data in the literature. In an experimental study, Mendes *et al.* [25] simulated a PSA commercial unit. They concluded that to affect of pressure rising in the adsorption step as a result of feed flow rate increases (and constant product flow rate), increasing production pressure more than 3 bar causes decrease both purity and recovery of oxygen. The experimental results by these authors together with the simulation results of this work are shown in Fig. 1. As obvious in this figure, the simulation and presented model in this work predicts the results of other experimentally work with a relatively high accuracy. In another case study, Mendes *et al.* [26], the PSA unit performance was studied by experiments and simulations. They reported that to affect of purge flow rate on oxygen purity and recovery, increase of the purge flow rate will cause to decrease oxygen recovery while its purity will be increase. The experimental results of these authors together with the predictions of current work are also shown in Fig. 2. In this consideration also it can be seen that the results of simulation indicated a very good agreement with current literature experimental work.

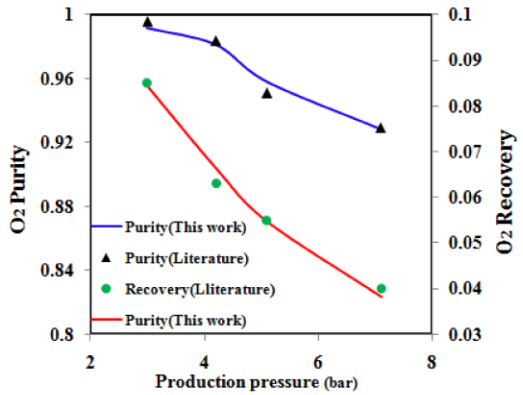

Fig. 1 O_2 purity a recovery as a function of production pressure, compare the model prediction in this work and experimental data by Mendes *et al.* **[24].**

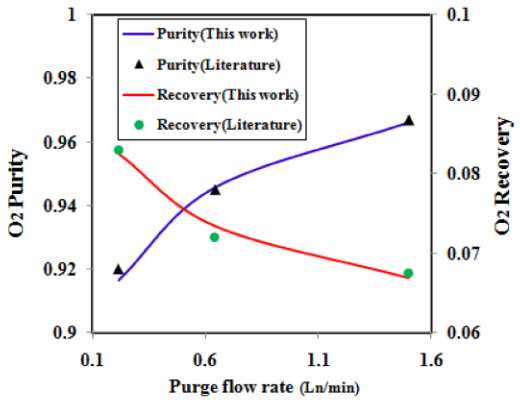

Fig. 2 O_2 purity and recovery as a function of purge flow rate, compare the model prediction in this work and experimental data by Mendes et al. **[25]**

Fig. 3 shows the adsorption isotherms of N_2, O_2, and Ar on zeolite 5A and 13X at 293.15K. The isotherms imply that zeolite 5A and 13X cannot separate argon from oxygen because of almost same adsorption amount. However, the adsorption capacity of N_2 is larger than that of O_2 and Ar especially, for zeolite 13X. The net adsorption amount of N_2 on zeolite 13X almost was higher than that of zeolite 5A with an increase in adsorption pressure. In the other hand, the net adsorption amount of O_2 on zeolite 5A was higher than that of zeolite 13X. Also the breakthrough simulation results indicated the difference between adsorption capacities of two types of zeolites.

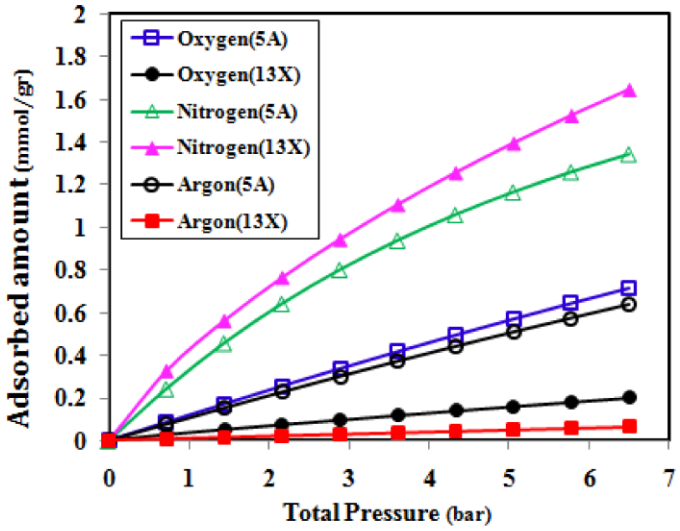

Figure 3 Adsorption isotherm of O_2, N_2 and Ar on zeolite 5A and 13X at 293.15K.

The breakthrough curves for N_2 and O_2 on a) zeolite 13X and b) zeolite 5A beds are shown in Fig. 4. As an initial condition, a non-adsorptive gas was assumed to pressurize the bed to adsorption pressure. As shown in this figure, O_2 was the first breakthrough component at about 240 and 280 sec for zeolite 5A and zeolite 13X, respectively. The breakthrough curve for O_2 was relatively broad and showed a small excursion. As the O_2 concentration increases slightly with time the breakthrough of the N_2 occurs at about 560 and 640 sec for zeolite 5A and zeolite 13X, respectively. Then, the O_2 concentration began to decrease with a tail at the beginning of the breakthrough of the N_2. In particular, Fig. 5 depicts the difference between adsorption capacities of a) O_2 and b) N_2 on two types of zeolites. The areas between two curves in these figures show these differences. Fig. 5-a shows the adsorption capacity of O_2 on zeolite 5A is larger than zeolite 13X as the inter-area of two curves, while Fig. 5-b indicates the adsorption capacity of N_2 on zeolite 5A is smaller as the inter-area of two curves. Fig. 6 shows that increase of the purge-to-feed (P/F) ratio will be led to increasing oxygen purity. This is due to useful bed desorption in the low pressure step with more purge gas volume. Needless to say that oxygen recovery will be reduce with the P/F ratio due to supplying the purge flow from the main product stream of the unit. However, oxygen recovery under zeolite 13X is almost as oxygen recovery under zeolite 5A. In this figure it also can be seen that oxygen purity always under zeolite 5A has a higher value than zeolite 13X. Fig. 7 depicts the influence of the feed flow rate on process performance of the PSA unit for two types of zeolites. By referring to this figure, oxygen purity decreases while oxygen recovery increases as the feed flow rate increases. Increase of the feed flow rate with regard to physical nature of the adsorbent outrages the breakthrough time of the bed and subsequently oxygen purity decreases. In other hand, oxygen recovery increases when the product flow increases as a result of feed flow increasing. With regard to this figure, oxygen purity has an almost the same value for two types of zeolites when the feed flow rate is about less than 23 Ln/min. It was evident that the process performance (O_2 purity) of zeolite 13X is worse than that of zeolite 5A for the flow rates more than 23 Ln/min. It also can be seen from this figure that oxygen recovery is higher value significantly for the zeolite 5A. The effect of adsorption pressure on oxygen purity and recovery is shown in Fig. 8. Oxygen purity and recovery both decrease when adsorption pressure increases (same conditions as figure 1). As indicated,

oxygen recovery has an almost the same value for two types of zeolites, while oxygen purity of zeolite 5A takes precedence over zeolite 13X when the adsorption pressure was higher than 3.5 bar.

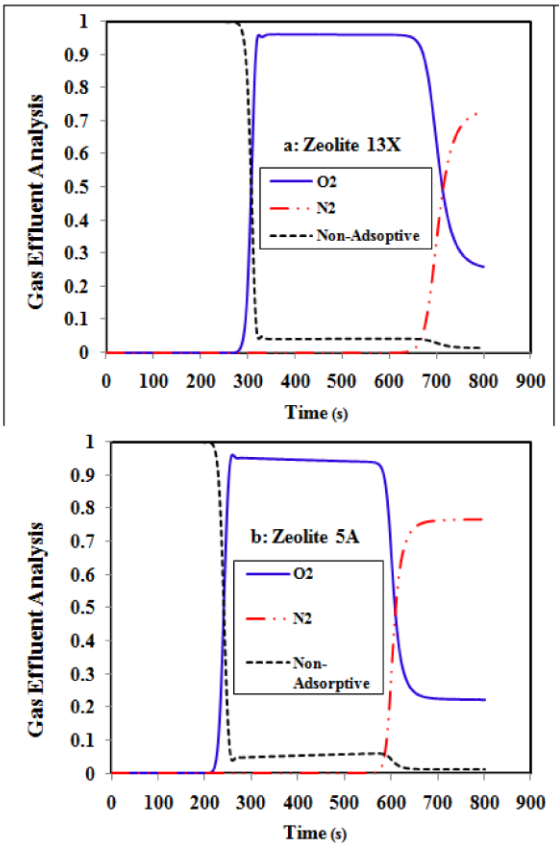

Fig. 4 Simulated concentration breakthrough curves at 6 atm adsorption pressure and 5 LSTP/min feed flow rate, (adsorption bed was initially saturated with a non-adsorptive gas at 6 atm and 298 K), a: zeolite 13X & b: zeolite 5A.

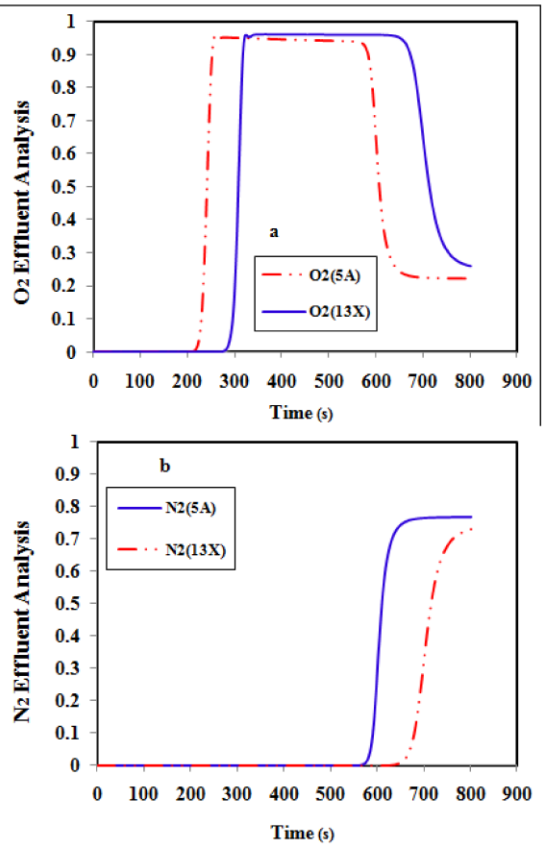

Fig. 5 The differences between adsorption capacities for zeolite 5A & 13X, a: oxygen and b: nitrogen.

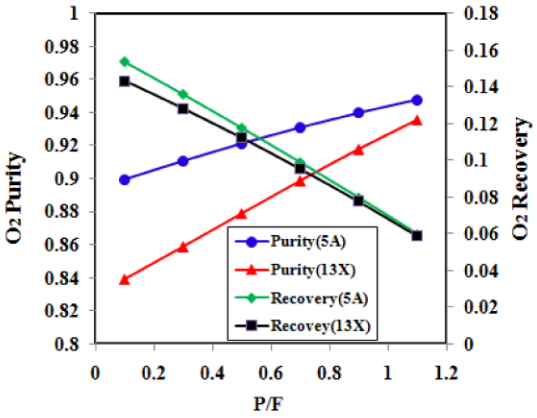

Fig. 6 Oxygen purity and recovery as a function of P/F

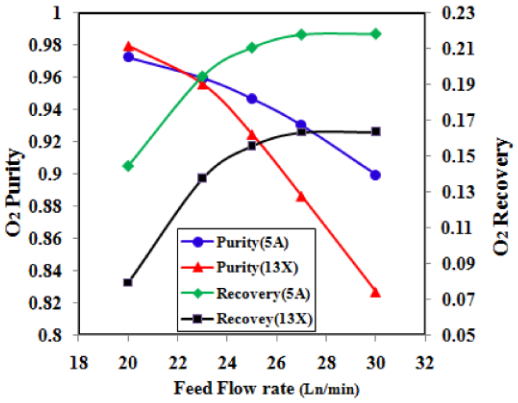

Fig. 7 Oxygen purity and recovery as a function of feed flow rate, (P_H = 6 bar).

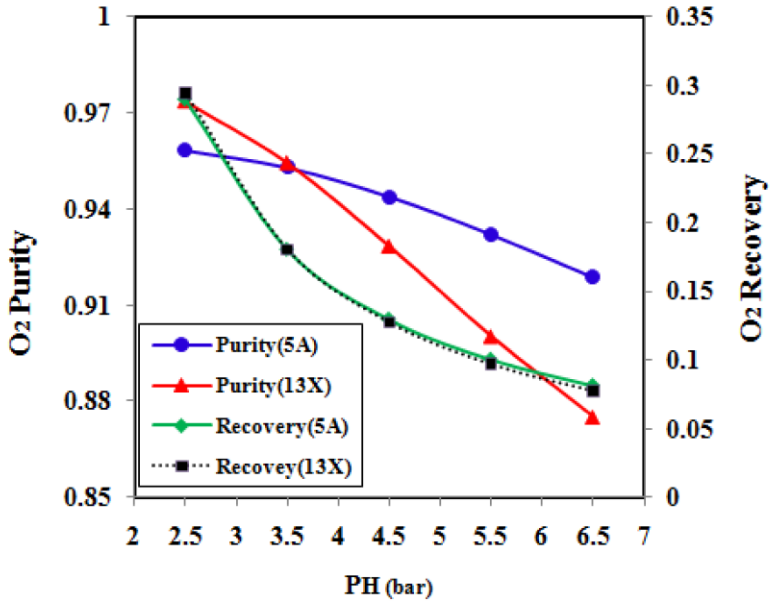

Fig. 8 Effect of higher operating pressure on oxygen purity and recovery (PL=1 bar, P/F=0.1, AD=20 sec., ED=5 sec., BD=15 sec.).

4. Conclusions

Two types of zeolite adsorbents, namely, zeolite 5A and zeolite 13X in a laboratory scale PSA unit for the same conditions are studied by numerical simulation. Simulation results indicated a satisfactory compliance with some current experimentally literatures. In addition, the effects of adsorption step pressure, feed flow rate and purge-to-feed (P/F) ratio on oxygen purity and recovery are studied. The adsorption isotherms of N_2, O_2 and Ar on zeolite 5A and 13X were compared in the range of 0 to 6.5 bar. Also the breakthrough curves of N_2 and O_2 on zeolites 5A and 13X are studied. Increase of the P/F ratio will be cause to increase oxygen purity and decrease its recovery. Oxygen recovery increases and oxygen purity decreases as feed flow rate increases. Both oxygen purity and recovery are increased with increasing adsorption pressure. Furthermore, comparison of two types of zeolites adsorbents shows that the process performance (in terms of purity and recovery) of an O_2-PSA unit is in may well conditions when the zeolite 5A is used instead of zeolite 13X.

Nomenclature

A_w cross-sectional area of the wall (cm^2)
AD adsorption step
B equilibrium parameter for the Langmuir model (atm^{-1})
BD blow down step
Cp_g, C_{ps}, C_{pw} gas, pellet, and wall heat capacities, respectively (cal/g.K)
D_L axial dispersion coefficient (cm^2/s)
G purge to feed ratio (kg_{feed}/kg_{purge})
hi internal heat-transfer coefficient ($cal/cm^2.K.s$)
ho external heat-transfer coefficient ($cal/cm^2.K.s$)
ΔH average heat of adsorption (cal/mol)
k parameter for the LDF model
K_L axial thermal conductivity (cal/cm.s.K)
L bed length (cm)
P total pressure (atm)
P_r reduced pressure, dimensionless
PG purge step
PR pressurization step
P/F ratio of purge flow rate to feed flow rate

PH/PL ratio of operating pressures
q, q*, q amount adsorbed, equilibrium amount adsorbed, and average amount adsorbed, respectively (mol/g)
q_m equilibrium parameter for the Langmuir model (mol/g)
R gas constant (cal/mol.K)
R_p radius of the pellet (cm)
R_{Bi}, R_{Bo} inside and outside radii of the bed, respectively (cm)
T time (s)
T_{atm} temperature of the atmosphere (K)
T, T_w pellet or bed temperature and wall temperature, respectively (K)
u interstitial velocity (cm/s)
y_i mole fraction of species i in the gas phase
z axial distance in the bed from the inlet (cm)

Greek Letters

α particle porosity
ε, ε_t voidage of the adsorbent bed and total void fraction, respectively
ρ_g, ρ_p, ρ_B, ρ_w gas density, pellet density, bulk density, and bed wall density, respectively (g/cm^3)

Subscripts

B bed
H higher operating pressure
i component i
L lower operating pressure
p pellet
g gas phase
s solid
w wall

References

[1] Castle, W.F. Air Separation and Liquefaction: Recent Developments and Prospects for the Beginning of the New Millennium. *Int. J. Ref.* 2002, 25, 158.
[2] Ruthven, D. M. *Principles of Adsorption and Adsorption Process*; John Wiley & Sons, 1984.
[3] Skarstrom, C. W. Method and Apparatus for Fractionating Gaseous Mixtures by Adsorption. U.S. Patent 2,944,627, July 12, 1960.
[4] Skarstrom, C. W. Oxygen Concentration Process. U.S. Patent 3,237,377, March 1, 1966.
[5] Fuderer, A.; Rudelstorfer, E. Selective Adsorption Process. U.S. Patent 3,986,849, October 19, 1976.
[6] Malek, A.; Farooq, S. Study of a Six-Bed Pressure Swing Adsorption Process. *AIChE J.* 1997, 43, 2509.
[7] Malek, A.; Farooq, S. Hydrogen Purification from Refinery Fuel Gas by Pressure Swing Adsorption. *AIChE J.* 1998, 44, 1985.
[8] Sircar, S.; Golden, T. C. Purification of Hydrogen by Pressure Swing Adsorption. *Sep. Sci. Technol.* 2000, 35, 667.
[9] Yang, R. T. Air Separation by Pressure Swing Adsorption Using Superior Adsorbents (Final Technical Report). Department of Chemical Engineering University of Michigan, 2001.
[10] Santos, J. C.; Magalhaes, F.D.; Mendens, A. Contamination of Zeolites Used in Oxygen Production by PSA: Effects of Water and Carbon Dioxide. *Ind. Eng. Chem. Res.* 2008, 47, 6197.
[11] Farooq, S.; Ruthven, D. M. A Comparison of Linear Driving Force And Pore Diffusion Models for a Pressure Swing Adsorption Bulk Separation Process. *Chem. Eng. Sci.*, 1990, 45 (1), 107.
[12] Farooq, S.; Rathor, M. N.; Hidajat, K. A Predictive Model for a Kinetically Controlled Pressure Swing Adsorption Separation Process. *Chem. Eng. Sci.* 1993, 48(24), 4129.
[13] Hassan, M. M.; Ruthven, D. M.; Raghvan, N. S. Air Separation by Pressure Swing Adsorption on a Carbon Molecular Sieve. *Chem. Eng. Sci.* 1986, 41 (5), 1333.

[14] Ruthven, D. M.; Farooq, S. Air Separation by Pressure Swing Adsorption. *Gas Sep. Purif*. 1990, 4, 141.
[15] Fernandez, G. F.; Kenney, C. N. Modeling of the Pressure Swing Air Separation Process. *Chem. Eng. Sci.* 1983, 38 (6), 827.
[16] S. Farooq, D. M. Ruthven, H. A. Boniface. Numerical Simulation of a Pressure Swing Adsorption Oxygen Unit. *Chem. Eng. Sci.* 1989, 44 (12), 2809.
[17] Farooq, S.; Ruthven, D. M. Numerical Simulation of a Kinetically Controlled Pressure Swing Adsorption Bulk Separation Process Based on a Diffusion Model. *Chem. Eng. Sci.* 1991, 46 (9), 2213.
[18] Kent S. Kneabel, Frank B. Hill. Pressure Swing Adsorption: Development of an Equilibrium Theory for Gas Separations. *Chem. Eng. Sci.* 1985, 40(12) , 2351.
[19] Jee J-G; Kim M-B; Lee C-H. Pressure Swing Adsorption to Purify Oxygen Using a Carbon Molecular Sieve. *Chem. Eng. Sci.* 2005, 60, 869-882.
[20] Jee, J. G.; Park, H. J. ; Haam, S. J. ; Lee, C. H. Effects of Nonisobaric and Isobaric Steps on O2 Presure Swing Adsorption for an Aerator. *Ind. Eng. Chem. Res.* 2002, 41, 4383.
[21] Ruthven, D. M.; Farooq, S.; Knaebel, K. S. *Pressure Swing Adsorption*; VCH Publishers: New York, 1994.
[22] Wever, T. W.; Chakravort, R. K. Pore and Solid Diffusion Models for Fixed-Bed Adsorbers. *AIChE J.* 1974, 20, 228.
[23] Jee, J. G.; Lee, S. J.; Lee, C. H. Comparison of the Adsorption Dynamics of Air on Zeolite 5A and Carbon Molecular Sieve Beds. *Korean J. Chem. Eng.* 2004, 21, 1183.
[24] Kostroski, K. P.; Wankat, P. C. High Recovery Cycles for Gas Separations by Pressure Swing Adsorption. *Ind. Eng. Chem. Res.* 2006, 45, 8117.
[25] Mendes, A. M. M.; Costa, C. A. V.; Rodrigues, A. E. Analysis of Nonisobaric Steps in Nonlinear Bicomponent Pressure Swing Adsorption Systems, Application to Air Separation. *Ind. Eng. Chem. Res.* 2000, 39, 138
[26] Mendes, A. M. M.; Costa, C. A. V.; Rodrigues, A. E. Oxygen Separation from Air by PSA: Modelling and Experimental Results Part I: Isothermal Operation. *Sep. Purif. Technol.* 2001, *24*, 173.
[27] Yang, R. T. Adsorbents: Fundamentals and Applications. New Jersey: John Wiley & Sons, Inc., 2003.
[28] Keller, J.; Staudt, R. Gas Adsorption Equilibria: Experimental Methods and Adsorption Isotherms. Boston: Springer Science + Business Media, Inc., 2005.
[29] Mofarahi, M.; Javadi Shokroo, E. Numerical Simulation of a Pressure Swing Adsorption for Air Separation. *7th International Chemical Engineering Congress & Exhibition*, Iran, 2011.

To whom correspondence should be addressed. E-mail: ejavadi@nsf-partshimico.tk, The Parthia Chemistry Co., Postcode: 71 888 41111, Fax: +98 7116362782.

Appl Petrochem Res
DOI 10.1007/s13203-014-0080-z

RESEARCH NOTE

Study of feed temperature effects on performance of a domestic industrial PSA plant

Ehsan Javadi Shokroo · Mohammad Shahcheraghi · Mehdi Farniaei

Received: 10 April 2014 / Accepted: 17 July 2014

Abstract The Parsian N_2-PSA industrial plant, situated in the southern pars zone of Iran, was studied numerically by mathematical modeling and numerical simulation. The model coupled PDEs are solved using fourth order Runge–Kutta scheme. In this work, we are dealing with the feed temperature and investigating its effect on the N_2 purity and recovery, which is known as an operating variable. Finally, the results of simulations showed that the feed temperature near to 25 °C is well suited to N_2 production with respect to its purity and recovery. In addition, as the feed temperature increases N_2 productivity decreases.

Keywords Pressure swing adsorption · Industrial plant · N_2 production · Numerical simulation · Carbon molecular sieve

Nomenclature

A_w	Wall cross-sectional area (cm^2)
AD	Adsorption step
B	L-F parameter (atm^{-1})
BD	Blow down step
cp_g	Gas heat capacities (cal/g.K)
cp_s	Pellet heat capacities (cal/g K)
cp_w	Wall heat capacities (cal/g K)
D_L	Axial dispersion coefficient (cm^2/s)
ED	Equalization to depressurization step
EP	Equalization to pressurization step
h_i	Internal heat-transfer coefficient (cal/cm^2 K s)
h_o	External heat-transfer coefficient (cal/cm^2 K s)
ΔH	Average heat of adsorption (cal/mol)
ID	Idle step
K	Parameter for the LDF model
K_L	Axial thermal conductivity (cal/cm s K)
L	Bed length (cm)
P	Total pressure (atm)
PP	Providing purge step
Pr	Reduced pressure (—)
PG	Purge step
PR	Pressurization step
q	Amount adsorbed (mol/g)
q^*	Equilibrium amount adsorbed (mol/g)
q_m	Saturated amount adsorbed (mol/g)
R	Gas constant (cal/mol K)
R_p	Radius of the pellet (cm)
R_{Bi}	Inside outside radius of the bed (cm)
R_{Bo}	Outside outside radius of the bed (cm)
t	Time (s)
T	Gas phase temperature (k)
T_{atm}	Temperature of the atmosphere (K)
T_w	Wall temperature (K)
u	Interstitial velocity (cm/s)
y_i	Mole fraction of species i in gas phase
Z	Axial distance (cm)

Greek letters

α	Particle porosity
ε	Voidage of the adsorbent bed
ε_t	Total void fraction
ρ_g	Gas density (g/cm^3)

E. J. Shokroo (✉) · M. Shahcheraghi · M. Farniaei
PART-SHIMI Company, Martyr Fahmideh Talent Foundation, Campus of Knowledge Based Companies, 87, Mirzaye Shirazi, 71 888 41111 Shiraz, Fars, Iran
e-mail: ehsan.javadi@hotmail.com

Published online: 13 August 2014

ρ_p Pellet density (g/cm^3)
ρ_B Bulk density (g/cm^3)
ρ_w Wall density (g/cm^3)

Subscripts

B Bed
i Component *i*
p Pellet
g Gas phase
s Solid
w Wall

Introduction

In general, three commercial methods are available for nitrogen purification, namely cryogenic, membrane technologies and pressure swing adsorption (PSA). PSA process is a wide operating unit for separation and purification of gases that operates based on capability of solid adsorption and selective separation of gases. The important operational parameter in this system is the pressure, and most industrial units operate at\or vicinity of the surrounding temperature. Today, the PSA process completely is known in a wide region of the processes, and this process was preferred in contrast to other conventional separation methods, especially for lower capacity and higher purity [23, 25, 33]. The nitrogen purification by pressure swing adsorption (N_2-PSA) system is well suited to rapid cycling, in contrast to other cyclic adsorption separation processes, and this has the advantage of reducing the absorbent inventory and therefore the capital costs of the system [23]. Use of PSA process to gas separation took place for the first time in 1958 by Skarstrom. He provided his recommended PSA cycles to enrich oxygen and nitrogen in air under the subject of heatless drier [30]. Thus, Skarstrom invented a two-bed PSA cycle with equalization step for oxygen production from air using zeolite 13X adsorbent in 1966 [31]. The main reasons for the success of this technology are many reforms that reached in this field and also is the new design and configuration for the cycles and devices [10, 16, 17, 29].

PSA process performance was strongly influenced by design parameters (such as: bed size, adsorbent physical properties, configuration and number of beds) and operating variables (such as: pressurization time, production time, purge time, feed flow rate, purge flow rate, production flow rate, temperature and/or pressure variations). So, this may be the maximum performance to obtain in terms of the best process variables. Thus, it is important that the behavior of the PSA operating variables was undertaking a review to know the optimum operating conditions. In recent years, use of this method was followed by researchers as a more important separation technique in air separation.

In modeling a kinetically controlled PSA process, the key requirement is an adequate representation of the mass transfer kinetics. For the systems showing kinetic selectivity, the mass transfer resistance is usually in the micropores and both linear driving force (LDF) [11], 1987; [1, 14] and micropore diffusion [7, 28] models. Shin and Knaebel [28] assumed that the diffusivities remain constant, while Farooq and Ruthven [7] allowed for the concentration dependence of the micropore diffusivity in accordance with the chemical potential gradient as the driving force. Detailed studies of diffusion in microporous adsorbents reveal that, for both zeolites [5, 26] and carbon molecular sieves [3, 15], the micropore diffusivity varies strongly with sorbate concentration.

Fernandez and Kenney [9] provided a theoretical analysis and adaptation to the experimental results for the separation of oxygen and nitrogen from air by a single bed pressure swing adsorption. They have compared the analytical approximations with the results of the experiments, and concluded that the approximately analytical solution can predict the adsorption bed dynamics for short cycle time. These authors also have reported that the exact numerical solution is an efficient method in the modeling and numerical simulation of the adsorption bed dynamics, especially in the case of long cycle time. Hassan et al. [11] proposed a simple dynamic model for the O_2-PSA process based on linear mass transfer rate relations and Langmuir equilibrium equation. These authors have assumed that the pressure remains constant during the adsorption and desorption steps. Farooq et al. [8] proposed a kinetically dynamic model for the O_2-PSA process, in which the adsorption is controlled by equilibrium instead of kinetic. Their testing system was a Skarstrom cycle [30]. The advantage of the kinetically proposed model by these researchers for the PSA systems is that the effects of mass transfer resistance and axial dispersion can easily be evaluated. The considered system by the authors is a simple two-bed PSA Skarstrom system, but utilizing the model is not limited for the multi-bed systems which are commonly used in large-scale units. Farooq & Ruthven [6] suggested a linear driving force model (LDF) assuming frozen solid concentration during pressurization and blowdown steps to numerical simulation of air separation process by adsorption method using carbon molecular sieve (CMS). A fix bed under a four-step cycle was used in the PSA experiments. The cycle steps were the same as the steps of Skarstrom fundamental cycle: (1) high-pressure production, (2) blowdown, (3) purge with product and, (4) pressurization with feed. The authors have concluded that a good agreement is between the simple LDF model and the experimental results and, also the LDF model has a high

compatibility with the more complicated pore-diffusion model. Farooq & Ruthven [24] modeled the PSA process dynamic behavior for the nitrogen recovery using zeolite 5A, zeolite 13X, and CMS using the theoretical and experimental investigation. The LDF and pore-diffusion models were also used to compare the rate of mass transfer in the adsorption beds. The experiments were performed in a dual-bed system with two configurations: (1) the Skarstrom cycle and (2) the Self-purging modified cycle. The comparison between simulation results and experiments showed that the simple LDF model can predict the effect of process variables, but the complicated pore-diffusion model indicated a better adaptation to the experimental results. Farooq & Ruthven [7] suggested a pore-diffusion model for modeling the bulk two-component gas separation process using a PSA system based on Langmuir equilibrium and also considering concentration dependency for diffusion coefficient. The PSA system used by the authors was investigated in two configurations: (1) Skarstrom cycle and modified Skarstrom cycle with pressure equalization step and self-purging. The concentration dependency for diffusion coefficient of micropore was also examined. The concentration dependency has a large effect on cyclic steady state (CSS) performance. Budner et al. [2] improved a thermal non-equilibrium model for the multicomponent adsorption process. They also have designed a software for the computation and simulation air separation process based on vacuum swing adsorption (VSA) technique using molecular sieve zeolite adsorbent. They have claimed that the developed and studied mathematical model using its software is able to design and optimize the VSA units for oxygen production. Mendes et al. [18] investigated a PSA system using zeolite 5A and Skarstrom cycle through simulations and experiments. They showed that the pressure increasing during pressurization step causes increasing dispersion in the PSA beds and finally results in decrease of product purity and recovery. Time reduction of depressurization in blowdown step down to 4 s does not affect on product purity and recovery. Taking the pressure equalization step in the Skarstrom cycle causes improvement of product purity and recovery. Mendes et al. [19] examined the PSA unit for oxygen separation from air using zeolite 5A through simulations and experiments. The mentioned PSA system was studied in two configurations as Skarstrom cycle and Skarstrom cycle with pressure equalization step. They showed that, as the production flow rate increases the product purity decreases; as the production step time increases the product purity reduces while its recovery increases. Shin et al. [27] found the optimal conditions for oxygen recovery and productivity using a two-bed PSA system with incomplete equalization step. According to their findings, use of the incomplete equalization step for PSA cycle is the leading cause of

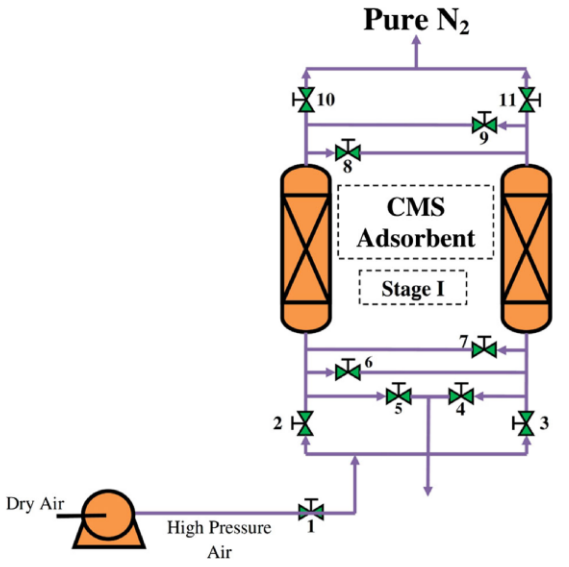

Fig. 1 Schematic diagram of Parsian N_2-PSA industrial plant [22]

productivity improvement in the case of feed pressurization. The maximum productivity occurs using the incomplete equalization step, but its level is less than that for the case of feed pressurization. On the other hand, the maximum recovery always is obtained using complete equalization step. Cruz et al. [4] proposed a heuristic method to optimizing cyclic adsorption separation processes (PSA/VSA), in which the system acts based on Skarstrom cycle with pressure equalization step. They studied the various configurations for equalization step, and they found that bottom-to-bottom configuration is just efficient when adsorbent productivity is low and the Skarstrom cycle is used. The top-to-top configuration always is the most efficient in terms of product recovery and power consumption. Moghadaszadeh et al. [21] investigated different process variables such as production recovery, cycle time, production and purge flow rates on oxygen purity. They examined a four-bed PSA pilot consisting of seven steps to oxygen separation from air using zeolite 13X. These authors showed that the increasing purge flow rate maximized the product purity. Also, increasing cycle time is the leading cause of power consumption decrease, while power requirement will be increased. Mofarahi et al. [20] investigated a four-bed PSA consisting seven steps to oxygen separation from air using zeolite 5A. They reported that as long as the adsorption pressure increases from 4 to 6 bar, the oxygen purity and recovery increase. The PSA unit performance is improved at higher cycle times. When production flow rate increases oxygen recovery increases, while oxygen purity will be reduced.

The Parsian N_2-PSA industrial plant, a two-bed PSA process, operates as modified Skarstrom cycle [23, 33].

Table 1 Model equations [23, 25, 33]

$$\frac{\partial C_i}{\partial t} - D_L \frac{\partial^2 C_i}{\partial z^2} + \frac{\partial (C_i.u)}{\partial z} + \rho_p.\left(\frac{1-\varepsilon}{\varepsilon}\right).\frac{\partial \bar{q}_i}{\partial t} = 0 \quad (1)$$

$$\frac{\partial C}{\partial t} - D_L \frac{\partial^2 C}{\partial z^2} + \frac{\partial (C.u)}{\partial z} + \rho_p.\left(\frac{1-\varepsilon}{\varepsilon}\right).\sum_{i=1}^{N}\frac{\partial \bar{q}_i}{\partial t} = 0 \quad (2)$$

$$-K_l \frac{\partial^2 T}{\partial z^2} + \varepsilon.\rho_g.c_{p,g}.\left(u\frac{\partial T}{\partial z} + T\frac{\partial u}{\partial z}\right) + \left(\varepsilon_t.\rho_g.c_{p,g} + \rho_B.c_{p,s}\right).\frac{\partial T}{\partial t} - \rho_B.\sum_{i=1}^{N}\left(\frac{\partial \bar{q}_i}{\partial t}.(-\Delta \bar{H}_i)\right) + \frac{2h_i}{R_{B,i}}(T - T_w) = 0 \quad (3)$$

$$\rho_w.c_{p,w}.A_w\frac{\partial T_w}{\partial t} = 2\pi R_{B,i}h_i(T - T_w) - 2\pi R_{B,o}h_o(T_w - T_{atm}); A_w = \pi\left(R_{B,o}^2 - R_{B,i}^2\right) \quad (4)$$

$$P(t) = a.t^2 + b.t + c \quad (5)$$

$$-\frac{dP}{dz} = a.\mu.u + b.\rho.u.|u|; a = \frac{150}{4R_p^2}.\frac{(1-\varepsilon)^2}{\varepsilon^2}; b = 1.75\frac{(1-\varepsilon)}{2R_p\varepsilon} \quad (6)$$

$$q_i = \frac{q_{m,i}.B_i.P_i}{1+\sum_{j=1}^{s}B_j.P_j}; q_{m,i} = k_1 + k_2.T; B_i = k_3.\exp(k_4/T); n_i = k_5 + k_6/T \quad (7)$$

$$\frac{\partial \bar{q}_i}{\partial t} = \omega_i.(\dot{q}_i - \bar{q}_i); \omega_i = \frac{15D_{ei}}{r_c^2}; \frac{15D_{ei}}{r_c^2} = C_i.P_r^{0.5}.(1 + B_i.P_i)^2 \quad (8)$$

Figure 1 shows a schematic diagram of the process. The six-step process used is as follows: (1) co-current feed pressurization (PR) of a partially pressurized bed by a previous pressurizing pressure equalization step (EP); (2) high-pressure adsorption (AD) step; (3) counter-current depressurizing pressure equalization (ED) step; (4) counter-current blow down (BD) step; (5) counter-current purge with a light product (PG) step; (6) co-current EP step.

In this work, the Parsian N_2-PSA industrial plant is studied by mathematical modeling and numerical simulation. Furthermore, the effect of feed temperature on the plant performance (N_2 recovery and productivity) is investigated.

Mathematical model

To develop a mathematical model for a PSA system, the below main assumptions were given:

a. Gas behaves an ideal gas.
b. The flow pattern is described by the axially dispersed plug-flow model.
c. Adsorbing properties throughout the tower would remain constant and unchanged.
d. Radial gradient is to be negligible.
e. Equilibrium equations for the components of the feed (N_2, O_2, Ar) can be expressed by three-component Langmuir–Freundlich isotherm.
f. Mass transfer rate is expressed by a linear driving force equation.
g. Thermal equilibrium between gas and solid phases is assumed.
h. Pressure drop along the bed is calculated by the Ergun's equation.

The model equations for the bulk phase in the adsorption bed are written in Table 1 [12, 13, 32].

For the coupled PDEs problem, the well-known Danckwerts boundary conditions are applied [23, 25, 33]. The adsorption isotherm parameters and diffusion rate constant of N_2, O_2 and Ar over CMS are shown in Table 2. In Table 3, the characteristics of adsorbent and adsorption bed are shown.

Results and discussion

The fourth order Runge–Kutta scheme (for the time derivatives) and the implicit finite difference scheme (for the space derivatives) were used to solve the mathematical model that consisted of coupled partial differential equations.

The plant operating conditions data supplied by Parsian Co. can be found in Table 4 [22]. In this simulation study, the feed (air) components were assumed to be N_2, O_2 and Ar. To validate the simulation results, the results of this work first were compared with the plant data. Figure 2 shows the simulated N_2 purity as a function of feed flow rate, with N_2-PSA industrial plant data. This figure also shows as the feed flow rate increases the nitrogen purity decreases, which are in correspondence with other PSA simulations results [23, 25, 33]. In addition, as obvious in this figure, the simulation and presented model in this work predict the results of the plant data with a fairly high accuracy. The effect of feed temperature on N_2 purity and recovery is indicated in Fig. 3. It can be seen from this figure that the increasing of the feed temperature is the leading cause of a reduction in the N_2 purity and an increment in the N_2 recovery. The adsorption is an inherently exothermic phenomenal, so the decreasing of

Table 2 Equilibrium\rate parameters and heat of adsorption of N_2, O_2 and Ar on CMS [12]

Parameter	Component		
	N_2	O_2	Ar
$k_1 \times 10^3$ (mol/g)	23.63	15.27	20.42
$k_2 \times 10^3$ (mol/g k)	−0.0638	−0.00323	−0.00530
$k_3 \times 10^4$ (1/atm)	361	22.9	239.7
k_4 (k)	1,444	9,66.1	324.6
k_5 (−)	1.692	1.187	1.646
k_6 (k)	−270	−106	−238.2
Heat of adsorption, $-\Delta H_i$ (cal/mol)	3,197.532	3,297.828	3,398.124

Table 3 The characteristics of adsorbent and adsorption bed

Adsorbent [12]		*Adsorption bed* [22]	
Adsorbent	CMS	Length L (cm)	245
Type	Sphere	Inside radius, $R_{B,i}$ (cm)	80
Micropore diameter, R_p (cm)	3 A	Outside radius, $R_{B,o}$ (cm)	80.50
Particle density, ρ_p (g/cm^3)	0.9	Heat capacity of column, Cp_w (cal/g k)	0.12
Bulk density, ρ_B (g/cm^3)	0.633	Density of column, ρ_w (g/cm^3)	7.83
Heat capacity, Cp_s (cal/g k)	0.22	Internal heat-transfer coefficient, h_i (cal/cm^2 k s)	9.2×10^{-4}
Particle porosity, α	0.30	External heat-transfer coefficient, h_o (cal/cm^2 k s)	3.4×10^{-4}

Table 4 Industrial N_2-PSA operating condition [22]

Composition, mol (%)	Feed	Product	Tail
N_2	79.00	99.99	N/A
O_2	20.00	0.01	N/A
Ar	1.00	N/A	N/A
Pressure (bar)	7.00	6.50	1.00
Temperature (°C)	35.00	40.00	25.00
Flow rate (N m^3/h)	319.800	N/A	N/A

the N_2 purity with the feed temperature has occurred in the normal way. In other hand, the incremental behavior of the N_2 recovery through the increasing of the feed temperature is caused by gas molar compression in the adsorption (AD) step, which means that the N_2 volume increases in the product stream. This figure shows that the feed temperature near to 25 °C is well suited to N_2 production in terms of its purity and recovery. Figure 4 depicts as the feed temperature increases N_2 productivity decreases. Productivity is defined as the ratio of moles of N_2 in the product stream to the kg of the adsorbent per cycle time. The cyclic partial concentration of N_2 at the top of the bed during a whole cycle is shown in Fig. 5. It is evident also from this figure that the process performance (N_2 purity) is modified to correspond to lower feed temperature (25 °C) because of the cyclic concentration of N_2 placed at an upper level. In other words, it can reach the high pure N_2 (as the current purity in the plant) using higher feed flow rates when the feed temperature is near to 25 °C, which causes the increasing of N_2 recovery.

Conclusions

The Parsian N_2-PSA, located in the southern pars zone of Iran, has been simulated. The effect of feed temperature on the process performance is studied by a mathematical

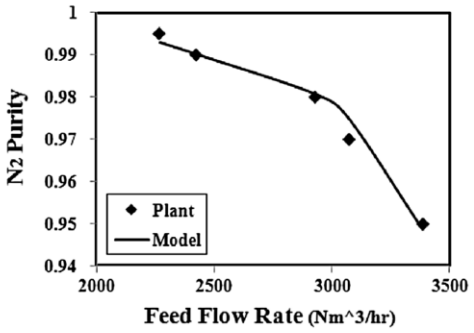

Fig. 2 Simulated purity and plant data of N_2-PSA industrial process as a function of feed flow rate

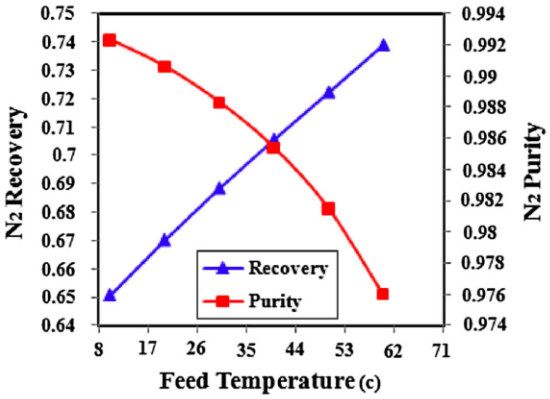

Fig. 3 N_2 purity and recovery as a function of feed temperature

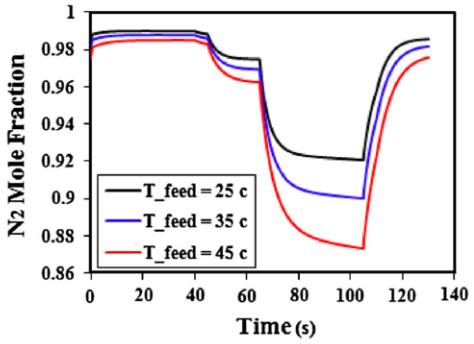

Fig. 5 Cyclic partial concentration of N_2 during a whole cycle at the top of the bed

modeling numerical simulation. The mathematical model in the gas phase takes into account the balances in energy, mass and momentum and the coupled PDEs are solved using fourth order Runge–Kutta scheme. Results showed

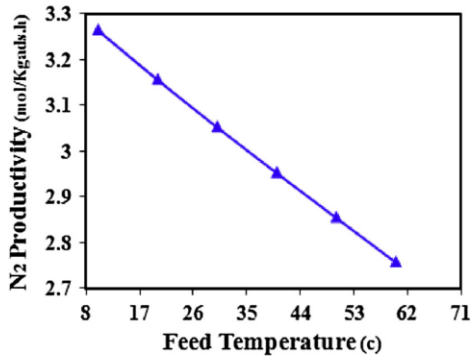

Fig. 4 Effect of feed temperature on the N_2 productivity

that the unit performance (in terms of N_2 purity and recovery) is in may well conditions when the feed temperature is near to 25 °C. Furthermore, as the feed temperature increases N_2 productivity decreases.

Acknowledgments The authors gratefully acknowledge the Parsian Gas Refining Co. for agreement with this research.

References

1. Ackley MW, Yang RT (1990) Kinetic separation by pressure swing adsorption: method of characteristics. A1ChE J 36:1229–1238
2. Budner Z, Dula J, Podstawa W, Gawdzik A (1999) Study and modeling of the Vacuum Swing Adsorption (VSA) process employed in the production of oxygen. Ins Chem Eng, 77, Part A, 405–412
3. Chihara K, Suzuki M, Kawazoe K (1978) Concentration dependence of micropore diffusivities-diffusion of propylene in molecular sieving carbon 5A. J Chem Eng Japan 11:153–155
4. Cruz P, Magalhaes FD, Mendes A (2005) On the optimization of cyclic adsorption separation processes. AIChE J 51:1377–1395
5. Doetsch IH, Ruthven DM, Loughlin KF (1974) Sorption and diffusion of n-Heptane in 5A Zeolite. Can J Chem 52:2717–2724
6. Farooq S, Ruthven DM (1990) A comparison of linear driving force and pore diffusion models for a pressure swing adsorption bulk separation process. Chem Eng Sci 45:107–115
7. Farooq S, Ruthven DM (1991) Numerical simulation of a kinetically controlled pressure swing adsorption bulk separation process based on a diffusion model. Chem Eng Sci 46:2213–2224
8. Farooq S, Ruthven DM, Boniface HA (1989) Numerical simulation of a pressure swing adsorption oxygen unit. Chem Eng Sci 44(12):2809–2816
9. Fernandez G, Kenney CN (1983) Modeling of the pressure swing air separation process. Chem Eng Sci 38(6):827–834
10. Fuderer A, Rudelstorfer E (1976) Selective adsorption process, US Patent 3,986,849

11. Hassan MM, Raghavan NS, Ruthven DM (1986) Air Separation by pressure swing adsorption on a carbon molecular sieve. Chem Eng Sci 41:1333–1343
12. Jee JG, Kim MB, Lee CH (2005) Pressure swing adsorption to purify oxygen using carbon molecular sieve. Chem Eng Sci 60:869–882
13. Jee JG, Park HJ, Haam SJ, Lee CH (2002) Effects of nonisobaric and isobaric steps on O_2 pressure swing adsorption for an aerator. Ind Eng Chem Res 41:4383
14. Kapoor A, Yang RT (1989) Kinetic separation of methane-carbon dioxide mixture by adsorption on molecular sieve carbon. Chem Eng Sci 44:1723–1733
15. Kawazoc K, Suzuki M, Chihara K (1974) Chromatographic study of diffusion in molecular-sieving carbon. J Them Eng Jpn 7:151–157
16. Malek A, Farooq S (1985) Hydrogen purification from refinery fuel gas by pressure swing adsorption. AIChE J 44:1985
17. Malek A, Farooq S (1997) Study of a six-bed pressure swing adsorption process. AIChE J 43:2509
18. Mendes AMM, Costa CAV, Rodrigues AE (2000) Analysis of nonisobaric steps in nonlinear bicomponent pressure swing adsorption systems: application to air separation. Ind Eng Chem Res 39:138–145
19. Mendes AMM, Costa CAV, Rodrigues AE (2001) Oxygen separation from air by PSA: modeling and experimental results part I: isothermal operation. Sep Purif Tech 24:173–188
20. Mofarahi M, Towfighi J, Fathi L (2009) Oxygen separation from air by four-bed pressure swing adsorption. Ind Eng Chem Res 48:5439–5444
21. Moghadaszadeh Z, Towfighi J, Mofarahi M (2008) Study of a four-bed pressure swing adsorption for oxygen separation from air. Int J Chem Bio Eng 1(3):140–144
22. Parsian GAS Refinement Co., N2-PSA plant, http://www.nigc-parsian.ir/
23. Ruthven DM (1984) Principle of adsorption and adsorption processes. John Wiley & Sons Inc, New York
24. Ruthven DM, Farooq S (1990) Air separation by pressure swing adsorption. Gas Sep Purif 4:141–148
25. Ruthven DM, Farooq S, Knaebel KS (1994) Pressure swing adsorption. VCH Publishers Inc, New York
26. Ruthven DM, Loughlin KF (1971) The sorption and diffusion of n-butane in linde 5a molecular sieve. Chem Eng Sci 26:1145–1154
27. Shin HS, Kim DH, Koo KK, Lee TS (2003) Performance of a two-bed pressure swing adsorption process with incomplete pressure equalization. Adsorption 6:233–240
28. Shin HS, Knaebel KS (1988) An experimental study of diffusion-induced separation of gas mixtures by pressure swing adsorption. AIChE J 34:1409–1416
29. Sircar S, Golden TC (2000) Purification of hydrogen by pressure swing adsorption. Sep Sci Technol 35:667
30. Skarstrom CW (1960) Method and apparatus for fractionating gaseous mixture by adsorption, US Patent, No. 2,944,627
31. Skarstrom CW (1966) Oxygen concentration process, US Patent, No. 3,237,377
32. Shokroo EJ, Shahcheraghi M, Farrokhizadeh A, Farniaei M (2014) The Iranian Jam Petrochemical's H_2-PSA enhancement using a new steps sequence table. Pet Coal 56(1):13–18
33. Yang RT (1987) Gas separation by adsorption processes. Butterworth, Reprinted by Imperial College Press, London

Korean J. Chem. Eng., 33(4), 1391-1401 (2016)
DOI: 10.1007/s11814-015-0232-6

pISSN: 0256-1115
eISSN: 1975-7220

Comparative study of zeolite 5A and zeolite 13X in air separation by pressure swing adsorption

Ehsan Javadi Shokroo*,†, Danial Jafari Farsani, Hadiseh Khalilpour Meymandi*, and Nadia Yadollahi***

*PART-SHIMI Knowledge Based Company, Shiraz, Iran
**Bidboland Refining Co., NIGC, Bidboland, Iran
(*Received 23 June 2015 • accepted 6 November 2015*)

Abstract−The performance of zeolites 5A and 13X is numerically investigated in oxygen separation from air by a two-bed PSA system. The effect of operating variables such as adsorption step time, P_H/P_L ratio and cycle time was investigated on product purity and recovery. The simulation results showed that nitrogen adsorption capacity on zeolite 13X was slightly more than the one on zeolite 5A. In the completely same operating conditions, zeolite 5A had a larger mass transfer zone than zeolite 13X. Therefore, the adsorption and desorption rate of nitrogen on zeolite 5A is less than zeolite 13X. Moreover, for the equal volume of adsorbed nitrogen on both adsorbents, zeolite 5A is more capable rather than zeolite 13X to desorb much more volume of nitrogen at certain time. Furthermore, for achieving oxygen with purity of 96%, utilizing zeolite 5A is more economical than zeolite 13X, when $5.5<P_H/P_L<7$ and 75<cycle time≤90.

Keywords: Pressure Swing Adsorption, Zeolite 5A, Zeolite 13X, Separation, Numerical Simulation

INTRODUCTION

Air separation is one of the most important gas separation processes in the chemical industry. The two most commonly methods used for the separation of oxygen and nitrogen from air are as follows: 1. Cryogenic distillation (by use of the relative volatility difference between two components). 2. Adsorption processes such as pressure swing adsorption (PSA), which works based on the selective adsorption capability of a component on a suitable adsorbent. PSA technology is used to separate some gas species from a gas mixture under pressure according to the molecular characteristics of the species and affinity for an adsorbent material. This process operates at near-ambient temperatures. Specific adsorptive materials such as zeolites, activated carbon, molecular sieves are used as adsorbents to adsorb the target gas species at high pressure. The process then swings to low pressure for the purpose of desorbing the adsorbed material [1].

In addition to PSA, there is also temperature swing adsorption (TSA), which is based on adsorption at operating conditions and regeneration at an elevated temperature. Similar to other adsorption processes, there are at least two stages in TSA processes: adsorption and desorption. Desorption in the cycle of this process includes two stages of heating and cooling. After ending the heating stage, the bed cooling operation starts in order that the first adsorption condition is obtained [1,2].

Generally, the common adsorption processes of air separation are divided into two categories. The first category consists of processes which make use of zeolites as nitrogen adsorbent under the equilibrium conditions and oxygen is a process product. The second one contains processes which utilize carbon molecular sieves (CMSs) as oxygen adsorbent. Based on kinetic separation in this kind of category, oxygen is adsorbed owing to its faster permeation and higher selectivity. Moreover, nitrogen is produced as a product in such these processes. The operating conditions, product purity and type of cycles are completely different in these two categories. As a matter of fact, producing oxygen from air depends on its applications in different industries.

Oxygen is one of the most important products in the chemical industry. This chemical element is used in various processes, such as refineries, manufacturing metal and other industrial operations. For instance, oxygen with high purity is used in different chemical processes like steel construction, paper industries, wastewater treatment and glass production. In 1907, oxygen was produced for the first time, when Linde built a first cryogenic distillation bed for air separation [3].

A widely used unit operation for gas separation or purification is pressure swing adsorption used in most of the commercial adsorption applications [4-8]. Before 1980, PSA systems were used with adsorption pressure greater than atmospheric pressure and desorption pressure near atmospheric conditions. In comparison with cryogenic distillation process, these systems are low-cost in terms of initial investment (because of their simplicity), whereas they are costly in terms of energy consumption. Vacuum swing adsorption (VSA) systems (a kind of operations which work with adsorption pressure of slightly more than atmospheric pressure and desorption pressure of about 0.2 atm) have been developed due to availability of modified adsorbents and the less cost of vacuum equipment, rather than feed compression.

Over the past 40 years, several processes of PSA and VSA systems have been designed in order that pure oxygen from air mix-

†To whom correspondence should be addressed.
E-mail: ehsan.javadi@hotmail.com

ture is produced. In O_2-PSA industrial units the ratio of high pressure, in the adsorption step, to low pressure, in the desorption step, (P_H/P_L), is considered to be one of the most important factors owing to determine required energy [9]. Typically, the pressure ratio of 4 and higher than 4 is utilized in the industries. Furthermore, many units with low capacity make use of two-bed systems based on Skarstrom cycle, which are sometimes associated with an equalization step in order to improve the recovery.

Selecting a suitable adsorbent is a critical parameter to design a PSA process. Generally, finding a suitable adsorbent is the first step in developing adsorption separation process. As the separation factor usually varies with temperature and considerably with composition, choosing appropriate conditions for maximizing the separation factor is considered to be a major issue in the process design. Sometimes an initial selection of suitable adsorbents can be directly achieved according to available Henry's law constants.

Most of the time, selecting the adsorbents can be easily achieved with measurement of chromatographic retention times (MCRT). Moreover, to achieve a quick and actual estimation of separation factors, chromatographic methods are better than the other methods because of their prediction in adsorption kinetic.

Zeolites 5A and 13X are the most commonly used adsorbents in air separation for oxygen production. The unique properties of zeolites are originated from this fact that their surfaces are formed with negatively charged oxides. Moreover, the presence of isolated cations above their surface structure is another reason for their uniqueness. Despite knowing the selectivity of O_2/N_2 by zeolite, there was no progress in the case of air separation by adsorption process until 1960 [9], even after the innovation of synthetic zeolites 5A and 13X and PSA cycles. The innovation of zeolites 5A and 13X by Milton (1959) created conditions which were always available [3]. Zeolites are aluminosilicate crystallines of alkaline or earth alkaline elements such as sodium, potassium and calcium. More detailed description of the zeolite structures is accessible in the literature [11]. There are many studies which have been done on the separation of oxygen from air [12-26]. By these innovations, the industrial ideologists were e ncouraged to examine the feasibility of air separation at ambient temperature by applying adsorption processes, while the temperature for cryogenic processes was 77 K. From an economical point of view, the history of PSA technology development can be associated with reducing the cost of oxygen production via this process which is illustrated in Fig. 1.

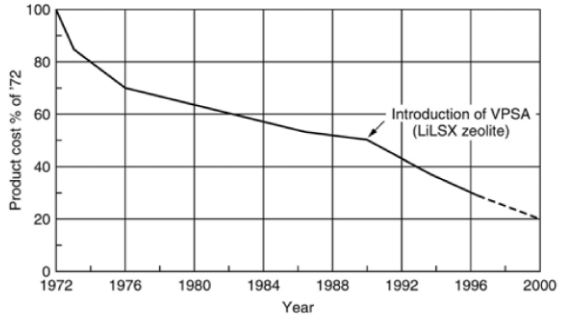

Fig. 1. Cost of oxygen production by applying PSA process (in constant dollars). Zeolites 5A and 13X were used before 1990 and zeolite LiLSX was used afterwards [10].

Several investigations and experimental researches have been separately done in order to separate oxygen from air by PSA process using zeolites 5A and 13X [9]. However, there are not any investigations in accordance with the range of operating conditions of these two adsorbents in order to compare their effects on the process performance. Despite there being many investigations which were performed on the dynamics of a zeolite adsorption and desorption, there are not any investigations on the PSA process performance according to the type of adsorbent. For instance, the adsorption and desorption experiments for N_2/O_2 system on zeolite 5A, 10X, and 13X beds were performed by Jee et al. [27] to study the dynamic characteristics of air separation adsorption processes. Although zeolites 5A and 13X are both commonly used for oxygen separation from air in the PSA process, there are still unanswered questions. For example, whether to use 5A or 13X at different operating conditions when the product purity is more important than recovery. Is zeolite 5A better than zeolite 13X when a product recovery with an acceptable level of purity is considered? Or which type of zeolite should be used when both purity and recovery of oxygen are expected to be in the acceptable range? Answering these important questions requires strong and effective studies which have been investigated in the current study.

Two processes of oxygen separation from air by means of PSA technique, using zeolites 5A and 13X as adsorbents, are simulated at the same operating conditions in this study. The influence of adsorbent type on O_2-PSA process performance is examined. Furthermore, the importance of zeolite type in the quality and quantity of oxygen has been interpreted according to different operational variables. The simulated PSA process is a six-step process with the following sequence: (I) co-current feed pressurization (PR); (II) high-pressure adsorption (AD) step; (III) counter-current depressurizing pressure equalization (ED) step; (IV) counter-current blow down (BD) step; (V) counter-current purge with a light product (PG) step; (VI) co-current pressurizing pressure equalization (EP) step.

MATHEMATICAL MODEL

To develop a mathematical model for a PSA system, the following assumptions were made:

1. Gas behaves as an ideal gas;
2. Total pressure versus time remains constant during adsorption and purge steps;
3. Total pressure changes nonlinearly with time during pressurization, pressure equalization and blow down steps;
4. The flow pattern is axially assumed as plug-flow model;
5. Equilibrium equations for air are expressed as triple Langmuir-Freundlich isotherm (oxygen, nitrogen and argon);
6. Rate of mass transfer is presented by linear driving force (LDF) relations;
7. Bed is clean at initial state and there is no gas flow in it;
8. Air is considered a mixture of oxygen and argon (21%) and nitrogen (79%) as feed.

According to these assumptions, dynamic behavior of system in terms of mass, energy and momentum balances can be expressed

as follows:

Dimensionless partial mass balance for gas phase in the adsorption bed is [9,20,25,26]:

$$-\left(\frac{1}{P_e^m}\right)\cdot\frac{\partial^2 y_i}{\partial\hat{z}^2}+y_i\cdot\frac{\partial\hat{u}}{\partial\hat{z}}+\hat{u}\cdot\left(\frac{\partial y_i}{\partial\hat{z}}+y_i\cdot\left(\frac{1}{\hat{P}}\cdot\frac{\partial\hat{P}}{\partial\hat{z}}-\frac{1}{\hat{T}}\cdot\frac{\partial\hat{T}}{\partial\hat{z}}\right)\right)$$
$$+\frac{\partial y_i}{\partial\tau}+y_i\cdot\left(\frac{1}{\hat{P}}\cdot\frac{\partial\hat{P}}{\partial\tau}-\frac{1}{\hat{T}}\cdot\frac{\partial\hat{T}}{\partial\tau}\right) \quad (1)$$
$$+\left(\frac{\rho_p\cdot R\cdot T_0\cdot\hat{T}}{P_0\cdot\hat{P}}\right)\cdot\left(\frac{1-\varepsilon}{\varepsilon}\right)\cdot\left(q_{m,i}\cdot\frac{\partial\hat{q}_i}{\partial\tau}+\hat{q}_i\cdot\frac{\partial q_{m,i}}{\partial\tau}\right)=0$$

Dimensionless equilibrium loading of i^{th} component for solid phase in the adsorption bed is:

$$\frac{\partial q_{m,i}}{\partial\tau}=\frac{\partial q_{m,i}}{\partial\hat{T}}\times\frac{\partial\hat{T}}{\partial\tau}=k_{2,i}T_0\times\frac{\partial\hat{T}}{\partial\tau} \quad (2)$$

Dimensionless loading of i^{th} component for solid phase in the adsorption bed is (LDF relation):

$$\frac{\partial\hat{q}_i}{\partial\tau}=\alpha_i\cdot\left(\frac{\beta_i\cdot y_i^{ni}}{1+\sum_{j=1}^{N}\beta_j\cdot y_j^{nj}}-\hat{q}_i\right)-\left(\frac{\hat{q}_i}{q_{m,i}}\cdot\frac{\partial q_{m,i}}{\partial\tau}\right) \quad (3)$$

According to Eq. (3), the LDF relation depends on various parameters, such as equilibrium parameter for the Langmuir model, mole fraction of species i in the gas phase, average amount adsorbed and equilibrium parameter for the Langmuir model.

The equilibrium of triple Langmuir-Freundlich isotherm is as follows:

$$\hat{q}_i^*=\frac{\beta_i y_i^{ni}}{1+\sum_{j=1}^{N}\beta_j\cdot y_j^{nj}} \quad (4)$$

where β, n and q_m are as follows:

$$q_{m,i}=k_1+k_2T_0\hat{T} \quad (5)$$

$$\beta_i=k_3\exp\left(\frac{k_4}{T_0\hat{T}}\right) \quad (6)$$

$$n=k_5+\frac{k_6}{T_0\hat{T}} \quad (7)$$

Table 1. Equilibrium parameters and adsorption heat of oxygen, nitrogen and argon on zeolites 5A and 13X

Parameters	Zeolite 5A [21,22]		Zeolite 13X [20]	
	N_2	O_2	N_2	O_2
$k_1\times10^3$ (mol/g)	6.21	7.252	12.52	6.705
$k_2\times10^5$ (mol/g·K)	−1.27	−1.820	−1.785	−1.435
$k_3\times10^4$ (1/atm)	1.986	54.19	2.154	3.253
k_4 (K)	1970	662.6	2333	1428
k_5	2.266	−1.101	1.666	−0.3169
k_6 (K)	−396.5	656.4	−245.2	387.8
Heat of adsorption (cal/mol)	5470	3160	4390	3060
LDF constant (s^{-1})	0.05	0.15	0.197	0.62

Adsorption isotherm parameters and diffusion rate constants of oxygen, nitrogen and argon over zeolites 5A and 13X are presented in Table 1.

Overall dimensionless mass balance for gas phase in the adsorption bed is [12,19,23,28]:

$$\left(\frac{1}{\hat{P}}\right)\cdot\frac{\partial\hat{P}}{\partial\tau}+\frac{\partial\hat{u}}{\partial\hat{z}}+\frac{\hat{u}}{\hat{P}}\cdot\frac{\partial\hat{P}}{\partial\hat{z}}-\left(\frac{1}{\hat{T}}\right)\cdot\left(\frac{\partial\hat{T}}{\partial\tau}+\hat{u}\frac{\partial\hat{T}}{\partial\hat{z}}\right)$$
$$+\left(\frac{\rho_p\cdot R\cdot T_0\cdot\hat{T}}{P_0\cdot\hat{P}}\right)\cdot\left(\frac{1-\varepsilon}{\varepsilon}\right)\cdot\sum_{i=1}^{3}\left(q_{m,i}\cdot\frac{\partial\hat{q}_i}{\partial\tau}+\hat{q}_i\cdot\frac{\partial q_{m,i}}{\partial\tau}\right)=0 \quad (8)$$

Dimensionless energy balance for gas phase in the adsorption bed is [13-15,18,24]:

$$-\left(\frac{1}{P_e^h}\right)\cdot\frac{\partial^2\hat{T}}{\partial\hat{z}^2}+\varepsilon\cdot\left(\hat{u}\frac{\partial T}{\partial z}+\hat{T}\frac{\partial\hat{u}}{\partial\hat{z}}\right)+\left(\varepsilon_t+\frac{\rho_B\cdot c_{p,s}}{\rho_g\cdot c_{p,g}}\right)\cdot\frac{\partial\hat{T}}{\partial\tau}$$
$$-\left(\frac{\rho_B}{T_0\cdot\rho_g\cdot c_{p,g}}\right)\cdot\sum_{i=1}^{3}\left[\left(q_{m,i}\cdot\frac{\partial\hat{q}_i}{\partial\tau}+\hat{q}_i\cdot\frac{\partial q_{m,i}}{\partial\tau}\right)\cdot(-\Delta\overline{H}_i)\right] \quad (9)$$
$$+\left(\frac{2h_i\cdot L}{R_{B,i}\cdot U_0\cdot\rho_g\cdot c_{p,g}}\right)\cdot(\hat{T}-\hat{T}_w)=0$$

Dimensionless energy balance for the wall of adsorption bed is:

$$\frac{\partial\hat{T}_w}{\partial\tau}=\left[\frac{2\pi\cdot R_{B,i}\cdot h_i\cdot L}{\rho_w\cdot c_{p,w}\cdot A_w\cdot U_0}\right]\cdot(\hat{T}-\hat{T}_w)$$
$$-\left[\frac{2\pi\cdot R_{B,o}\cdot h_o\cdot L}{\rho_w\cdot c_{p,w}\cdot A_w\cdot U_0}\right]\cdot\left(\hat{T}_w-\frac{T_{atm}}{T_0}\right) \quad (10)$$

Cross-sectional area of adsorption bed wall is:

$$A_w=\pi\cdot(R_{B,o}^2-R_{B,i}^2) \quad (11)$$

Dimensionless boundary conditions for mass and energy balances are as follows:

Pressurization and adsorption steps:

$$\left(\frac{\partial y_i}{\partial\hat{z}}\right)\Big|_{\hat{z}=0}=-P_e^m\cdot\hat{u}\cdot(y_i|_{\hat{z}=0^-}-y_i|_{\hat{z}=0^+});\ \frac{\partial y_i}{\partial\hat{z}}\Big|_{\hat{z}=1}=0 \quad (12)$$

$$\left(\frac{\partial\hat{T}}{\partial\hat{z}}\right)\Big|_{\hat{z}=0}=-P_e^h\cdot\hat{u}\cdot(\hat{T}|_{\hat{z}=0^-}-\hat{T}|_{\hat{z}=0^+});\ \frac{\partial\hat{T}}{\partial\hat{z}}\Big|_{\hat{z}=1}=0 \quad (13)$$

$y_i|_{z=0^-}$ and $T|_{z=0^-}$ are composition of i^{th} component in the inlet feed and the feed temperature in Eqs. (12) and (13), respectively.

Blow down and equalization to depressurization steps:

$$\frac{\partial y_i}{\partial\hat{z}}\Big|_{\hat{z}=0}=\frac{\partial y_i}{\partial\hat{z}}\Big|_{\hat{z}=1}=0;\ \frac{\partial\hat{T}}{\partial\hat{z}}\Big|_{\hat{z}=0}=\frac{\partial\hat{T}}{\partial\hat{z}}\Big|_{\hat{z}=1}=0 \quad (14)$$

Purge step:

$$\left(\frac{\partial y_i}{\partial\hat{z}}\right)\Big|_{\hat{z}=0}=0;\ \left(\frac{\partial y_i}{\partial\hat{z}}\right)\Big|_{\hat{z}=1}=-P_e^m\cdot\hat{u}\cdot(y_i|_{\hat{z}=1^+}-y_i|_{\hat{z}=1^-}) \quad (15)$$

$$\left(\frac{\partial\hat{T}}{\partial\hat{z}}\right)\Big|_{\hat{z}=0}=0;\ \left(\frac{\partial\hat{T}}{\partial\hat{z}}\right)\Big|_{\hat{z}=1}=-P_e^h\cdot\hat{u}\cdot(\hat{T}|_{\hat{z}=1^+}-\hat{T}|_{\hat{z}=1^-}) \quad (16)$$

where, $y_i|_{z=L^+}$ and $T|_{z=L^+}$ are concentration of the i^{th} component in the product of AD step and the output flow temperature of AD step, respectively.

Equalization to pressurization step:

$$\left(\frac{\partial y_i}{\partial \hat{z}}\right)\Big|_{\hat{z}=0} = -P_e^m \cdot \hat{u} \cdot (y_i|_{\hat{z}=0^-} - y_i|_{\hat{z}=0^+}); \frac{\partial y_i}{\partial \hat{z}}\Big|_{\hat{z}=1} = 0 \quad (17)$$

$$\left(\frac{\partial \hat{T}}{\partial \hat{z}}\right)\Big|_{\hat{z}=0} = -P_e^h \cdot \hat{u} \cdot (\hat{T}|_{\hat{z}=0^-} - \hat{T}|_{\hat{z}=0^+}); \frac{\partial \hat{T}}{\partial \hat{z}}\Big|_{\hat{z}=1} = 0 \quad (18)$$

$y_i|_{z=0^-}$ and $T|_{z=0^-}$ are concentration of i^{th} component in the outlet flow of ED step and the outlet flow temperature of ED step in Eqs. (17) and (18), respectively.

Ergun equation is utilized to investigate the pressure drop across the adsorption bed [16,17].

$$-\frac{d\hat{P}}{d\hat{z}} = [a \cdot \mu \cdot U_0 \cdot \hat{u} + b \cdot \rho \cdot U_0^2 \cdot \hat{u} \cdot |\hat{u}|] \cdot \left(\frac{L}{P_0}\right) \quad (19)$$

$$a = \frac{150}{4R_p^2} \cdot \frac{(1-\varepsilon)^2}{\varepsilon^2}; \; b = 1.75 \frac{(1-\varepsilon)}{2R_p \varepsilon} \quad (20)$$

Moreover, a non-linear equation for variable pressure step is used to study the pressure changes versus dimensionless time [16,17]:

$$\hat{P}(\tau) = A \cdot \tau^2 + B \cdot \tau + C \quad (21)$$

Physical properties of adsorbents and characteristics of adsorption bed are depicted in Tables 2 and 3, respectively.

RESULTS AND DISCUSSION

The fourth-order Runge-Kutta Gill scheme was used to solve a mathematical model considered as coupled partial differential equations. The experimental data obtained from the literature has been simulated to validate the simulation results in this study [17,20,21]. An experimental and simulation study of a PSA unit which is running a traditional Skarstrom cycle and a Skarstrom cycle with co-current equalization owing to separate oxygen from air using a 5A zeolite has been proposed by Mendes et al. in 2001.

Table 2. Physical properties of beds and adsorbents

Characteristic	Zeolite 5A [21,22]	Zeolite 13X [20]
Type	Sphere	Sphere
Average pellet size, R_p (cm)	0.157	0.07
Pellet density, ρ_p (g/cm^3)	1.16	1.17
Heat capacity, C_{ps} (cal/g·K)	0.32	0.32
Bed porosity, ε	0.314	0.391
Bed density, ρ_B (g/cm^3)	0.795	0.713

Table 3. Adsorption bed properties [29]

Length, L (cm)	76
Inside radius, R_{Bi} (cm)	2.138
Outside radius, R_{Bo} (cm)	2.415
Heat capacity of the column, C_{pw} (cal/g·K)	0.12
Density of column, ρ_w (g/cm^3)	7.83
Internal heat-transfer coefficient, h_i (cal/cm^2·K·s)	9.2×10^{-4}
External heat-transfer coefficient, h_o (cal/cm^2·K·s)	3.4×10^{-4}
Axial thermal conductivity, K_L (cal/cm·s·K)	6.2×10^{-5}
Axial dispersion coefficient, D_L (cm^2/s)	1×10^{-5}

The effects of production pressure, purge and product flow rates, and production step duration on the product purity and recovery are investigated for both cycles and compared. Furthermore, a lin-

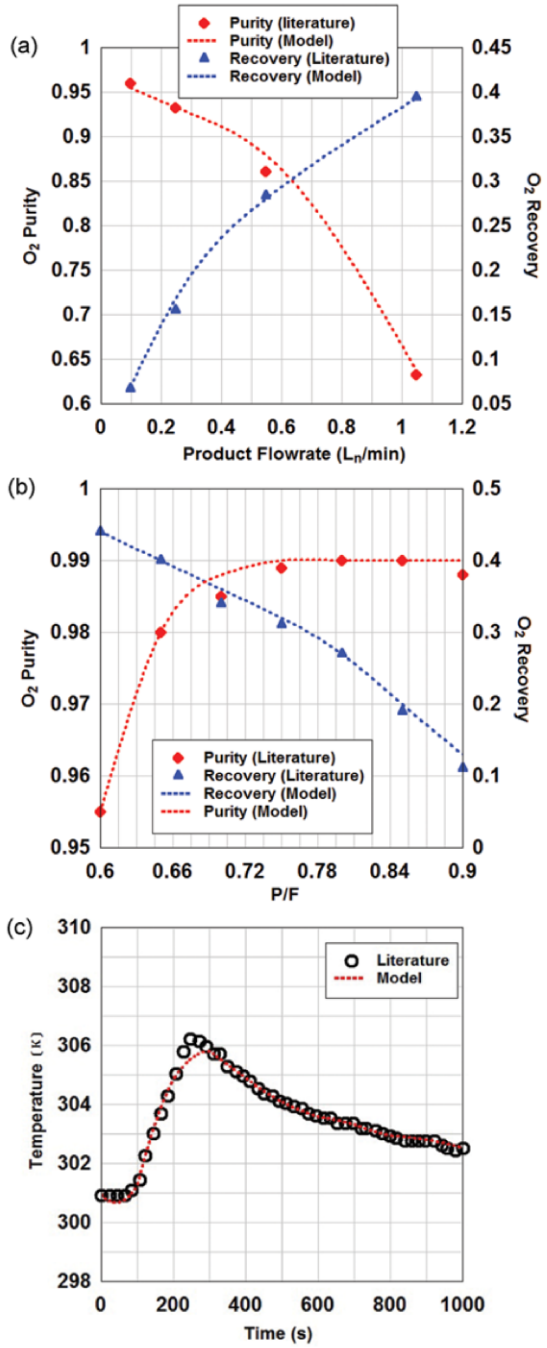

Fig. 2. (a) Numerical simulation of experimental data in this work [17]. (b) Numerical simulation of experimental data in this work [20]. (c) Numerical simulation of experimental data in this work [21].

ear driving force representation of the dusty gas intra particle mass transport is considered in their model [17]. Moreover, a small-scale two-bed six-step PSA process using zeolite 13X was performed by Jee et al. to provide oxygen-enriched air. The effects of different operating parameters such as the P/F ratio, adsorption pressure, feed flow rate, and adsorption step time were investigated experimentally under the nonisothermal condition. They showed that there is a strong effect of feed flow rate on O_2 purity [20]. The effects of adsorption and desorption on zeolite 5A and CMS beds were investigated in a mixture of $N_2/O_2/Ar$ by Jee et al. in 2004. A non-isothermal mathematical model was applied to simulate the adsorption dynamics in their studies [21].

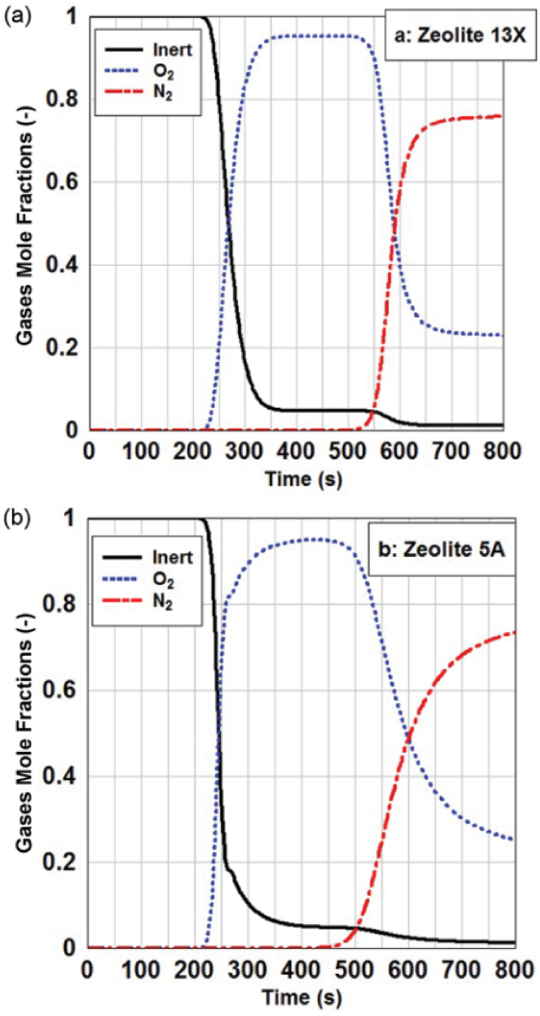

Fig. 3. (a) The simulated breakthrough curves of zeolite 13X for oxygen and nitrogen at adsorption pressure of 6 bar and feed flow rate of 5 LSTP/min. The adsorption bed was initially saturated with a non-adsorptive gas. (b) The simulated breakthrough curves of zeolite 5A for oxygen and nitrogen at adsorption pressure of 6 bar and feed flow rate of 5 LSTP/min. The adsorption bed was initially saturated with a non-adsorptive gas.

Figs. 2(a) and (b) indicate the effect of product flow rate and P/F on the purity and recovery of oxygen during PSA process, respectively. The impact of temperature variations in gas phase during adsorption as a function of time is illustrated in Fig. 2(c). It is obviously seen that there is a relatively high accuracy in the simulation of experimental data [29]. Breakthrough curves for nitrogen and oxygen on both zeolites 13X and 5A are shown in Figs. 3(a) and (b), respectively. The term "break-through time" is originated from the response of initially cleaned bed per a flow with a constant composition. As an initial condition, it is assumed that the adsorption bed is pressurized with a non-adsorptive gas. As shown in Fig. 3(a), oxygen exits from the top of zeolite 13X earlier than nitrogen at a time of approximately 230 seconds [29].

As time is passing, high roll-up phenomenon is observed in the case of oxygen. Owing to high roll-up phenomenon effect, oxygen concentration is approximately 4.5 times more than feed concentration during the time of 400-500 seconds. Occurring high roll-up phenomenon in the case of oxygen is because there is a competitive adsorption between oxygen and nitrogen molecules to be adsorbed on the adsorbent.

This competitive adsorption can be developed according to nitrogen and oxygen properties like polarizability, dipole moment and quadruple moment. The isotropic polarizability is defined as the average of the diagonal terms of the polarizability tensor. Nitrogen and oxygen molecules are symmetrical and thus they are not dipole. Both of these molecules are diatomic molecules. The polarizability of oxygen and nitrogen is 1.562 and 1.710 ($Å^3$), respectively. Furthermore, the bond description of oxygen molecule is double bond (O=O); however, the nitrogen bond description is triple bond (N#N). Moreover, the electric quadruple moment of nitrogen is (xx, yy, zz)=(0.697, 0.697, −1.394). Besides, the molecular diameters of oxygen and nitrogen are 3.8 Å and 4.2 Å, correspondingly [30].

The adsorption kinetics and equilibrium have been investigated in this study. In fact, the adsorption capacity will be greater for more polarity molecules which is consistent with adsorption equilibrium. On the other hand, the rate of adsorption will be greater for molecules with smaller sizes, which is based on the adsorption kinetics.

The superiority of adsorption equilibrium mechanism than adsorption kinetic mechanism in zeolite adsorbents for separation of oxygen and nitrogen has been depicted in the literature [1].

Oxygen is affected by the high roll-up phenomenon because nitrogen adsorption on the adsorbent sites is much more than oxygen adsorption. Therefore, oxygen concentration is relatively increased rather than feed concentration. While time reaches nitrogen breakthrough at the time of 550 seconds, oxygen concentration is starting to be reduced. As clearly shown in Fig. 3(a), the high roll-up phenomenon does not occur in the case of nitrogen due to its strong adsorption on zeolite 13X adsorbent. Fig. 3(b) presents the breakthrough curves in zeolite 5A. According to this figure, although oxygen penetration on zeolite 5A is similar to the one on zeolite 13X, nitrogen penetration occurs at the time of 450 seconds. By comparing Figs. 3(a) and 3(b), the breakthrough curves for zeolite 5A is slightly broader than zeolite 13X. In addition, the

capacity of nitrogen adsorption on zeolite 13X is slightly more than the one on zeolite 5A. Moreover, the high roll-up phenomenon occurs in both zeolites 5A and 13X in the case of oxygen. The adsorption capacity in the adsorption bed depends on the factors such as pressure, temperature, flow rate [9,20]. Actually, the adsorption and desorption cycle of a PSA system operates by pressure increasing and decreasing. Adsorption and desorption phenomenon are inherently exothermic and endothermic, respectively. Therefore, the optimal setting of temperature is very important owing to better performance of adsorption and desorption phenomenon. On the other hand, the adsorption of impurities on the adsorbent bed is a function of retention time on the adsorbent. Consequently, the flow rate factor is necessary for better performance of system.

The concentration of nitrogen on zeolites 13X and 5A in terms of different adsorption pressures and time are presented in Figs. 4(a) and (b), respectively. As pressure increases, the adsorption rate of more strongly adsorbed component increases [9,20]. As it is expected, nitrogen adsorption capacity on zeolites 13X and 5A enhances with pressure increasing. Although nitrogen adsorption capacity is approximately the same on both adsorbents, nitrogen breakthrough on zeolite 13X occurs with a steeper slope rather than zeolite 5A in different adsorption pressures. Furthermore, the effect of increasing the adsorption pressure on zeolite 13X is more effective than the other zeolite and the adsorption capacity increases gradually. Therefore, the rate of nitrogen adsorption on zeolite 13X is more than the one on zeolite 5A due to different kinetic parameters of these two zeolites. It is depicted in Table 1 that the nitrogen LDF coefficient for zeolite 13X is almost four-times more than the one on zeolite 5A. On the other hand, the rate of nitrogen adsorption on zeolite 13X is approximately four-times more than the one on zeolite 5A in the completely same conditions. The difference in the rate of adsorption can be investigated in the different mass transfer zones (MTZs) of these two zeolite beds.

Oxygen concentration along the bed length for zeolites 13X and 5A in different times have been depicted in Figs. 5(a) and (b), respectively. Obviously, the slope of oxygen concentration curves in the case of zeolite 13X is faster than zeolite 5A. On the other hand, there is a larger MTZ for zeolite 5A rather than zeolite 13X in the

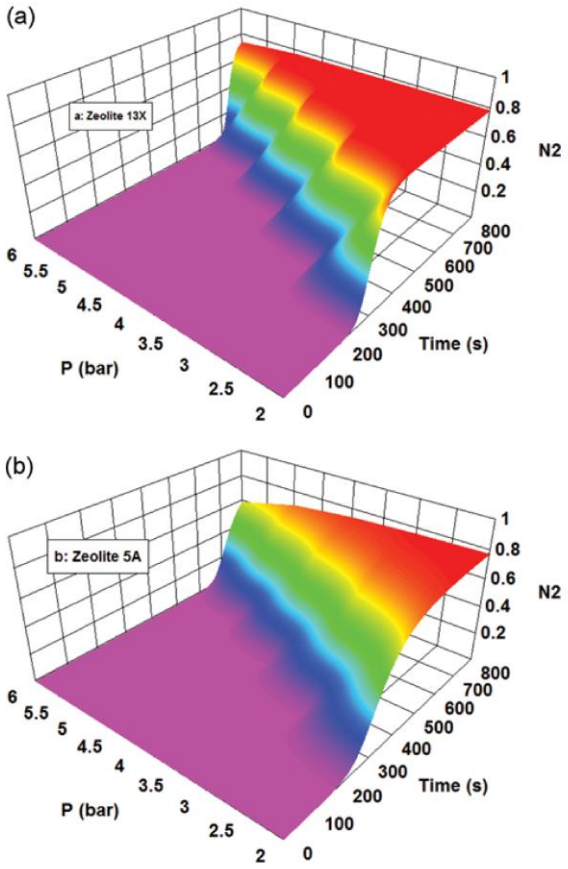

Fig. 4. (a) The outlet mole fraction of nitrogen form zeolite 13X at different adsorption pressures and feed flow rate of 4 LSTP/min. The adsorption bed was initially saturated with a non-adsorptive gas. (b) The outlet mole fraction of nitrogen form zeolite 5A at different adsorption pressures and feed flow rate of 4 LSTP/min. The adsorption bed was initially saturated with a non-adsorptive gas.

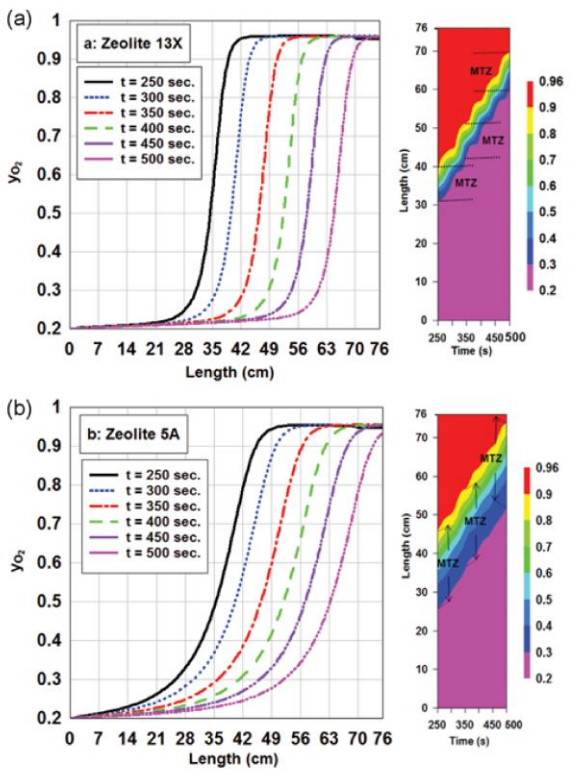

Fig. 5. (a) Distribution of oxygen concentration along the length of zeolite 13X during adsorption process in different times. The feed flow rate is 5 LSTP/min and the adsorption pressure is 6 bar. (b) Distribution of oxygen concentration along the length of zeolite 5A during adsorption process in different times. The feed flow rate is 5 LSTP/min and the adsorption pressure is 6 bar.

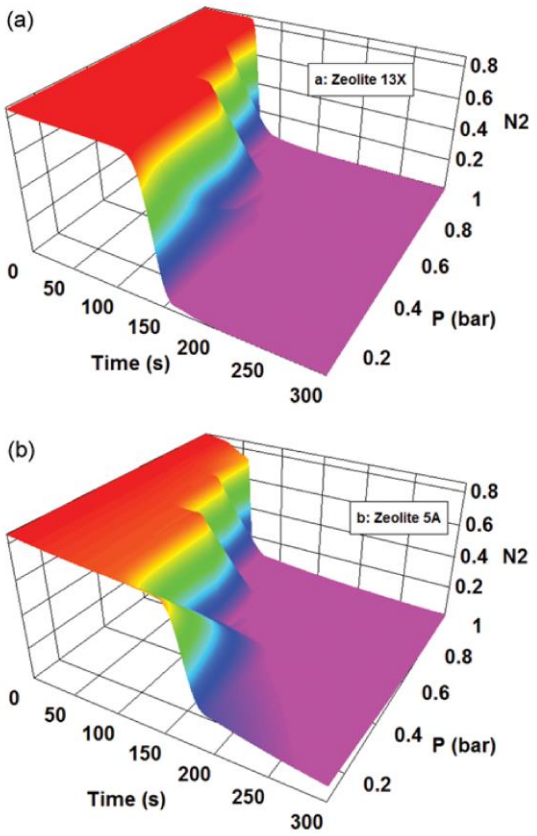

Fig. 6. (a) The outlet simulated concentration of gas phase from zeolite 13X during desorption at pressure of 0.1 bar. The desorption bed was completely clean in the initial state. (b) The outlet simulated concentration of gas phase from zeolite 5A during desorption at pressure of 0.1 bar. The desorption bed was completely clean in the initial state.

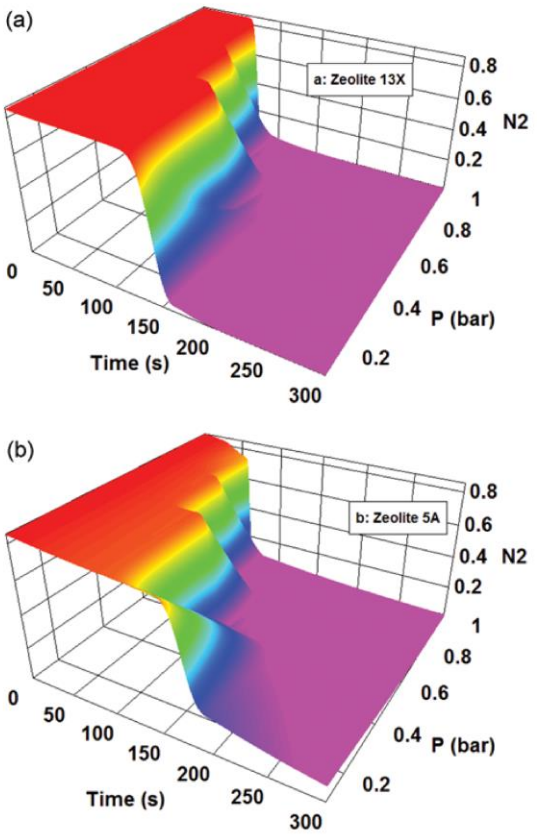

Fig. 7. (a) The outlet concentration of nitrogen from zeolite 13X in the gas phase as a function of desorption pressure and time. Desorption process is applied with a non-adsorptive gas. (b) The outlet concentration of nitrogen from zeolite 5A in the gas phase as a function of desorption pressure and time. Desorption process is applied with a non-adsorptive gas.

completely equal conditions. The bed with smaller MTZ has larger adsorption rate in the completely same conditions [9,20,22]. Moreover, it is considerable to mention that the transfer rate of MTZ is almost equal for both adsorbents.

In the dynamic study of adsorption beds it is considerable to investigate desorption curves. The desorption curves of zeolites 13X and 5A are illustrated in Figs. 6(a) and (b), respectively. To simulate desorption over the beds, it is assumed that a pure inert gas is utilized for cleaning the beds. By passing the inert gas through the bed in a pressure of 0.1 bar, nitrogen with high concentration is first desorbed from top of the bed. As nitrogen is desorbed, a little adsorbed oxygen is removed from the bed with nitrogen. As time passes and the desorbed volume of nitrogen and oxygen gases decreases, the concentration of inert gas in the outlet of bed begins to increase. By comparing Figs. 6(a) and (b), it is considerable to point out:

1. The main drop of nitrogen concentration in the outlet of zeolite 13X occurs at the time of about 125 seconds, while this concentration drop in the outlet of zeolite 5A occurs at the time of about 155 seconds;

2. However nitrogen concentration in the outlet of zeolite 13X approaches zero after about 180 seconds, nitrogen concentration in the outlet of zeolite 5A does not approach zero after approximately 300 seconds and its value is almost 10%.

Besides, according to these figures, nitrogen desorption capacity from zeolite 5A is more than zeolite 13X. On one hand, for the equal volume of adsorbed nitrogen on adsorbents, zeolite 5A is more capable than zeolite 13X owing to desorb much more volume of nitrogen in a certain time. This can be justified in the adsorption and desorption hysteresis loops of zeolites 13X and 5A. On the other hand, in the completely same conditions, the rate of nitrogen desorption from zeolite 13X is more than the one on zeolite 5A owing to smaller MTZ in zeolite 13X rather than zeolite 5A. Similarly to adsorption capacity, the desorption capacity in adsorbent beds depends on some parameters such as pressure, temperature, time, flow rate [9,20], which have been described in details

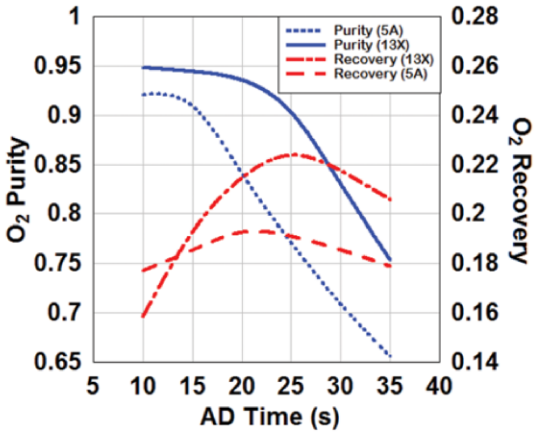

Fig. 8. The simulated purity and recovery of oxygen as a function of adsorption time. The feed flow rate is 20 LSTP/min, adsorption pressure is 6 bar, desorption pressure is 1 bar and the ratio of P/F is 0.1. ED and BD time steps are 5 and 15 seconds, respectively.

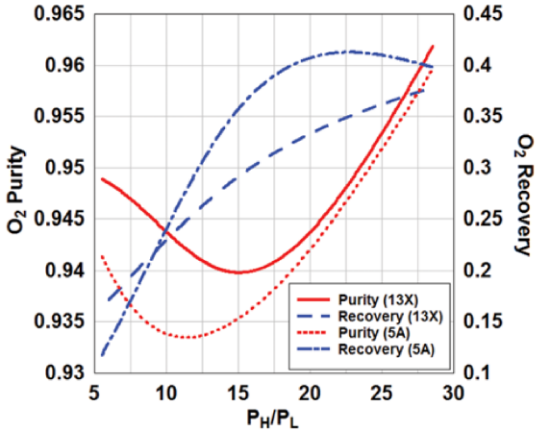

Fig. 9. The simulated purity and recovery of oxygen versus the ratio of operational pressures. The feed flow rate is 2 LSTP/min and the ratio of P/F is 0.1. ED and BD time steps are 5 and 15 seconds, respectively.

above.

Figs. 7(a) and (b) propose nitrogen concentration in the bed outlets for different desorption pressures as a function of time. The desorption amount of more strongly adsorbed component reduces by increasing the pressure [9,20]. As expected, nitrogen desorption capacity from both zeolites 13X and 5A increases by reducing the pressure. Despite the rate of nitrogen desorption from zeolite 13X is more than zeolite 5A, the capacity of nitrogen desorption from zeolite 5A is more than the one on zeolite 13X. As mentioned above, the adsorption capacity and the rate of adsorption are based on molecules with more polarity and molecules with small sizes, respectively. Therefore, there is smaller pore size on zeolite 13X rather than zeolite 5A. In addition the polarity of zeolite 5A is more than zeolite 13X [11]. The importance of this issue can be followed in product recovery and productivity curves.

Fig. 8 shows oxygen purity and recovery as a function of adsorption time for both zeolites. As obvious, there is a light effect on oxygen purity for both adsorbents with increasing the adsorption time at first. Afterwards, the product purity begins to decline with a sharp slope by increasing the time more than 15 and 20 seconds for zeolites 5A and 13X, respectively. The reason for oxygen purity behavior versus the adsorption time is due to breakthrough time. In the PSA process, the adsorption time is determined according to the study on breakthrough curves. In fact, the adsorption time is a required time for occurring breakthrough time. After this time, the product purity decreases while the entire capacity of the bed has not been utilized before this time.

Therefore, the adsorption time must be close to the breakthrough time in order that the best process performance in terms of adsorption time is achieved [31]. The rate of oxygen recovery for both adsorbents increases at first and then it reduces. It is considerable to note that the slope of recovery curve for zeolite 13X is gradually greater than zeolite 5A in incremental zone, while the slope of recovery curve is approximately equal for both zeolites in decreased zone. It is depicted that the performance of a PSA system for oxygen separation from air can work better, where zeolite 13X is utilized under simulated operational conditions. Fig. 9 shows the effect of O_2-PSA system performance versus P_H/P_L for a 60-second cycle. Where $8>P_H/P_L$, the performance of PSA process in terms of oxygen purity and recovery on zeolite 13X is better than zeolite 5A. This result can also validate the curve behavior in Fig. 8. Where $8\leq P_H/P_L\leq 28.5$, the rate of product recovery using zeolite 5A is more than zeolite 13X. Moreover, it is better to apply $25\leq P_H/P_L\leq 28.5$ (VSA system), for both adsorbents, in order to achieve oxygen with high purity and recovery. It occurs because purity and recovery are at their maximum values in Fig. 9. The high value of P_H/P_L ratio for N_2/O_2 system gives the meaning of VSA system. Because pressure higher than 6 bar is not required for oxygen production in a PSA system, which is considered as a zeolite adsorbent system [9]. Due to this fact, when the value of P_H/P_L is high, the desorption pressure is approximately zero which is VSA system. When a VSA system is utilized, the desorption phenomenon is done in vacuum conditions due that the adsorbents are well decontaminated in the desorption step. Therefore, the purity in the adsorption step and recovery will reach their maximum values.

Consequently, the overall results obtained from Fig. 9 are as follows:

1. It is better to apply zeolite 13X in O_2-PSA system to achieve an optimal process performance in terms of product purity and recovery in the range of $5\leq P_H/P_L\leq 8$ in comparison with zeolite 5A.

2. Applying a PSA system in the range of $8\leq P_H/P_L\leq 28.5$ with zeolite 5A operates better than zeolite 13X, when much more oxygen recovery is considered. Note that the performance of mentioned unit will improve by increasing the ratio of P_H/P_L (in Fig. 9, the optimal ratio of P_H/P_L is 22.5).

3. The performance of oxygen separation unit using a VSA system ($25\leq P_H/P_L\leq 28.5$) is almost the same for both zeolites 13X and 5A.

Cycle time is another variable which is effective for the performance of the PSA unit in oxygen separation from air. Figs. 10(a) and (b) show that oxygen purity depends on cycle time in differ-

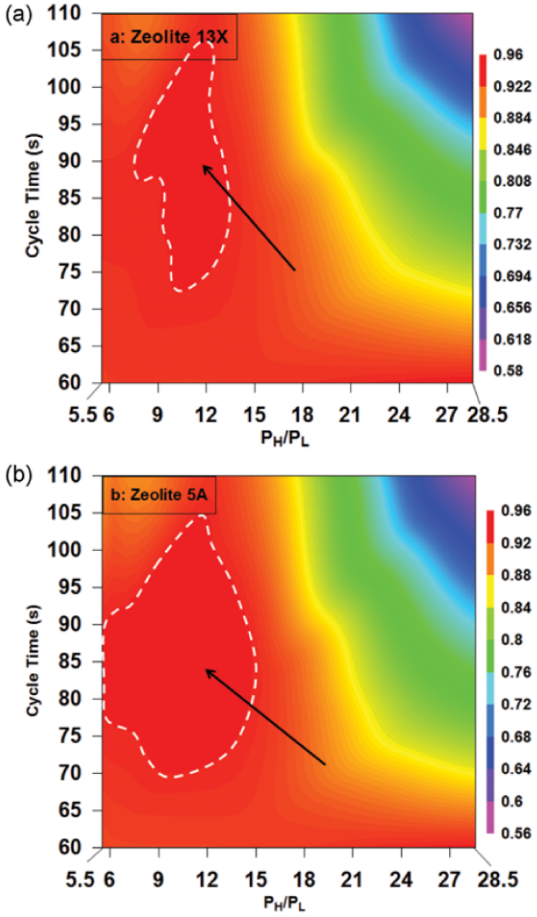

Fig. 10. (a) The distribution of oxygen concentration versus the ratio of operational pressures in different cycle times for zeolite 13X. The product flow rate is 2 LSTP/min and the ratio of P/F is 0.1. (b) The distribution of oxygen concentration versus the ratio of operational pressures in different cycle times for zeolite 5A. The product flow rate is 2 LSTP/min and the ratio of P/F is 0.1.

ent ratios of P_H/P_L for both zeolites 13X and 5A, respectively. The difference in PSA process performance in oxygen separation utilizing zeolites 5A and 13X can be seen by white dashed line in the surrounded area in Figs. 10(a) and (b). Applying higher cycle time and adjusting the ratio of $15>P_H/P_L$ leads to high purity product. According to the definition, the productivity of the PSA unit over the utilized adsorbent is the ratio of received product rate to the used cycle time [20].

On one hand, applying a higher cycle time will increase the unit productivity. On the other hand, increasing the ratio of P_H/P_L will increase the operating costs.

It is suggested that at a low ratio of P_H/P_L and with respect to maintaining high product purity, it is possible to increase the cycle time. According to the white dashed line in the surrounded area in Figs. 10(a) and (b), it is understandable that zeolite 5A is more economical than zeolite 13X when a higher cycle time is applied, because the cycle time can be increased at a low ratio of P_H/P_L. Accordingly, applying zeolite 5A is more economical than zeolite 13X while $5.5<P_H/P_L<7$ and 75<cycle time≤90, in order that oxygen purity of 96% is achieved.

CONCLUSIONS

Two types of zeolites, zeolite 5A and zeolite 13X, were simulated in a laboratory scale of PSA unit in the same operational conditions. Desorption and adsorption dynamics of zeolites 5A and 13X were investigated to study the behavior of these zeolites. Furthermore, the dependency of PSA process performance in terms of product purity and recovery over operational variables such as adsorption time, P_H/P_L and cycle time was compared in this study.

The results obtained from dynamic simulation of beds showed that:

The breakthrough curves for zeolite 5A are broader than zeolite 13X. Moreover, nitrogen adsorption capacity on zeolite 13X is relatively more than the one on zeolite 5A. In addition, the high roll-up phenomenon occurs for both zeolites in the case of oxygen. There is a larger mass transfer zone (MTZ) for zeolite 5A rather than zeolite 13X in the completely same conditions. Therefore, the adsorption rate of zeolite 13X is much more than the one on zeolite 5A. The rate of nitrogen desorption from zeolite 13X is more than zeolite 5A owing to its smaller MTZ. On the other hand, for equal volume of adsorbed nitrogen on the both adsorbents, zeolite 5A is more capable to desorb much more volume of nitrogen rather than zeolite 13X at certain time.

The effect of P_H/P_L on PSA process performance was modeled. The results obtained from this simulation are as follows:

1. Zeolite 13X is more effective than zeolite 5A in the O_2-PSA system. Furthermore, an optimal process performance in terms of product purity and recovery in the range of $5\leq P_H/P_L\leq 8$ is achieved by applying zeolite 13X rather than zeolite 5A.

2. The performance of zeolite 5A in the range of $8\leq P_H/P_L\leq 28.5$ in a PSA system is more effective than zeolite 13X. Note that the performance of a PSA system will improve via increasing the ratio of P_H/P_L.

3. It is shown that in a VSA system ($25\leq P_H/P_L\leq 28.5$), the performance of oxygen separation unit is approximately identical by applying both zeolites 5A and 13X.

Furthermore, simulation results of the cycle time effects showed that:

Applying zeolite 5A is more economical than zeolite 13X in order to achieve oxygen with purity of 0.96, when $5.5<P_H/P_L<7$ and 75<cycle time≤90.

ACKNOWLEDGEMENT

The authors gratefully acknowledge BIDBOLAND refinery plant is in agreement with this research.

NOMENCLATURE

A_w : cross-sectional area of the wall [cm^2]

AD : adsorption step
BD : blow down step
Cp_g, C_{ps}, C_{pw} : gas, pellet, and wall heat capacities, respectively [cal/g·K]
D_L : axial dispersion coefficient [cm^2/s]
G : purge to feed ratio [kg_{feed}/kg_{purge}]
hi : internal heat-transfer coefficient [$cal/cm^2 \cdot K \cdot s$]
ho : external heat-transfer coefficient [$cal/cm^2 \cdot K \cdot s$]
$\Delta\overline{H}$: average heat of adsorption [cal/mol]
k_1 : parameter for the LDF model [mol/g]
k_2 : parameter for the LDF model [mol/g·K]
k_3 : parameter for the LDF model [1/atm]
k_4 : parameter for the LDF model [K]
k_5 : parameter for the LDF model [-]
k_6 : parameter for the LDF model [K]
K_L : axial thermal conductivity [cal/cm·s·K]
L : bed length [cm]
P : total pressure [atm]
$\overline{P}$: dimensionless pressure [P/P_0]
P_e^h : heat peclet number [$u_0 \cdot L \cdot \rho_g \cdot c_{p,g}/K_L$]
P_e^m : mass peclet number [$u_0 \cdot L/D_L$]
P_r : reduced pressure, dimensionless
PG : purge step
PR : pressurization step
P/F : ratio of purge flow rate to feed flow rate
P_H/P_L : ratio of operating pressures
q, q*, $\hat{q}$: amount adsorbed, equilibrium amount adsorbed, and average amount adsorbed, respectively [mol/g]
q_m : equilibrium parameter for the Langmuir model [mol/g]
R : gas constant [cal/mol·K]
R_p : radius of the pellet [cm]
R_{Bi}, R_{Bo} : inside and outside radial of the bed, respectively [cm]
T : temperature [K]
$\overline{T}$ dimensionless temperature [T/T_0]
T_{atm} : temperature of the atmosphere [K]
T, T_w : pellet or bed temperature and wall temperature, respectively [K]
t : time [s]
τ : dimensionless time [t^*u_0/L]
u : interstitial velocity [cm/s]
$\overline{u}$: dimensionless velocity [u/u_0]
y_i : mole fraction of species i in the gas phase
z : axial distance in the bed from the inlet [cm]
$\overline{z}$: dimensionless length

Greek Letters

α : particle porosity
β : equilibrium parameter for the Langmuir model in the form of dimensionless
ε, ε_t : voidage of the adsorbent bed and total void fraction, respectively
ρ_g, ρ_p, ρ_B, ρ_w : gas density, pellet density, bulk density, and bed wall density, respectively [g/cm^3]

Subscripts

B : bed
H : higher operating pressure
i : component i
L : lower operating pressure
p : pellet
g : gas phase
s : solid
w : wall

REFERENCES

1. C. A. Grande, Advances in Pressure Swing Adsorption for Gas Separation, ISRN Chemical Engineering, Article ID 982934, **2012**, 13 (2012), DOI:10.5402/2012/982934.
2. M. Rosen, L. Mulloth, D. Affleck and Y. Wang, Development and Testing of a Temperature-Swing Adsorption Compressor for Carbon Dioxide in Closed-Loop Air Revitalization Systems, SAE Technical Paper 2005-01-2941 (2005), DOI:10.4271/2005-01-2941.
3. R. M. Milton, Molecular Sieve Adsorbents, US Patent, 2,882,243 (1959).
4. A. Mivechian and M. Pakizeh, *Korean J. Chem. Eng.*, **30**(4), 937 (2013).
5. S.-C. Jang, S.-I. Yang, S.-G. Oh and D.-K. Choi, *Korean J. Chem. Eng.*, **28**(2), 583 (2011).
6. Y. H. Kim, D. G. Lee, D. K. Moon, S.-H. Byeon, H. Ahn and C. H. Lee, *Korean J. Chem. Eng.*, **31**(1), 132 (2014), Available from: 10.1007/s11814-013-0201-x.
7. M. Zaman and J. H. Lee, *Korean J. Chem. Eng.*, **30**(8), 1497 (2013).
8. V. Hoshyargar, F. Fadaei and S. N. Ashrafizadeh, *Korean J. Chem. Eng.*, **32**(7), 1388 (2015).
9. D. M. Ruthven, S. Farooq and K. S. Knaebel, *Pressure Swing Adsorption*, New York, VCH Publications, Inc. (1994).
10. R. T. Yang, *Adsorbents: Fundamentals and Applications*, New Jersey, Wiley (2003).
11. D. M. Ruthven, *Principle of Adsorption and Adsorption Processes*, New York, Wiley (1984).
12. C. Chou and W.-C. Huang, *Ind. Eng. Chem. Res.*, **33**(5), 1250 (1994).
13. L. Lin, *Numerical Simulation of Pressure Swing Adsorption Process*, Dissertation Presented for the Degree of Bachelor of Science, XIDIAN University, Xi'an, China (1990).
14. J. A. Ritter and Y. Liu, *Ind. Eng. Chem. Res.*, **37**, 2783 (1998).
15. K. G. Teague, Jr. and T. F. Edgar, *Ind. Eng. Chem. Res.*, **38**, 3761 (1999).
16. A. M. M. Mendes, C. A. V. Costa and A. E. Rodrigues, *Ind. Eng. Chem. Res.*, **39**, 138 (2000).
17. A. M. M. Mendes, C. A. V. Costa and A. E. Rodrigues, *Sep. Purif. Technol.*, **24**, 173 (2001).
18. S. J. Wilson, C. C. K. Beh, P. A. Webley and R. S. Todd, *Ind. Eng. Chem. Res.*, **40**, 2702 (2001).
19. S. U. Rege, R. T. Yang, K. Qian and M. A. Buzanowski, *Chem. Eng. Sci.*, **56**, 2745 (2001).
20. J. G. Jee, J. S. Lee and C. H. Lee, *Ind. Eng. Chem. Res.*, **40**, 3647 (2001).
21. J. G. Jee, S. J. Lee and C. H. Lee, *Korean J. Chem. Eng.*, **21**, 1183 (2004).
22. J. G. Jee, H. G. Park, S. J. Haam and C. H. Lee, *Ind. Eng. Chem. Res.*, **41**, 4383 (2002).

23. S. T. Y. Choong, W. R. Paterson and D. M. Scott, *Jurnal Teknologi*, **38**, 65 (2003).
24. J. C. Santos, A. F. Portugal, F. D. Magalhaes and A. Mendes, *Ind. Eng. Chem. Res.*, **43**, 8328 (2004).
25. S. P. Reynolds, A. D. Ebner and J. A. Ritter, *Ind. Eng. Chem. Res.*, **45**, 3256 (2006).
26. K. P. Kostroski and P. C. Wankat, *Ind. Eng. Chem. Res.*, **45**, 8117 (2006).
27. J.-G. Jee, M.-K. Park, H.-K. Yoo, K. Lee and C.-H. Lee, *Sep. Sci. Technol.*, **37**(5), 3465 (2002).
28. S. J. Lee, J. H. Jung, J. H. Moon, J. G. Jee and C. H. Lee, *Ind. Eng. Chem. Res.*, **46**, 3720 (2007).
29. M. Mofarahi and J. S. Ehsan, *Petroleum Coal*, **55**(3), 216 (2013).
30. T. N. Olney, N. M. Cann, G. Cooper and C. E. Brion, *Chem. Phys.*, **223**(1), 59 (1997).
31. S. Jain, A. S. Moharir, P. Li and G. Wozny, *Sep. Purif. Technol.*, **33**, 25 (2003).

Applied Chemical Engineering (2018) Volume 2
doi: 10.63019/ace.v1i2.568

Simulation study of pressure swing adsorption to purify helium using zeolite 13X

Ehsan Javadi Shokroo[1,2], Mehdi Farniaei[1], Mehdi Baghbani[1]

[1] *FAPKCO Engineering Group, Elite Foundation for Southern Zone, Shiraz, Iran*

[2] *Faculty of Engineering, Selinus University of Sciences and Literature, 40138 Bologna BO, Italy*

ABSTRACT

A two-bed pressure swing adsorption system on a commercial type of zeolite 13X adsorbent has been studied numerically over a wide range of operating conditions to helium separation from gaseous mixture. The model includes energy, mass and momentum balances. The coupled partial differential equations are solved using fully implicit forth order Rung-Kutta scheme in the simulation. The effects of adsorption step pressure, adsorption step time and feed flow rate on the helium purity and recovery were investigated. Results shown that as the adsorption step pressure increases the helium purity will be increased. In addition, the helium recovery increases, and the helium purity decreases when the feed flow rate increases. Finally, the simulation results indicated a very good agreement with some current literature experimentally work.

Keywords: *Pressure swing adsorption; helium recovery; mathematical modeling; numerical simulation; zeolite 13X*

1. Introduction

Helium is a chemical element with symbol He and atomic number 2. It is a colorless, odorless, tasteless, non-toxic, inert, monatomic gas, the first in the noble gas group in the periodic table. The He boiling and melting points are the lowest among all the elements.

Helium is the second lightest element and is the second most abundant element in the observable universe, being present at about 24% of the total elemental mass, which is more than 12 times the mass of all the heavier elements combined. Helium was first detected as an unknown yellow spectral line signature in sunlight during a solar eclipse in 1868 by French astronomer Jules Janssen. In 1903, large reserves of helium were found in natural gas fields in parts of the United States, which is by far the largest supplier of the gas today.

Liquid helium is used in cryogenics (its largest single use, absorbing about a quarter of production), particularly in the cooling of superconducting magnets, with the main commercial application being in MRI scanners. Helium's other industrial uses-as a pressurizing and purge gas, as a protective atmosphere for arc welding and in processes such as growing crystals to make silicon wafers-account for half of the gas produced. A well-known but minor use is as a lifting gas in balloons and airships[4]. On Earth it is relatively rare 5.2 ppm by volume in the atmosphere.

Pressure swing adsorption (PSA) process is a wide operating unit to separation and purification of gases that operates based on capability of solids adsorption and selective separation of gases. The important operational parameter in this system is the pressure, and most industrial units operate at\or vicinity of the surrounding temperature. Today, the PSA process completely is known in a wide region of the processes, and this process was preferred in contrast to other conventional separation methods especially, for lower capacity and higher purity.

Linde Group developed the world's first air separation plant for the production of oxygen in 1902 and the first production facility was set up as early as 1903. Since then it is one of the world's largest helium supplier and since 1994 Linde has been the sole provider of helium and helium separators by the method of swing adsorption. Bhushan[1] purified helium by gas adsorption method in 2011 .The purifier was designed to purify up to 40% impurity to give 4.5

doi: 10.63019/ace.v1i2.568

grade or 99.995% pure helium by high pressure and low temperature cryosorption process. Activated carbons have been used for a long time at low temperature for cryogenic applications. The pore geometry and size can be used to optimize the carbon structure for a specific application. In 1978, Stoll *et al.*[2]commissioned a fully automatic large capacity helium purifier which included operation, regeneration, re-cooling and re-pressurization time. In 2007, E. vancleve *et al.*[3] developed a cryogenic pulsed laser deposition (PLD) system to deposit lithium films onto a quartz crystal microbalance (QCM) and Adsorption isotherms of 4He on lithium were measured. PLD system was used to form lithium substrates and the first helium adsorption measurements on this surface were reported. In 2008, Nisith Kr. Das[4] employed a technique known as Pressure swing adsorption to concentrate a lean amount of helium present in natural gas through selective physical elimination of N_2,CO_2, CH_4 and heavier hydrocarbons in a stepwise cycle sequence at present time intervals. In 2011, D. Martins *et al.*[5]reported on the low temperature adsorption properties of He, H2, and N2, using three activated carbons with different pore size distributions. In 2012, R. Majidia *et al.* [6]used the molecular dynamics simulation to study the helium adsorption on the CNCs with declination angle of 240° and300°. The results indicated that the adsorption capacity of the CNCs became considerable by decreasing the declination angle. In the same year, Nisith Kr. Das *et al.*[7]developed helium purification system using a three-bed seven-step pressure swing adsorption (PSA). It removed impurities like N_2 and O_2 from a ternary mixture leaving out high-purity helium from the gas mixture. The PSA system operated successfully resulting in high-purity helium (>99.9%) with a yield of around 89%. The adsorption capability of carbon dioxide on 5A molecular sieve (5AMS) was investigated in a fixed-bed apparatus with two-road gas mixing system by dynamic column breakthrough method with helium as the carrier gas for helium purification system of high-temperature gas-cooled reactor (HTGR) in 2013 by Chang Hua *et al.*[8].

In 2014, Bartolomei *et al.*[9]performed quantum dynamical simulations on reliable new force fields in order to assess the graphdiyne capability for helium chemical and isotopic separation.

In this work, a semi-industrial PSA unit for helium recovery from gaseous mixture was simulated. In this process the effect of some operating variables such as adsorption time, feed flow rate, and adsorption pressure on process performance was investigated. The simulated PSA process is a six-step process with the following sequence (Fig.1): (I) co-current feed pressurization (PR); (II) high-pressure adsorption (AD) step; (III) counter-current depressurizing pressure equalization (ED) step; (IV) counter-current blow down (BD) step; (V) counter-current purge with a light product (PG) step; (VI) co-current pressurizing pressure equalization (EP) step. The sequence time table of the PSA process was also depicted in Table 1.

No.	1	2	3	4	5	6
Time(sec.)	25	60	10	25	60	10
Column 1	PR	AD	ED	BD	PG	EP
Column 2	BD	PG	EP	PR	AD	ED
SV1	on	on	off	on	on	off
SV2	off	off	on	off	off	off
SV3	off	off	off	off	off	on
SV4	on	on	off	on	on	off
SV5	on	on	off	on	on	off
SV6	on	on	off	on	on	off

2

SV7	off	off	off	off	on	off
SV8	off	on	off	off	off	off
SV9	off	off	off	off	on	off
SV10	off	on	off	off	off	off
SV11	off	on	off	off	on	off
SV12	off	on	off	off	off	off
SV13	off	off	off	on	on	off

Table 1. Step sequence of the PSA process.

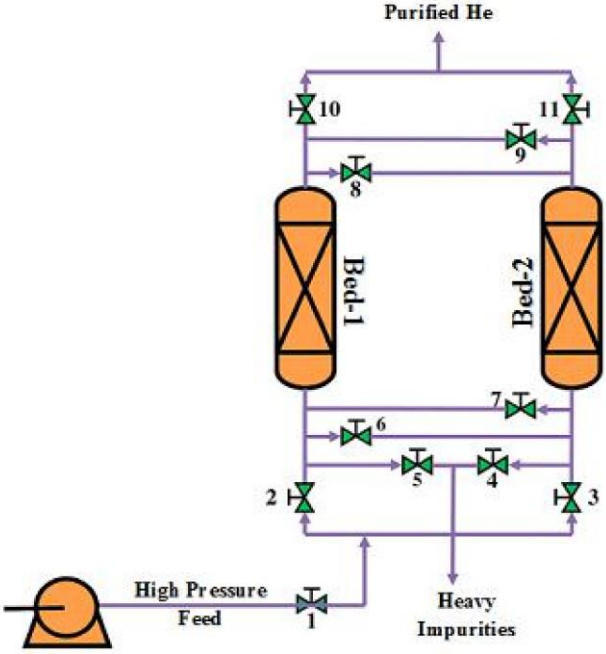

Figure 1. Schematic diagram of He-PSA.

2. Mathematical model

In order to develop a mathematical model for an adsorption bed, the following assumptions were made:

1- Gas behaves as an ideal gas;

2- The flow pattern is axially assumed as plug-flow model;

3- Equilibrium equations for air are expressed as multi-component Langmuir-Freundlich isotherm;

4- Rate of mass transfer is presented by linear driving force (LDF) relations;

5- Bed is clean at initial state and there is no gas flow in it;

According to these assumptions, dynamic behavior of system in terms of mass, energy and momentum balances can be expressed as follows:

Dimensionless partial mass balance for gas phase in the adsorption bed is [9,20,25,26]:

$$-\left(\frac{1}{P_e^{\,m}}\right).\frac{\partial^2 y_i}{\partial \hat{z}^2}+y_i.\frac{\partial \hat{u}}{\partial \hat{z}}+\hat{u}.\left(\frac{\partial y_i}{\partial \hat{z}}+y_i.\left(\frac{1}{\hat{P}}.\frac{\partial \hat{P}}{\partial \hat{z}}-\frac{1}{\hat{T}}.\frac{\partial \hat{T}}{\partial \hat{z}}\right)\right)+\frac{\partial y_i}{\partial \tau}+$$
$$y_i.\left(\frac{1}{\hat{P}}.\frac{\partial \hat{P}}{\partial \tau}-\frac{1}{\hat{T}}.\frac{\partial \hat{T}}{\partial \tau}\right)+\left(\frac{\rho_p.R.T_0.\hat{T}}{P_0.\hat{P}}\right).\left(\frac{1-\varepsilon}{\varepsilon}\right).\left(q_{m,i}.\frac{\partial \hat{q}_i}{\partial \tau}+\hat{q}_i.\frac{\partial q_{m,i}}{\partial \tau}\right) \quad (1)$$

Dimensionless equilibrium loading of ith component for solid phase in the adsorption bed is:

$$\frac{\partial q_{m,i}}{\partial \tau}=\frac{\partial q_{m,i}}{\partial \hat{T}}\times\frac{\partial \hat{T}}{\partial \tau}=k_{2,i}T_0\times\frac{\partial \hat{T}}{\partial \tau} \quad (2)$$

Dimensionless loading of ith component for solid phase in the adsorption bed is (LDF relation):

$$\frac{\partial \hat{q}_i}{\partial \tau}=\alpha_i.\left(\frac{\beta_i.y_i^{\,ni}}{1+\sum_{j=1}^{N}\beta_j.y_j^{\,nj}}-\hat{q}_i\right)-\left(\frac{\hat{q}_i}{q_{m,i}}.\frac{\partial q_{m,i}}{\partial \tau}\right) \quad (3)$$

According to equation (3), the LDF relation depends on various parameters such as: equilibrium parameter for the Langmuir model, mole fraction of species i in the gas phase, average amount adsorbed and equilibrium parameter for the Langmuir model.

The equilibrium of triple Langmuir-Freundlich isotherm is as follows:

$$\hat{q}_i^{*}=\frac{\beta_i y_i^{ni}}{1+\sum_{j=1}^{N}\beta_j.y_j^{nj}} \quad (4)$$

Where β, n and q_m are as follows:

$$q_{m,i}=k_1+k_2T_0\hat{T} \quad (5)$$

$$\beta_i=k_3\exp\left(\frac{k_4}{T_0\hat{T}}\right) \quad (6)$$

$$n=k_5+\frac{k_6}{T_0\hat{T}} \quad (7)$$

Overall dimensionless mass balance for gas phase in the adsorption bed is[12,19,23,28]:

$$\left(\frac{1}{\hat{P}}\right).\frac{\partial \hat{P}}{\partial \tau}+\frac{\partial \hat{u}}{\partial \hat{z}}+\frac{\hat{u}}{\hat{P}}.\frac{\partial \hat{P}}{\partial \hat{z}}-\left(\frac{1}{\hat{T}}\right).\left(\frac{\partial \hat{T}}{\partial \tau}+\hat{u}\frac{\partial \hat{T}}{\partial \hat{z}}\right)+\left(\frac{\rho_p.R.T_0.\hat{T}}{P_0.\hat{P}}\right).\left(1-\right.$$
$$\left.\sum_{i=1}^{3}\left(q_{m,i}.\frac{\partial \hat{q}_i}{\partial \tau}+\hat{q}_i.\frac{\partial q_{m,i}}{\partial \tau}\right)=0\right. \quad (8)$$

Dimensionless energy balance for gas phase in the adsorption bed is[13-15,18,24]:

$$-\left(\frac{1}{P_e^{\,h}}\right).\frac{\partial^2 \hat{T}}{\partial \hat{z}^2}+\varepsilon.\left(\hat{u}\frac{\partial T}{\partial \hat{z}}+\hat{T}\frac{\partial \hat{u}}{\partial \hat{z}}\right)+\left(\varepsilon_t+\frac{\rho_B c_{p,s}}{\rho_g c_{p\,g}}\right).\frac{\partial \hat{T}}{\partial \tau}-\left(\frac{\rho_B}{T_0.\rho_g c_{p\,g}}\right.$$
$$\left.\sum_{i=1}^{3}\left[\left(q_{m,i}.\frac{\partial \hat{q}_i}{\partial \tau}+\hat{q}_i.\frac{\partial q_{m,i}}{\partial \tau}\right).\left(-\Delta\bar{H}_i\right)\right]+\left(\frac{2h_i L}{R_{B,i}U_0\rho_g c_{p,g}}\right).\left(\hat{T}-T_w^{\,\wedge}\right)=\right. \quad (9)$$

Dimensionless energy balance for the wall of adsorption bed is:

$$\frac{\partial \widehat{T}_w}{\partial \tau} = \left[\frac{2\pi.R_{B,i}.h_i.L}{\rho_w.c_{p,w}.A_w.U_0}\right].\left(\widehat{T} - \widehat{T}_w\right) - \left[\frac{2\pi.R_{B,o}.h_o.L}{\rho_w.c_{p,w}.A_w.U_0}\right].\left(\widehat{T}_w - \frac{T_{atm}}{T_0}\right) \quad (10)$$

Cross-sectional area of adsorption bed wall is:

$$A_w = \pi.\left(R_{B,o}^2 - R_{B,i}^2\right) \quad (11)$$

Ergun equation is utilized in order to investigate the pressure drop across the adsorption bed[16,17].

$$-\frac{d\widehat{P}}{d\widehat{z}} = \left[a.\mu U_0 \widehat{u} + b.\rho U_0^2 \widehat{u}.|\widehat{u}|\right].\left(\frac{L}{P_0}\right) \quad (12)$$

$$a = \frac{150}{4R_p^2}.\frac{(1-\varepsilon)^2}{\varepsilon^2}; b = 1.75\frac{(1-\varepsilon)}{2R_p\varepsilon} \quad (13)$$

Zeolite 13X	Physical properties of adsorbents and characteristics of adsorption bed are depicted in Tables 2 and 3, respectively.
	Characteristic
Sphere	Type
0.07	Average pellet size, R_P (cm)
1.17	Pellet density, ρ_p (g/cm^3)
0.32	Heat capacity, C_{ps} (cal/g.K)
0.391	Bed porosity, ε
0.713	Bed density, ρ_B (g/cm^3)

Table 2. Physical properties of bed and adsorbent [20].

Characteristic	Zeolite 13X
Length, L (cm)	76
Inside radius, R_{Bi} (cm)	2.138
Outside radius, R_{Bo} (cm)	2.415
Heat capacity of the column, C_{pw} (cal/g.K)	0.12
Density of column, ρ_w (g/cm^3)	7.83
Internal heat-transfer coefficient, h_i (cal/cm^2.K.s)	**9.2×10^{-4}**
External heat-transfer coefficient, h_o (cal/ cm^2.K.s)	**3.4×10^{-4}**
Axial thermal conductivity, K_L (cal/cm.s.K)	**6.2×10^{-5}**
Axial dispersion coefficient, D_L (cm^2/s)	1×10^{-5}

Table 3. Adsorption bed properties[29].

3. Results and discussion

The fourth order Runge-Kutta Gill scheme was used to solve a mathematical model considered as coupled partial differential equations. The experimental data obtained from literatures has been simulated in order to validate the simulation results in this study[17,20,21]. An experimental and simulation study of a PSA unit which is running a traditional Skarstrom cycle and a Skarstrom cycle with co-current equalization owing to separate oxygen from air using a 5A zeolite has been proposed by Mendes *et al*. in 2001. Moreover, a small-scale two-bed six-step PSA process using zeolite 13X was performed by Jee *et al*. in order to provide oxygen-enriched air. They showed that there is a strong effect of feed flow rate on O_2 purity [20]. The effects of adsorption and desorption on zeolite 5A and CMS beds were investigated in a mixture of N_2/O_2/Ar by Jee *et al*. in 2004. A non-isothermal mathematical model was applied in order to simulate the adsorption dynamics in their studies[21].

Figures 2(a) and (b) indicate the effect of product flow rate and P/F on the purity and recovery of oxygen during PSA process, respectively. The impact of temperature variations in gas phase during adsorption as a function of time is illustrated in **Figure 2**(c). It is obviously seen that there is a relatively high accuracy in the simulation of experimental data [29].

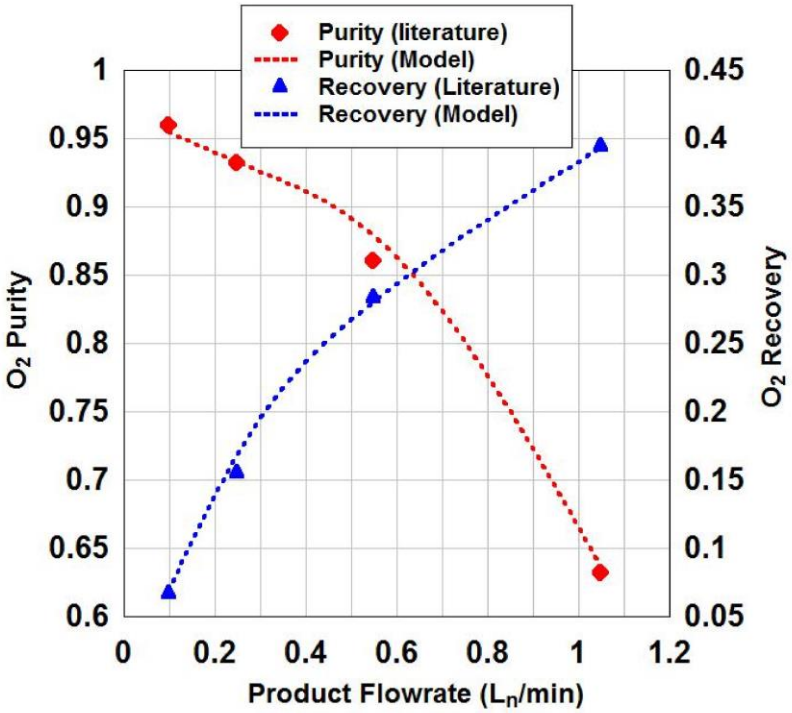

Figure 2a. Numerical simulation of experimental data in this work [17].

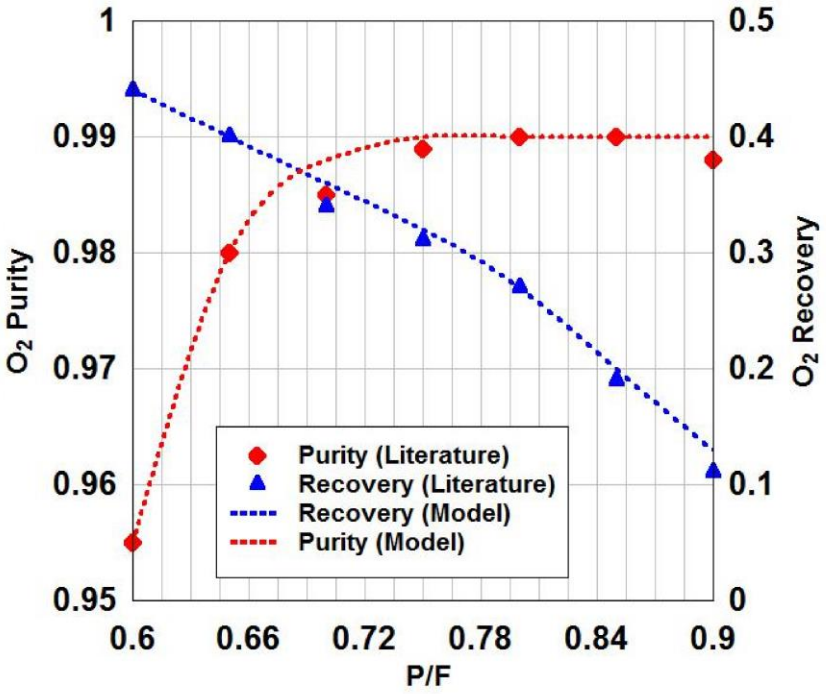

Figure 2b. Numerical simulation of experimental data in this work[20].

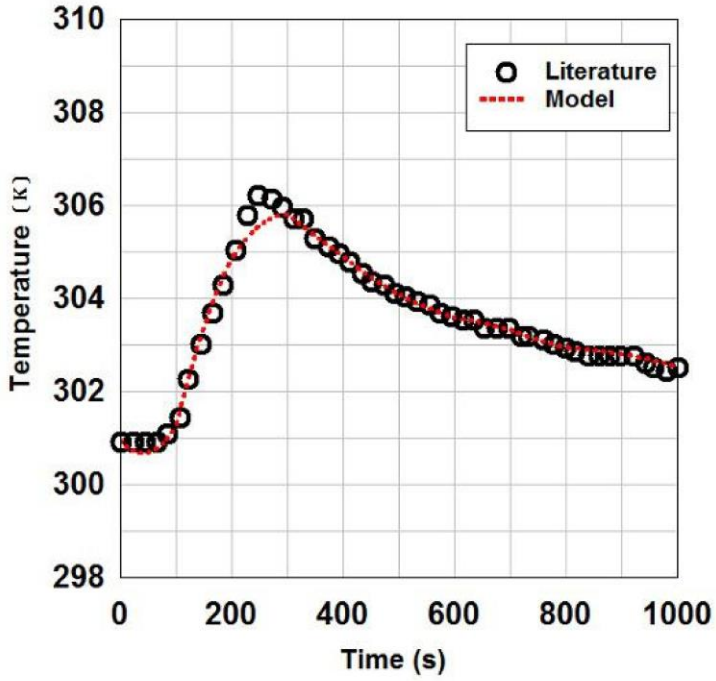

Figure 2c. Numerical simulation of experimental data in this work[21].

Figure 3 shows the effects of feed flow rate on helium purity and recovery at adsorption pressure of 8.5 bar and adsorption time of 20 sec. In this figure it can be seen that the increase in feed leads to a decrease in the helium purity while helium recovery has increased. The feed flow will rise at a constant purge flow in these simulations, which the P/F decreases and subsequently helium purity decreases. At a certain purge flow rate when the feed amount increases therefore, the P/F ratio is reduced and finally, the product purity decreases. In the other word, dead space of the bed in the adsorption step will rise with the feed flow rate. Thus, purging the bed in the purge step requires more purgative flow. In these simulations, a constant purge flow rate causes a reduction in the helium purity with the feed flow rate.

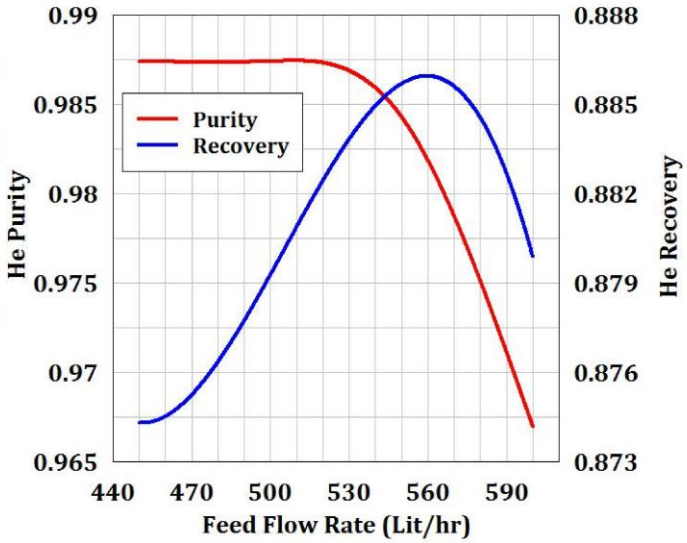

Figure 3. Helium purity and recovery variations versus feed flow rate.

The variations of helium purity and recovery in terms of adsorption step time at pressure of 5.5 bar and P/F of 0.1

are shown in figure 4. It is clear from this figure that increase of adsorption time leads to reduction in helium purity. It is due to the well-known breakthrough time of the adsorption beds Thus, the adsorption time should be near to the breakthrough time in order to achieve the maximum process performance in terms of adsorption time. In fact, the adsorption time is a required time for occurring breakthrough time. After this time, the product purity is decreased while the entire capacity of the bed has not utilized before this time. Therefore, the adsorption time must be close to the breakthrough time in order that the best process performance in terms of adsorption time is achieved [20]. With referring to this figure, the best time for adsorption is 25 sec. Furthermore it should be noted that, the helium recovery is in reverse order with its purity at all points. It was evident that the recovery reduces as the gas volume of the feed increases through increasing the adsorption time. Fig. 5 shows the effect of adsorption step pressure on the process performance. It is apparent from this figure that the higher adsorption pressure improves the PSA unit performance. As the adsorption pressure increases, the amount of adsorbed heavy species on the adsorbent will be increased and therefore, the helium purity increases. For the favorable isotherm systems, if the pressure is increased the highly adsorbed species are more adsorbed and the product purity will be increased. This result was seen in the literature [20-28]. Helium concentration profile curves are depicted in figure 6. It is obvious from this figure that the helium purity has a minimum and maximum quantity in the blow down step because of depressurized bed and the pressurization step as result of the cleansed bed, respectively.

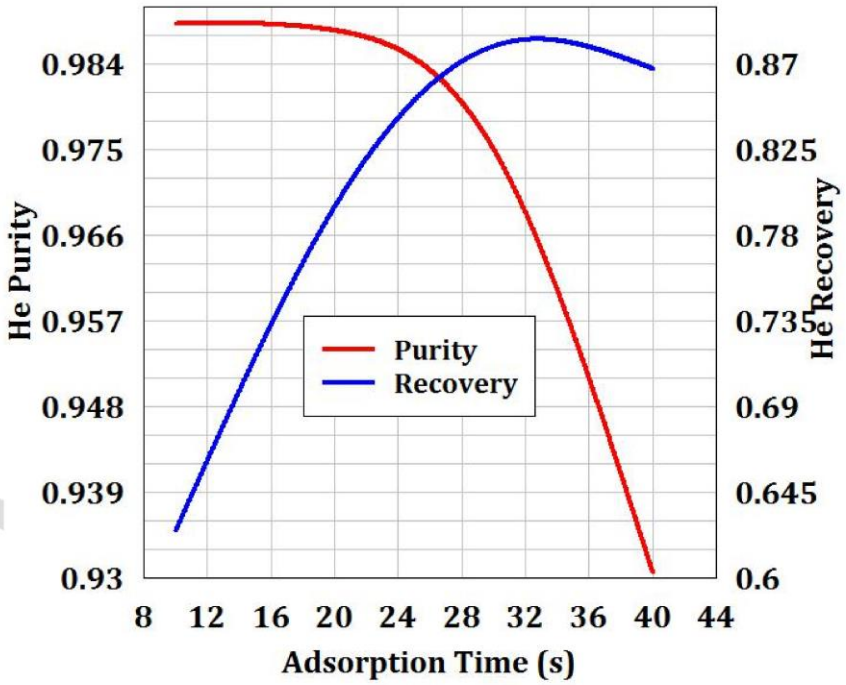

Figure 4. Variations of helium purity and recovery in terms of adsorption step time.

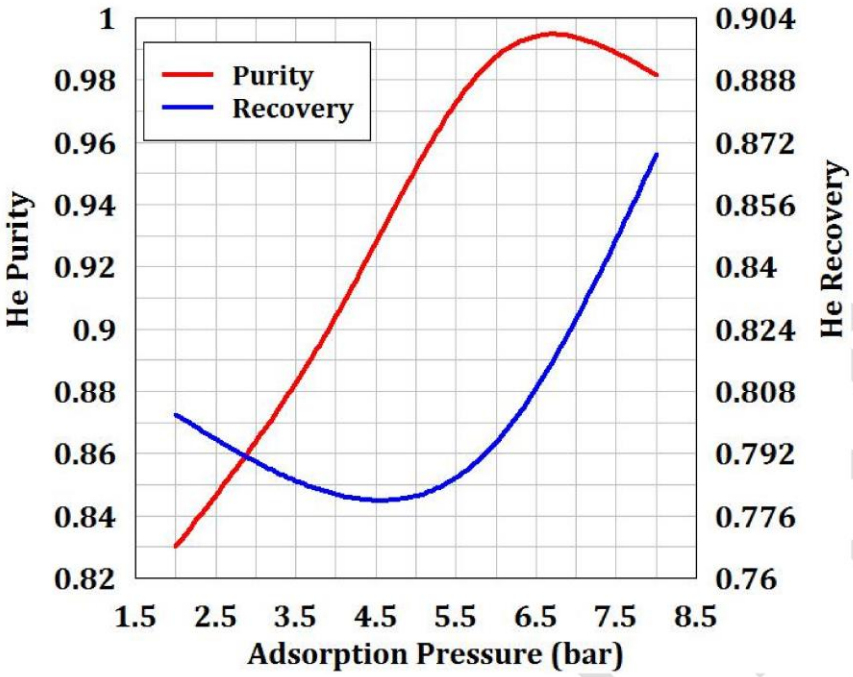

Figure 5. Variations of helium purity and recovery in terms of adsorption step pressure.

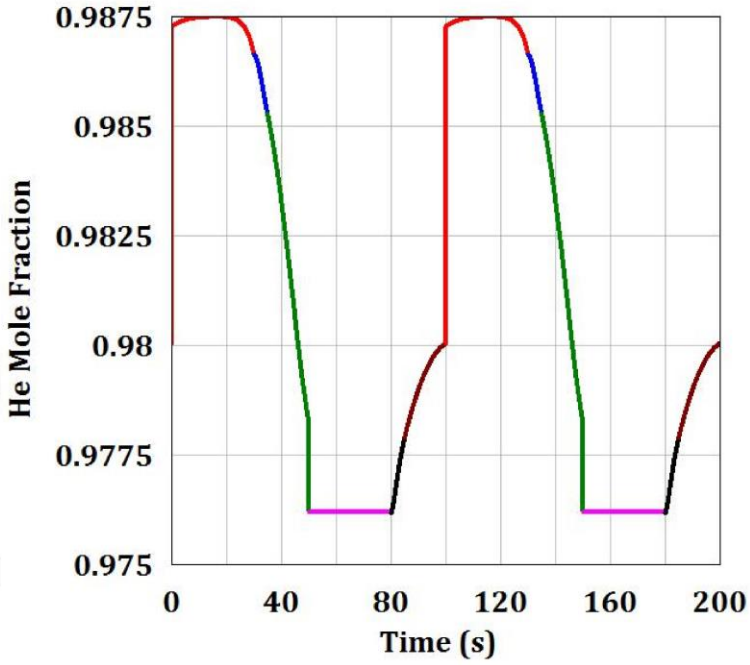

Figure 6. Helium concentration profile along a whole cycle at the top of the bed.

4. Conclusions

Helium separation from gaseous mixture in a two-bed pressure swing adsorption setup on a commercial type of zeolite 13X adsorbent has been studied numerically over a wide range of operating conditions. The influences of adsorption step pressure, adsorption step time and feed flow rate on the process performance were investigated. Results

shown that as the adsorption step pressure increases the helium purity will be increased. The time of the adsorption step is clearly defined through the physical properties of the bed such as length, diameter, adsorbent type as well as the feed flow rate. Furthermore, the helium recovery increases, and the helium purity decreases when the feed flow rate increases. Finally, a considerable agreement was found between the experimental data and the simulation results for various operating variables.

References

1. Bhushan J. Helium Purification by Gas Adsorption method master of technology thesis, Rourkela, 2011.
2. Stoll AP, Taylor LG, Steel AJ. Helium Purifiers Proceedings of the Seventh International Cryogenic Engineering Conference (ICEC7), 1978; 642 – 647.
3. Van Cleve E, Taborek P, Rutledge JE. Helium adsorption on lithium substrates. Journal of Low Temperature Physics 2007; 5.
4. Das Nkr., Chaudhuri H, Bhandari RK, *et al*. Purification of helium from natural gas by pressure swing adsorption. Current Science 2008; 95(12).
5. Martins D, Catarino I, Lopes D, *et al*. Low temperature adsorption versus pore size in activated carbons. International Cryocooler Conference, Inc., Boulder , CO 2011.
6. Majidia R, Ghanbarzadeh S, Jodaee asl N. Molecular dynamics simulation of helium adsorption on carbon nanocones with disclination angles of 240° and 300°" 4th. International Conference on Nanostructures (ICNS4) 2012.
7. Das NKr, Kumar P, Mallik C, *et al*. Development of a helium purification system using pressure swing Adsorption. Current Science 2012; 103(6).
8. Ch.Hua, W.Zong-Xin, Y.Mei-Sheng , *et al*. Experimental investigation and modeling of adsorption of carbon dioxide on 5A molecular sieve for helium purification of high-temperature gas-cooled reactor. Energy Procedia 2013; 39: 208 – 226.
9. Bartolomei M, Carmona-Novillo E, Hernández MI., *et al*. Graphdiyne pores: 'Ad hoc' openings for helium separation applications. The Journal Of Physical Chemistry 2014; 118(51).
10. Grande CA, *et al*. Advances in pressure swing adsorption for gas separation. International Scholarly Research Notices Chemical Engineering 2012.
11. Rosen MS, *et al*. Development and testing of a temperature-swing adsorption compressor for carbon dioxide in closed-loop air revitalization systems. SAE International, Paper 2005; 2941(1): 1-6.
12. Milton RM., *et al*. U. S. Patent, No. 2, 1959; 882,243.
13. Mivechian A, *et al*. Hydrogen recovery from Tehran refinery off-gas using pressure swing adsorption, gas absorption and membrane separation technologies: Simulation and economic evaluation. Korean Journal of Chemical Engineering 2013; 30(4): 937-948.
14. Jang SC, *et al*. Adsorption dynamics and effects of carbon to zeolite ratio of layered beds for multi component gas adsorption. Korean Journal of Chemical Engineering 2011; 28(2): 583-590.
15. Kim YH, *et al*. Effect of bed void volume on pressure vacuum swing adsorption for air separation. Korean Journal of Chemical Engineering 2014; 31(1): 132-141.
16. Zaman M, *et al*. Carbon capture from stationary power generation sources: A review of the current status of the technologies. Korean Journal of Chemical Engineering 2013; 30(8): 1497-1526.
17. Hoshyargar V, *et al*. Mass transfer simulation of nanofiltration membranes for electrolyte solutions through generalized Maxwell-Stefan approach. Korean Journal of Chemical Engineering.
18. Ruthven DM., *et al*. Pressure Swing Adsorption, New York, VCH Publications, Inc 1994
19. Yang RT, *et al*. Adsorbents: Fundamentals and Applications, New Jersey: John Wiley & Sons, Inc 2003.
20. Ruthven DM, *et al*. Principle of adsorption and adsorption processes. New York: John Wiley & Sons, Inc. 1984.
21. Chou CT, *et al*. Simulation of a four-bed pressure swing adsorption process for oxygen enrichment. Industrial & Engineering Chemistry Research 1994; 33(5): 1250-1258.
22. L. Lin *et al*. Numerical simulation of pressure swing adsorption process. Dissertation Presented for the Degree of Bachelor of Science, XIDIAN University, Xi'an, China, 1990.
23. Ritter JA, *et al*. Tapered pressure swing adsorption columns for simultaneous air purification and solvent vapor recovery. Industrial & Engineering Chemistry Research, 1998; 37(7): 2783-2791.
24. Teague KG *et al*. Predictive dynamic model of a small pressure swing adsorption. Industrial & Engineering Chemistry Research 1999; 38(10): 3761-3775.
25. Mendes AMM, *et al*. Analysis of nonisobaric steps in nonlinear bicomponent pressure swing adsorption systems. Application to Air Separation Industrial & Engineering Chemistry Research 2000; 39(1): 138-145.

26. Mendes AMM, *et al*. Oxygen separation from Air by PSA: modeling and experimental results Part I: Isothermal Operation. Separation and Purification Technology 2001; 24(1): 173-188.
27. Wilson SJ, *et al*. The effects of a readily adsorbed trace component (Water) in a bulk separation PSA process: The case of oxygen VSA. Industrial & Engineering Chemistry Research 2001; 40(12): 2702-2713.
28. Rege SU, *et al*. Air-prepurifcation by pressure swing adsorption using single/layered Beds. Chemical Engineering Science 2001; 56(8): 2745-2759.
29. Jee JG, *et al*. Air separation by small-scale two-bed medical O2 pressure swing adsorption. Industrial & Engineering Chemistry Research 2001; 40(16): 3647-3658.
30. Jee JG, *et al*. Comparison of the adsorption dynamics of air on Zeolite 5A and carbon molecular sieve beds. Korean Journal of Chemical Engineering 2004; 21(6): 1183-1192.
31. Jee JG, *et al*. Effects of nonisobaric steps and isobaric steps on O2 pressure swing adsorption for an aerator. Industrial & Engineering Chemistry Research 2002; 41(17): 4383-4392.
32. Choong STY, *et al*. On the numerical simulation of rapid pressure swing adsorption for air separation. Jurnal Teknologi 2003; 38(F): 65-86.
33. Santos JC, *et al*. Simulation and optimization of small oxygen pressure swing adsorption units. Industrial & Engineering Chemistry Research 2004;43(26): 8328-8338.
34. Reynolds SP, *et al*. Enriching PSA cycle for the production of nitrogen from air. Industrial & Engineering Chemistry Research 2006; 45(9): 3256-3264.
35. Kostroski KP, *et al*. High recovery cycles for gas separations by pressure-swing adsorption. Industrial & Engineering Chemistry Research 2006; 45(24): 8117-8133.
36. Jee JG, *et al*. Adsorption and desorption characteristics of air on zeolite 5a, 10x, and 13x fixed beds. Separation Science and Technology 2002; 37(15): 3465-3490.
37. Lee SJ, *et al*. Parametric study of the three-bed pressure-vacuum swing adsorption process for high purity O2 generation from ambient air. Industrial & Engineering Chemistry Research 2007; 46(11): 3720-3728.
38. Mofarahi M, *et al*. Comparison of two pressure swing adsorption processes for air separation using zeolite 5A And zeolite 13X. Petroleum & Coal 2013; 55(3): 216-225.
39. Olney TN, *et al*. Absolute scale determination for photoabsorption spectra and the calculation of molecular properties using dipole sum-rules. Chemical Physics 1997; 223, 59-98.
40. Jain S, *et al*. Heuristic design of pressure swing adsorption: a preliminary Study. Separation and Purification Technology 2003; 33(1): 25-43.

Chapter 1

Introduction

1.1 Introduction

Flare is an extension stack or vertical tube which is used as one of the essential parts in oil wells, refineries, petrochemicals, and chemical plants to burn waste, flammable, poisonous, and depleted gases and liquids. It can prevent fire hazards, explosions, and employee damage. In fact, flares convert flammable and poisonous materials as well as corrosive fumes into less harmful compounds. Flares always produce heat and sound during activity. The environmental pollution, the amount and type of gases emitted from the flare depends on the combustion efficiency and the type of gas supplied to flare. Investigating the reduction of the flare network is important in two respects. First, the gas supplied to the flare has a significant economic value, and the second is the environmental damage caused by combustion of the above mentioned compounds in flare. According to World Bank data, in 2005, the total greenhouse gas produced in the world by flares was 213 million tons. Iran with a production of 28.5 million tons and 2.13% share is ranked second after Nigeria, which is equivalent to 14 billion cubic meters of natural gas worth 10 milliard dollars [1]. This amount of gas can be used for other purposes, including energy production. In oil, gas and petrochemical industries, one of the most important environmental issues is the proper disposal of waste gases available in units and industrial complexes and burning these gases is one of the most commonly used methods. Flares are suitable equipment for burning waste gases and releasing their combustion products in the environment. The combustion occurs at the upper end of the flare stack and in the place where the flare tip and pilot burner are located. Process variations and rising pressure in tanks, towers, and other industrial equipment can cause irreparable damage to industrial equipment and sometimes criminal injuries. The factors that can lead to these changes are the power outage, the change in the input feed, utilization of production units over their design capacity, inappropriate repair and maintenance, deviations from the correct methods, utilization instructions, and human errors. In such a situation, flares are considered as the most important method of immunization. In terms of stack inhibitor types there are three type of flares: Derrick, guyed supported, self-supported, and

tripod (for small industries). In terms of mixing agent with flare gas, to improve flame fuel, there are different types of flares such as steam-assisted, air-assisted, pressure-assisted, and non-assisted. In terms of altitude, there are elevated and ground flares. The construction of flare and burning gas in it have different environmental consequences and, if not done correctly, can have a major negative impact on human life, plants, animals, and the surrounding environment in the future. Air pollution is one of the most important negative consequences of burning of gas in flares. The publication of strict standards for gas diffusion and reduction of flaring is an effective step in controlling air pollution caused by burning of gas. Also, flaring the gas can cause thermal, noise, visual pollution due to the characteristics of the gas burned in it.

Figure 1-1: A picture of a real flaring gases from an oil platform in the Sea.

Flare is used to describe an unprotected flame that burns excess gas. This phenomenon occurs in oil installations, refineries, and petrochemical industries in order to ensure the safety of staff and equipment. In fact, fare gases are produced when processes do not have a complete function. Inappropriate performance may result from the following factors:

1. Change in input feed

2. Technical failure of equipment

3. Inappropriate repair and maintenance

4. Human errors

5. Deviation from utilization procedures

6. Power outage

7. Utilization over design capacity

1.2 Flare Classifications

The classification of flares is based on two bases [2,3]:

1.2.1 Based on the height of the flare tip from the ground

1.2.1.1 Elevated flare

In this type of flare, the design is based on the maximum flow of combustible material and the maximum allowable amount of radiation from the combustion which, in order to prevent incomplete combustion or smoke, water vapor is injected or has auxiliary air. This flare is firmly fixed on the ground by a special structure in terms of keeping and tightening.

1.2.1.2 Ground flare (closed flare)

The combustion action is carried out in the combustion compartment and the flame is inside the compartment. Therefore, the radiation does not spread to the outside and there is no need for water vapor or auxiliary air, also it can be installed inside the operational centers.

1.2.2 Based on the mixing agent

1.2.2.1 Flare with steam mixing agent

In this type, the flare has a burner with one tip, and a flow of steam is injected into the combustion section to ensure adequate air supply and good mixing of the air with combustible gases. Among the flares, this type of flare is abundant.

1.2.2.2 Flare with air mixing agent

In this type of flare, the air flow is used to provide the required air and mixing agent. Burner of this type of flare is cobweb-shaped with small pores and the minimum diameter for a burner is two feet. In this type of flare due to mixing pressures, the vertical flame is 50% shorter than other smoke-free flares and the length of the stack is smaller.

1.2.2.3 Flare with pressure mixing agent

In this type of flare, combustible gas flow pressure that exceeds 10 psi is used as a mixing agent in the flare tip. Burner of this type of flare is located near the ground and has several tips.

1.2.2.4 Flare without mixing agent

This type of flare is used for gases with low enthalpy and low carbon to hydrogen ratios. Most flares of industrial units have a vapour-liquid separator, also called knockout drum, in the upstream of the flare to remove large amounts of liquid that may be associated with gases. Vapour is often injected into the flame to reduce black smoke formation. In order to maintain the efficiency of the flare system, as a pilot flame, a small amount of gas is burned continuously, so that the system is always ready to carry out its main task (High-pressure safety system).

The flow diagram in figure 1-2 shows the components of a general flare system.

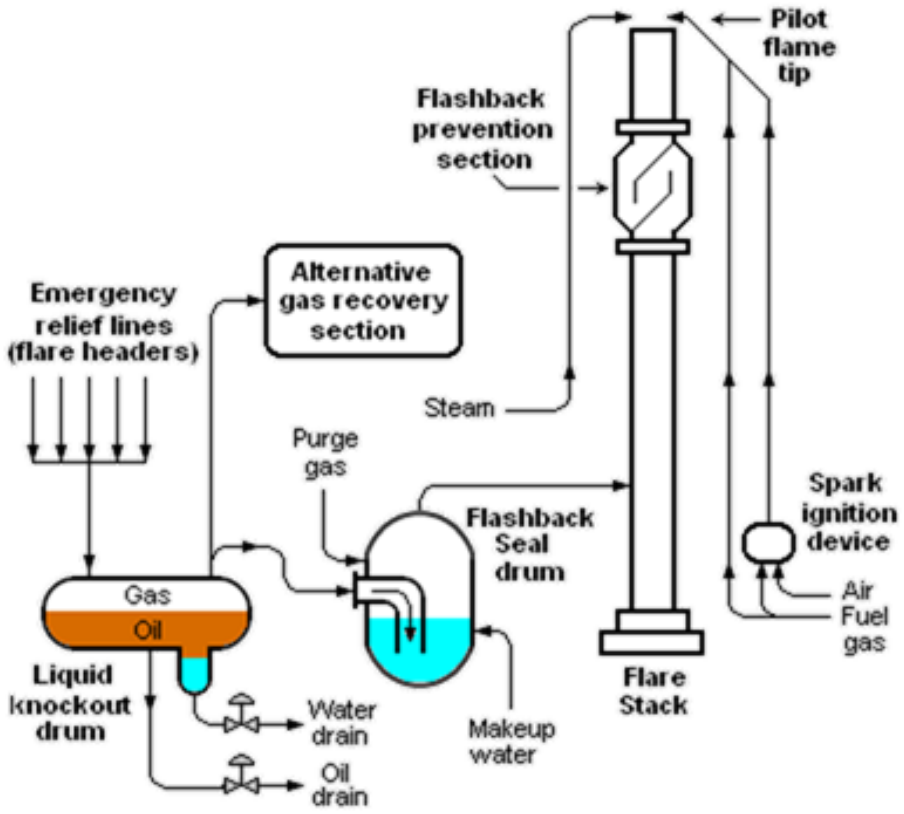

Figure 1-2: Components of a general flare system [4,5,6].

The flare component are as follow [4,5,6]:

1- A knock-out drum to remove any oil and/or water from released gases

2- A seal drum to prevent flame rejection from the top of the flare tower

3- An alternative gas recovery section for use when starting up and/or shutting down part of the plant and other required times; recovered gas is directed to the entire plant's gaseous system.

4- A steam injection system for creating an external momentum to effectively mixing the air with gas, which improves smoke-free combustion.

5- A pilot flame with a pilot burner system that burns constantly and is used to ignite gases at the required time.

The flare tower contains a section to prevent backfire in the upper part of the flare.

1.2.3 Different types of devices and systems

Flares used in petrochemical and hydrocarbon industries are generally divided into three categories:

1- Type I flares (with one outlet, one-directional flame)

2- Type II flares (multiple flares with multiple flame outputs, multi-directional flames)

3- Covered flares

1.2.3.1 Main Components of the Flare System

In a flare system, there are a set of special components, which use and have these components are optional. These optional components, such as smoke confine or liquid transfer components, require special monitoring. Optional equipment can help reduce system costs or operating system support.

1.2.3.2 Type I flares (with one outlet, one-directional flame)

For type I flares system, the essential and important components required and optional are as follow:

1- Flare torch with or without the capability of smoke catching

a: Torch with one or more pilot

b: Pilot dressing

c: A Pilot flame detector

2. The support structure, piping and sub-equipment

3. Purge gas reduction (converting) devices (optional)

4. Separator drum (Optional)

5. Seal drum (Optional)

6. Auxiliary equipment, including:

a. Smoke control equipment (optional)

b: Blowers (Optional)

c: Flow, composition, combustion heat (thermal value) measurement or image monitor (optional)

1.2.3.3 Multiple flares with multiple flame outputs

The main required and optional equipment for multiple flare systems are [3,4]:

1. Two or more multiple flames of flares

2. Pilots, pilot dressing, pilot torch detector

3. If it is elevated, the support structure and the sub-equipment

4. A fence to restrict access and reduce flame radiation and reduce the visibility (optional)

5. Separator drum (Optional)

6. Pool or liquid tank or seal drum (optional)

7- Piping

8. Auxiliary equipment:

a. Woodworking equipment and tools (optional)

b. Smoke control equipment

c: Flow, composition, combustion heat (thermal value) measurement or image monitor (optional)

1.2.3.4 Covered flare

The main required and optional components for covered flares are:

1- Flare torches with or without the ability to smoke confine

2. Enclosure and structure with a protective and resistant coating

3. A fence to restrict access to flare

4. Knockout drum (optional)

5. Seal drum (Optional)

6. Piping and optional heat shield

7. Auxiliary equipment:

a. Woodworking equipment and tools (optional)

b: Flow, composition, combustion heat (thermal value measurement) or image monitor (optional)

1.3 The destructive effects of flares in the oil industry

Oil industries in each country are among the advanced industries. Therefore, the pollution reduction program of these industries is constantly being implemented globally. Of course, pollution reduction programs differ from country to country, which sometimes depends on the national and local laws of the countries. Although the deleterious effects of flares on humans, plants and animals have not yet been provided quantitatively, studies and activities have already identified these harmful effects qualitatively [7]:

1- Active flares in gas fields or in refining operations directly generates greenhouse gases which undoubtedly leads to global warming.

2. The gases submitted to the flare in different conditions of its operation cause the release of various gases such as soot, unburned volatile organic compounds, carbon monoxide, nitrogen oxide gases, sulfur dioxides, and mercaptans.

The release of these gases threatens the health of people working in the environment. The harmful effects of these pollutants are summarized in Table 1-1.

3. Energy losses in flares are very important economically. The control and reduction of these losses can also reduce the emission of greenhouse gases and the heating of the earth.

4-Gases released from flares such as sulfur and nitrogen oxides in the vicinity of atmospheric water can produce significant amounts of acid. The acids can be dispersed thousands of kilometres away from the environment around the flare.

Table 1: The harmful effects of pollutants.

Name of Chemical substance	**chemical formula**	**Origin of production**	**Impact on health**
Ozone	O_3	Vehicles and	At low concentrations, it stimulates vision.

		refineries	At high concentrations causes respiratory problems especially in the elderly and children.
Hydrogen sulfide	H_2S	All oil industries	In low concentrations, it causes nausea, insomnia, headache, and affects vision. High concentration is lethal.
Nitrogen dioxide	NO_2	Vehicles and all oil industries	Affects the ends of the lungs and around the respiratory tract and exacerbates asthma. The high concentration of this gas causes the formation of methemoglobin, which prevents oxygen absorption by blood.

1.4 Application of recycled flare gases

In the following, a number of commonly used methods for recycled flare gases are presented.

1.4.1 The use of recycled flare gas as fuel gas

In many cases, the most basic and most practical way to use recycled flare gas is to use them as fuel in existing equipment. Typically, recycled flare gas is injected into the unit fuel gas system. Recycled flare gas can be used directly in equipment such as furnaces, heaters or low-pressure torches, or used as auxiliary fuel for equipment such as steam generators. In cases where the fuel consumed has a specific range for primary properties or high levels of H_2S are present in flare gases, recycled flare gas may be required to refine, sweetening or increased pressure, as appropriate. An important point in using flare gas as a fuel is that the flammability depends on

the ratio of the various compounds in the gas, not the thermal value of the gas expressed by the methane number. In fact, methane number is the main limiting factor for the use of flare gases as fuel. In figure 1-3, methane number is compared to a number of common fuel gas.

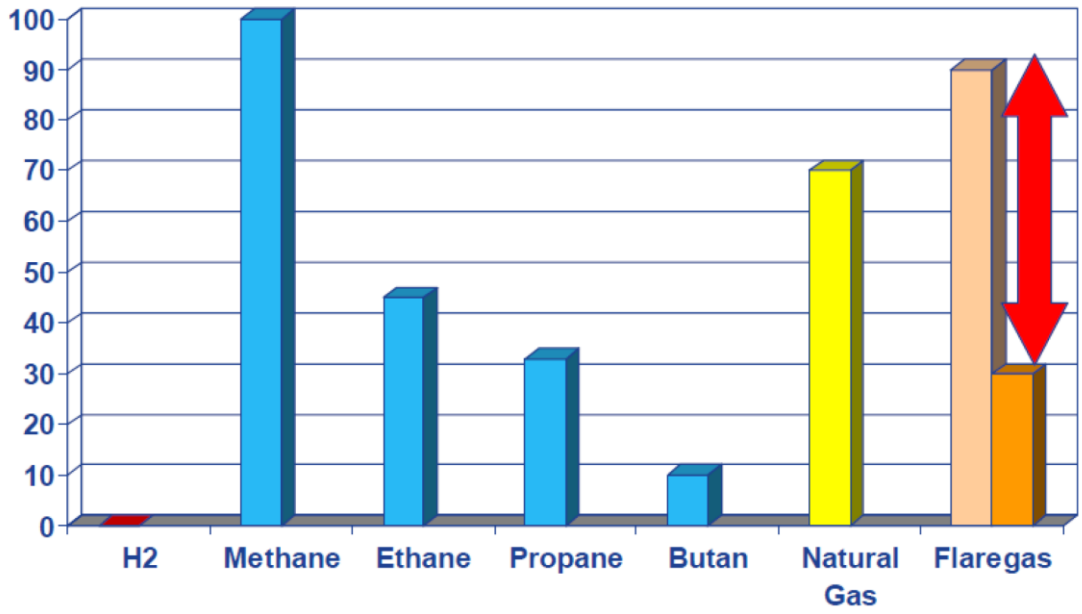

Figure 1-3: Comparison of methane parameters for common fuel gas [8].

The methane number is the parameter that describes the resistance of a gas to strike. This parameter is the same as the octane number for gasoline and indicates the volume ratio percentage of methane in a mixture of methane/hydrogen, which represents the resistance of the gas tested to impact in a test engine and under controlled conditions. In fact, it indicates the amount of gas knock and octane rating. Other important properties of the gas in the application as fuel are a low thermal value; which determines the energy content of a gas; and the low intensity of the flame, which is the rate at which oxidation occurs.

1.4.2 Generate electricity using flare gas

The solution for use of recycled flare gas to produce electricity is, in fact, a state of flare gas consumption as a fuel gas. Because of the importance and attractiveness of this solution, especially in locations away from the main electrical network such as offshore platforms or

wellhead facilities, or units with high electrical energy consumption, the production of electricity from flare gas is proposed as a separate solution.

1.4.3 Converting flare gas to heavy hydrocarbons or LPG

Recovery of heavy hydrocarbons or LPG from flare gases saves valuable hydrocarbons and allows them to be used locally. An interesting thing about LPG is its ease of storage and transmission, which is often used locally. Flare gases are rich in heavy hydrocarbons, so the separation of LPG and heavier sections of flare gas significantly reduces carbon emissions, and the thermal value of gas is recovered for local use. In some situations, the use of the LPG recovery system allows for the residual methane to be easily recovered in simple CNG and LNG units, to be used as a fuel gas or sent to a close consumer by piping.

Adsorption and cryogenic systems are traditionally used to recover LPG, which require the use of moving parts and extremely high-cost chemicals substance. A good solution is the use of membrane systems. In this system, a combination of two different membranes is used to recover LPG and also hydrogen. The first membrane passes the pure hydrogen in the gas, then the gas is transferred to another membrane that is able to pass the compounds. The remaining fluid flow from the membrane separation process is rich in hydrogen and lighter gas hydrocarbons, such as methane and ethane. Therefore, it can be used as a fuel or sent to a hydrogen purification unit [9] (see Figure 1-4).

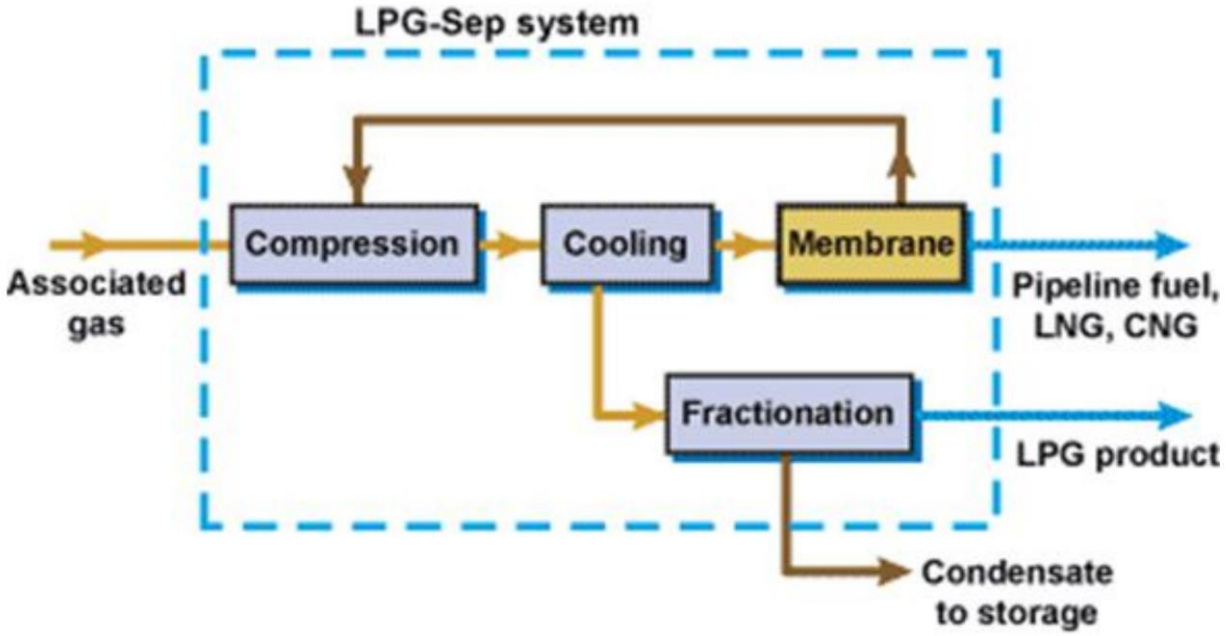

Figure 1-4: Schematic diagram of LPG membrane and hydrogen recovery from flare gas [10].

The collected gas streams are piped into a storage tank, are processed for the separation of impurities, and are separated into LPG components for use in the following applications:

• Commercial tanks

• Light naphtha as an industrial raw material

• Dilute gas as fuel for electricity generation projects

1.4.4 Conversion of recovered flare gases to the liquefied natural gas

Liquefied natural gas recycling due to the higher thermal value of hydrocarbons obtained is economical compared to primary gases used as fuels [11]. To recover liquefied natural gas, traditionally, cooling or turbine power plants are needed that require high capital and operating costs, while not suitable for offshore platforms. Therefore, the use of the membrane system shown in Figure 1-5 is proposed by Nemati Shahab & Omidkhah Nasrin.

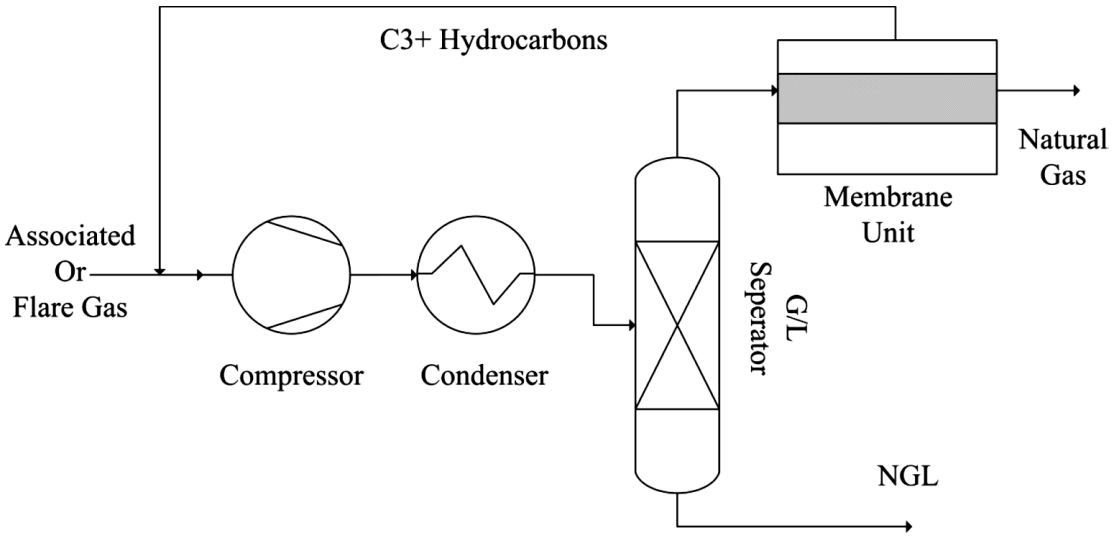

Figure 1-5: Schematic of liquefied natural gas recovery cycle from flare gas with membrane method [11].

The use of membranes is a simple and inexpensive way to separate and recover heavy hydrocarbons from flare gases. The membrane used is capable of passing only heavier hydrocarbons than methane. These hydrocarbons penetrate the membrane and, after compression and distillation, are recovered in liquid form. The main advantages of this system are:

• Optimum use of flare gases and significant reduction of flaring

• Removal of heavy hydrocarbons and water vapour and, as a result, reducing the dew point of a mixture of water and hydrocarbons in the gas pipe

• Proper size and weight for use on offshore platforms

• No use of moving parts and ease of operation

• Low installation and set up costs

1.4.5 Returning to the production or consumption process as a feed of other units

In many factories, by examining the conditions and processes of existing operating units, it appears that the recovered gases are in accordance with the feeds required by existing units, such as petrochemical feeds, methanol production units, naphtha, light hydrocarbons, and so on. In that case, the most economical way to recover will be to consume recycled flare gases as feeds for these units. In some cases, preparation and preliminary purification are needed to adapt to the desired feed.

1.4.6 Processes of converting flare gas to condensate

The processes of converting flare gas to condensate (GTL) are used in areas where the collection or re-injection of flare gas is not economically viable. These plants typically produce 25% naphtha and 75% high-quality diesel fuel with a methane number of at least 70 and zero sulfur content.

The main features of these systems are:

• Converting flare gas to diesel and naphtha

• Can be made in the form of portable units

• Quick and easy installation

• The ability to produce fuel for local consumption

1.4.7 Injecting associated gas into oil wells for enhanced oil recovery

Injection of associated gases is one of the ways to prevent it from burning. By re-injection of gas into reservoirs, can save 10 million cubic feet of gas a day in order to enhanced oil recovery. Research has shown that the use of high-hydrogen sulfide gas is also possible.

1.5 The basics of recycling flare gas

The most important point in designing the flare gas recovery system (FGR) is that the presence of this system, along with the existing flaring system, will not create a flaw in the flaring system emergency operation. Therefore, according to this point and the information and data required, the design of the compressor system and recovery of flare gases is carried out. This system collects gases that flow towards the flare and directs it to the gas processing unit. Emergency flows, as previously mentioned, always have a definite path to the flare where the combustion operation is performed safely. In general, there are two modes for the torch gas recycling system: recovery mode and flaring mode. During the recovery mode, a fast opening valve (FOV) blocks the path to the flare. This valve in addition to being reliable and no leakage should have no obstacle to open it immediately. Alternatively, a liquid sealant can be used. Of course, because of

the limited scope of control and the need for a wide range, it is not recommended to use. Of course, in order to increase the reliability of the system, another equipment is parallel to the fast opening valve in the flow path to operate as needed.

In terms of pressure limitations in the flare system, a pressure lift system, such as a compressor, blower, or ejector is used. Figure 1-6 shows a schematic diagram of flare gas recycling unit.

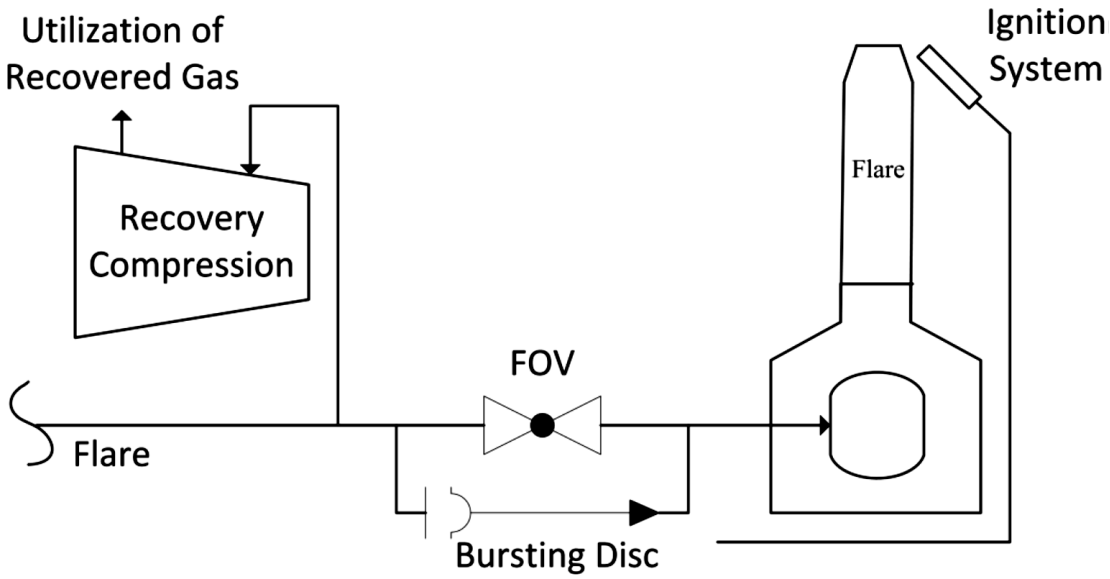

Figure 1-6: General schematic of flare gas recycling unit provided [12].

When a flaring mode is established, a fast opening valve or seal drum direct gas to the flare quickly. When the flare path is closed, a flow should always be present in the flare in order to provide a positive pressure. The source of positive pressure supply, which can be an inert gas, such as nitrogen or natural gas, prevents the air entering the flare system, as well as the recycling system. It is worth noting that failure to follow the above tips will result in a system explosion.

In order to design such a system, first, a general analysis of all the flare gases generators units and the existing flaring system should be available and, with such an analysis, the values of the variables should be collected. Since the general properties of the flow of the main pipeline of the flaring system, including flow intensity, temperature, pressure, and the combination of component percentage, are highly variable, a special flow pattern and properties are required to form the design parameters based on it. Regarding this issue, in the first step, during the course

of several weeks, the current state of this flow is fully measured and recorded, and simultaneously the composition of the percentage of samples obtained should be determined by the laboratory located in the studied unit (refinery). After the first step, a special system for compression and recovery of gases is presented and evaluated in terms of required technologies and possible costs. Economic calculations and determining the time of the returning capital will be performed through the re-utilization of gases supplied to the flare.

1.6 Effective factors in designing a recovery system

Since the flare system is essentially a security and safety system, so the most important point in designing a torch gas recovery system is that in normal operation of the flare should not be created an abnormality. Also, in designing the system, the following restrictions should also be considered.

1) If, in order to obtain the maximum pressure at the inlet of the gas recovery unit, the changes in the design of the flare seal drum are required to increase the pressure of the flare path, it should not be applied any limitation in performance of safety valve of units, especially those open with low pressure.

2) The flow of gas entering the flare path and its combination is not predictable. Therefore, it is necessary to design a unit that can operate under all conditions of gas release during normal operation.

3) The unit capacity should be compatible with all predicted conditions (flow and combinations of wasted gases in the frequent discharge of unit).

Effective factors in selecting and designing of the flare recovery system are:

1.6.1 The flow of gases supplied to flares in continuous mode

The gas supplied to flare is the most important factor in determining the scale and size of the equipment of the recovery system. Typically, this flow is considered in the normal operation of flare.

1.6.2 Maximum allowed the pressure in the surge tank

In order to determine the maximum allowed pressure, all flows conducted to flares should be investigated while the flare is closed. In order to reduce energy consumption in the recovery process of flare gases, the maximum pressure required to open the valve should be the highest amount.

1.6.3 The composition or molecular mass of the gas

The combination of gas has an important role in the selection of recovery equipment. The combination of gas also indicates the thermal and economic value of gas. For example, gases containing H_2S and CO_2 or other unwanted compounds have an impact on the type of recovery equipment and also the economic value of recovered gas.

1.6.4 Gas temperature

Flare gas temperature is also effective in the selection of recovery equipment. If the gas temperature is high, a cooling heat exchanger is required to compress the gas.

1.6.5 The output pressure of the recovery unit

The output pressure of the recovery unit is important because of facilitating the decision to use equipment such as compressors, blowers, ejectors, and so on.

1.6.6 The temperature of the output gas from the recycling system

Knowing the temperature of the output gas will help to provide the necessary heating or cooling equipment to reach the desired gas. For example, if an output gas temperature is high, a cooling heat exchanger is used to reduce its temperature.

1.6.7 The diameter and material of the flare gases transfer pipe

In order to estimate the cost of equipment such as FOV, rupture discs, and manual valves, should be considered the diameter and material of the flare gas transfer pipe.

1.6.8 Value of flare gas

The value of flare gases determines the revenue from the sale of recovered gases, which is important in the economic analysis of the project. These gases can be valued as fuel, or considered as feeds of a processing unit or even an injectable gas to enhanced oil recovery.

1.7 Determination of flare gas recovery system design parameters

Knowledge of quantitative variables is the most important factor in monitoring and controlling a system. Achieving these values requires the use of measuring equipment. The control of the flare system, as a system that guarantees the safety of the plant, is no exception to this and requires the use of measuring equipment. In this regard, gas flow and gas flow analysis is of great importance. In the design of the flare gas recovery system, the measurement and control of gases are very important. This means that accumulation, increased pressure, or lack of control and proper measurement of the input gases to the unit can cause very high risks and increase the risk of the recovery process. Flare gas measurement systems, in addition to working power in obstruction mode, should work in such a way as to minimize the pressure drop in the system. The most important methods for measuring flare gases include [13]:

1) Thermal Mass Metering

2) Differential Pressure Metering (Pitot tube)

3) Ultra-Sonic Metering (vortex)

4) Insertion Metering

5) Tracer Techniques

In cases where measurement systems are not available, the following methods can be used to measure gas flares. These methods, which have high uncertainty, are [13]:

1) Flare spectacle (Obtaining an approximate amount of gas flow from flame height)

2) Process simulation software by applying temperature and pressure values at the key points of the system

3) Mass balance (currently used in many refineries and process industries of the Iran)

The equipment used in the flare gas recovery unit should not have an absolute impact on the safety of operations. The system used should be of a non- interference or low-interference type. This equipment should also be able to measure a wide range of materials, or they can be measured from the purge to the gas blow down. Ultimately, this equipment should have the least maintenance required.

1.8 Determining the composition of gases in the flare system

Knowledge of gas analyzes in a flare system of an industrial unit is necessary for two reasons. First, by determining the composition of gases, a mass and energy balance can be studied in the whole plant, and an optimal program for recovery and determining the use of these gases can be developed. The second factor is the environmental requirements of government agencies that have put certain restrictions on the emission of pollutant gases. In the world, the second factor is the most important factor in determining the analysis of gases in the flare system, and therefore, special measuring equipment is used to record the composition of gases. Some of this equipment is continuously and others discontinuously analyze the sample of desired gas. In the flare systems, determining the gas analysis is important in two parts: one at the entrance to the stack (in order to balance the mass and energy, and planning the recovery plan) and the second after combustion (due to the environmental requirements).

Generally, there are ten types of gas analysis methods which based on these methods, fixed and portable equipment was developed for determining the gas analysis [7].

1) Spectrophotometry

2) UV Fluorescence

3) Chemiluminescence

4) Flame Ionization Detector

5) Photo Ionization Detector

6) Gas Chromatography

7) Mass Spectrometry

8) Electrochemical cell

9) UV / Visible Diode Array

10) Paramagnetic

It should be noted that, among the various methods for determining the gas analysis, gas chromatography (GC) method is the best methods for determining the analysis of gases submitted to flare.

1.9 Pressure swing adsorption

In general, separation is a process whereby a mixture of materials is converted into two or more different products. This operation can be considered as one of the most costly stages in the chemical and petrochemical industries. Adsorption is a kind of separation process in which some of the fluid phase components are transferred to a solid phase absorptive surface. In this process, the solid surface structure is different from the solid bulk structure. So that the surface is not completely saturated in terms of energy, and when the solid is exposed to a gas, the molecules of gas are bonded to the centres of the surfaces and absorbed by the solid. This is called gas adsorption by solid. Typically, small solid particles (adsorbents) are kept in the fixed bed and the gas continuously passes through the bed until the solid is almost saturated and the desired separation cannot be done. At this time, the flow is transferred to another bed until the saturated adsorbent is replaced or regenerated. The adsorption applications in the vapour phase include the recycling of organic solvents used in paints, the printing ink, and the solutions used for casting or coating the cloth. The adsorption on carbon is also used to remove contaminating materials such as H_2S, CO_2 and other smelly components from air circulation in ventilation systems. Drying of gases is often carried out by adsorption of water onto silica gel, alumina or another porous solid mineral. Zeolites or molecular sieves are natural or synthetic aluminum silicate that is effective

in the preparation of low dew point. Adsorption on molecular sieves are also used for the separation of oxygen and nitrogen, preparation of pure hydrogen as a synthesis gas and the separation of ordinary paraffin from branched paraffin and aromatic compounds. Adsorption from the liquid phase is used to separate organic components from wastewater, colourless impurities from sugar solutions and vegetable oil, and separation of water from organic liquids. Also, adsorption is used to recycle a reaction product that is not easily dispersed by distillation or crystallization. Some of the solids are separated by adsorption from both the vapour phase and the liquid phase, although most of the adsorbents with large pores are preferred for use in liquids. Direct use of adsorption was limited to air purification and exhaust gases from industrial centres by the early 1960s. But, following the important advances in recent decades, adsorption by solid phase has been used as a key process for the separation of gases in chemical and petrochemical industries. One of the important advances is the innovations about the synthesis of synthetic adsorbents and development of cyclic adsorption processes.

The existence of a recovery phase is a characteristic of cyclic processes in which the adsorption column is regenerated and used for use in the next cycle. The thermal swing is one of the cyclical processes. However, heat recovery due to the high amount of time required to heat and cool the adsorbent bed does not have much efficiency. Next cycles in this evolutionary process were pressure swing cycles that were invented by Skarstrom [14] and had more efficiency. Thereafter, the pressure swing cycles were widely developed by applying various changes in process steps, in terms of energy use and separation efficiency.

The pressure swing adsorption (PSA) process is an extensive operational unit for separating and purifying gases, based on the adsorption capacity of the solids and the selective separation of gases. The most important operating parameter in this system is pressure and most industrial units act at ambient or near ambient temperature. The term PSA is derived from the regeneration method, which is the reduction and pressure swing. The PSA process is well known today in a

wide range of processes and is preferred to other conventional separation methods, especially for higher purity. Therefore, much effort is being made to develop this technology. This process is used in many cases for the separation of gas mixtures, the most important of these are:

1- Air drying

2- Purification of natural gas

3- Purification of all kinds of industrial gases

4- Separation of hydrogen from hydrocarbon mixtures

5. Solvent Recovery

6- Separation of air components (production of oxygen and nitrogen)

7. Separation of normal paraffin from isoparaffin and aromatics.

In addition to the above, PSA technology has recently been developed for other separations, such as separation of gas isotopes in industrial nuclear processes, recovery of helium from air furnace gas by blowing air and hydrocarbon separation. This process was originally developed by Hasche and Dargan in 1927 for the recovery of sulfur dioxide from purifier gases using silica gel [15]. But the use of this process to produce oxygen and nitrogen from the air was first introduced by Skarstrom in 1958. In order to enrich oxygen and air nitrogen, he presented his proposed PSA cycles for air drying, named Heatless Dryer and removing carbon dioxide from the air [14]. Finally, in 1966, the PSA cycle was developed by Skarstrom in two beds with a pressure equivalent step using zeolite 13X [16]. Pressure Swing adsorption processes have common principles but can be applied in different ways. In all processes, the existence of a multi-step cycle is essential, but the number and type of steps in different methods will be different. Each method has its own characteristics and the choice of the method depends on the ultimate goal, available facilities and equipment, the desired mixture, and the absorbent used. The essential steps in the PSA process are four stages: pressurization step, production step, depressurization step, and purge step.

Generally, the relative advantages of PSA in comparison with other processes can be expressed as follows:

1- High purity percentage, especially for hydrogen, helium, and methane

2. There is no need for outside heat to recover

3- One stage process

4. The long lifetime of adsorbent

5. Need for less equipment

6. Ability to set off the purge flow as an operational variable

7- Fast and easy start and end

8. Simple and flexible operation with easy maintenance

9. Lower price and operating costs compared to the corresponding methods

10. Capable of producing with high flexibility minimizes maintenance capacity

11. Effective performance

12. The minimum cost of construction and insulation.

As with all adsorption separation processes, the need for the PSA process is the presence of a suitable absorbent that is selectable compared to a compound in a feed mixture (or a group of compounds). As previously noted, this selectivity may depend on the difference in the adsorption equilibrium or the difference in the diffusion rates.

In the PSA process, valuable products can be obtained from each step of adsorption or desorption (recovery) or from both of them.

The outlet flow from adsorption step is called raffinate or treated product, which the more strongly adsorbed species is traped by the adsorbent. The desorption flow, recovered during the recovery step, includes a strong adsorbing species in the concentrated form (relative to the feed), which, after passing this step, the resulting product is called extract product. The mandatory feature of the PSA process is that, during the recovery step, the predominant adsorbing species is

eliminated by lowering the total pressure, instead of using methods such as increasing the temperature or removing by displacing agent. The PSA process usually operates under isothermal conditions.

According to figure (1-7) useful capacity is the difference between two points, corresponding to the feed and regeneration pressures, on the same isotherm [17,18].

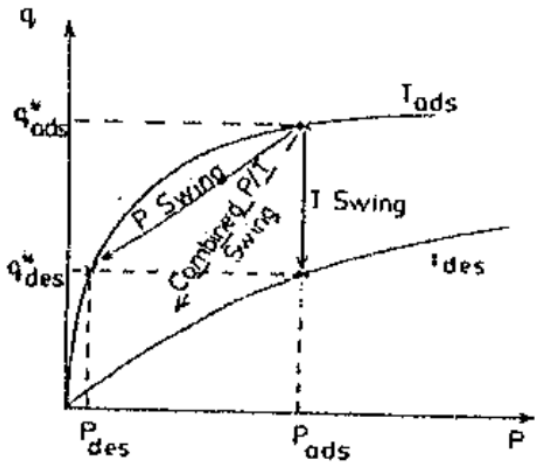

Figure 1-7: Change in pressure swing loading [17].

The feed step ends naturally before the strong adsorbing species penetrates the entire bed. However, the recovery step is usually completed before desorption occurs completely in the bed. In a cyclic steady state, the concentration distribution varies around an average position based on bed length. The main advantage of the PSA process compared to the other adsorption processes, such as temperature swing, is the faster change of pressure compared to the temperature. Therefore, it is possible that the PSA process works under a faster cycle. On the other hand, the main limitation of this process is its limited to weak adsorbing species. If a predominant adsorbing species is adsorbed very strongly, an uneconomic vacuum is needed to produce effective desorption during the recovery step. Therefore, the temperature swing will generally be a preference for very strong adsorbing compounds. Because in general, a small change in temperature leads to a relatively large change in the equilibrium constant of solid-gas adsorption.

The PSA process is not very different from conventional separation processes. But this process is comparable to other processes in terms of an essential characteristic: the PSA process acts under transient state (or unsteady state), however, most separation processes, such as absorption, extraction, and distillation operate under steady state. Therefore, the perceptual framework and design methods for these two categories of processes are completely different from each other. This difference in the mathematical part of processes can be better described. Steady state processes can be expressed mathematically by an ordinary differential equation (or a system consisting of ordinary differential equations), and in order to obtain a relationship between operational variables and process performance, only the integration of this equation is required. Conversely, transient processes are expressed by partial differential equations. This requires a more complex solution, and thus the relationship between operational variables and process performance is less evident.

In a basic state [14], the adsorption bed that undergo the process of pressure swing adsorption is subjected to four steps: pressurization, high-pressure-adsorption, blowdown, and purge.

It should be noted that if the purge step is performed under vacuum conditions, the process will be called the vacuum swing adsorption (VSA).

1.9.1 General features of the PSA process

There are six general features for the PSA system, which largely express both the advantages and limitations of this technology and determine its suitability for specific applications [17].

1.9.1.1 Product purity

The raffinate product (weak adsorbing or slow penetrating species) can be recovered in a very pure form, while the extraction product (strong adsorbing or fast penetrating species) is generally released in the form of impure and similar to a byproduct. Various corrections can be made on the PSA cycle to recovery a predominant adsorbing species, but this leads to increasing

complexity of the cycle. Therefore, the best process mode (in terms of product purity) is when only the raffinate product is needed.

1.9.1.2 Fractional recovery

In the PSA process, partial recovery (part of the feed flow that is recovered as a pure product) is relatively low in comparison with processes like distillation, absorption, and extraction. Recovery can be enhanced by defining additional steps in the cycle or increasing the number of beds, but both of these corrections will increase the capital cost. Therefore, a PSA process is at its best mode (in terms of recovery) when the unit feed is relatively inexpensive. However, high product yield alone is not a reason for the cost-effectiveness of the process.

1.9.1.3 Dilute impurities concentration

When the adsorbent with high selectivity is available, the PSA process can produce a reasonable amount of diluted impurities.

1.9.1.4 Energy Requirements

Like most separation processes, the energy efficiency of the PSA process is relatively low. The efficiency of the first law of thermodynamics (the ratio of separation work to consumed energy) is quite comparable to processes such as distillation or extraction compared to the PSA. On the other hand, in the PSA system, mechanical energy is used which is generally much more expensive than heat. The power consumption cost is an important component of the operational cost for the PSA system. If the unit feed is already available at a high pressure, these costs can be greatly reduced. Because, generally, the cost of product compression at high operational pressure is much lower than the cost of feed compression. Therefore, a PSA system is particularly useful when (in terms of energy requirements) the feed is available at high pressure.

1.9.1.5 Specifications of production scale

For most separation processes, operational costs increase almost linearly with throughput (operational capacity). Also, for the PSA process, the capital cost increases almost linearly with throughput, but for most processes, the capital cost curve is strictly non-linear and increasing the cost for larger units is less (Figure 1-8). As a result, when overall costs are considered, the economic justification for low-to-high throughput is satisfied by the PSA system and for higher scales by systems such as cryogenic distillation [17].

1.9.1.6 Pressure range

Vacuum swing adsorption is a PSA cycle with a desorption step at sub-atmospheric pressure. This type of process is a semantic choice. The performance of each PSA process is controlled by the absolute pressure ratio (adsorption pressure to desorption pressure). The desorption that occurs at sub-atmospheric pressure improves the process performance.

Therefore, increasing the absolute pressure ratio (adsorption to desorption) in certain conditions can increase the process throughput.

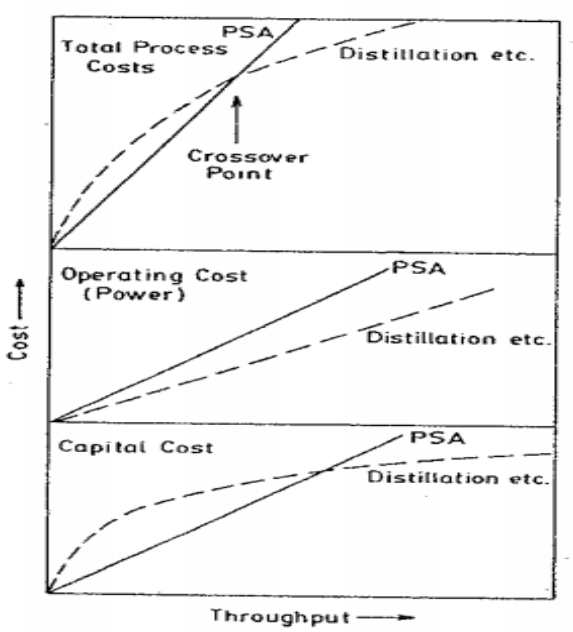

Figure 1-8: Change in cost with the product for air separation by cryogenic distillation and PSA processes [17].

1.10 Thesis objectives

Although the PSA process is not a new process, due to the high efficiency of this process, in order to improve its performance, every day a new achievement in applied fields is introduced by researchers around the world. Combining PSA knowledge with modern techniques gives this a modern look to this old process. The extensive separation place in the chemical and petrochemical industries shows the high need to study the separation processes such as PSA, for a proper separation.

In this project, nitrogen, methane, and ethane are simultaneously recovered from the flow of submitted gases to the oxychlorination unit flare by the PSA process and sent to the relevant units for reuse. For this purpose, an experimental pilot is constructed in the FAPKCO Industrial Engineering Group, and then the relevant tests are carried out in the oxychlorination unit of a domestic industrial Petrochemical Complex. This leads to providing quite realistic and reliable results for the proposed plan.

Chapter 2

Literature Review

2.1. Introduction

The use of the Pressure Swing Adsorption (PSA) process is developing as a process of separation for various applications around the world. In recent years, the application of this method in the separation of gas mixtures from each other has been further investigated by researchers. Because, generally, the PSA process is more cost-effective than other separation processes. Therefore, this process sometimes can be replaced by other separation processes in order to justify the economy. In the previous studies, various improvements have been made to the structure of the fundamental PSA cycle (Skarstrom cycle) in order to economize the process. The evolution of PSA is still ongoing around the worldwide and newer measures are being taken every day to develop this important process to achieve the best economic conditions. This chapter focuses on the most important studies on the application of the PSA process for the gas separation.

Since the early 1970s, PSA units have been utilized to separate the air components, but 1980s should be considered as the time of advancement and industrialization [19]. Currently, this method is also used on a low-level scale to produce oxygen for medical purpose and on an industrial scale to produce oxygen and nitrogen instead of a cryogenic method.

In general, the performance of the PSA process is strongly influenced by the design variables (bed size, physical properties of the adsorbent, the configuration and number of beds) as well as the operational parameters (pressurization time, production time, purge time, feed flow rate, purge flow rate, production flow rate, and variation of temperature or pressure). So, could be achieved maximum possible performance relate to an optimum amount of process variables.

Therefore, the sensitivity of the behaviour of PSA operations to process variables should be investigated in order to identify optimal operating conditions. For many years, associated petroleum gases have been burned or flared in oil fields. Flaring of the associated gases is usually performed to increase the safety of equipment and to prevent potential hazards such as explosions and other potential hazards due to increased pressure and flaring of high-pressure gases during petroleum extraction. But this process is the source of greenhouse gases emissions, including carbon dioxide, sulfur oxides, and nitrogen oxides. According to World Bank statistics in 2012, Russia, Nigeria, and Iran have the largest volumes of flare gas production in the world, respectively [20]. According to statistics of Global Gas Flaring Reduction Department in 2012, based on the satellite images, Iran's share of the total volume of burned gas in the world was about 11 percent, equivalent to 30 million cubic meters of natural gas per day [20]. Figure (2-1) shows the global volume of flared gases and oil production from 1996 to the end of 2016. Also, the data of top 30 gas flaring countries in the world from 2013-2016 is shonwn in figure (2-2).

Incomplete combustion in the flare leads to significant amounts of carbon monoxide, unburned hydrocarbons, very dangerous organic compounds such as benzene and toluene, as well as small amounts of sulfur compounds (such as carbon sulfide and carbonyl sulfide [9].

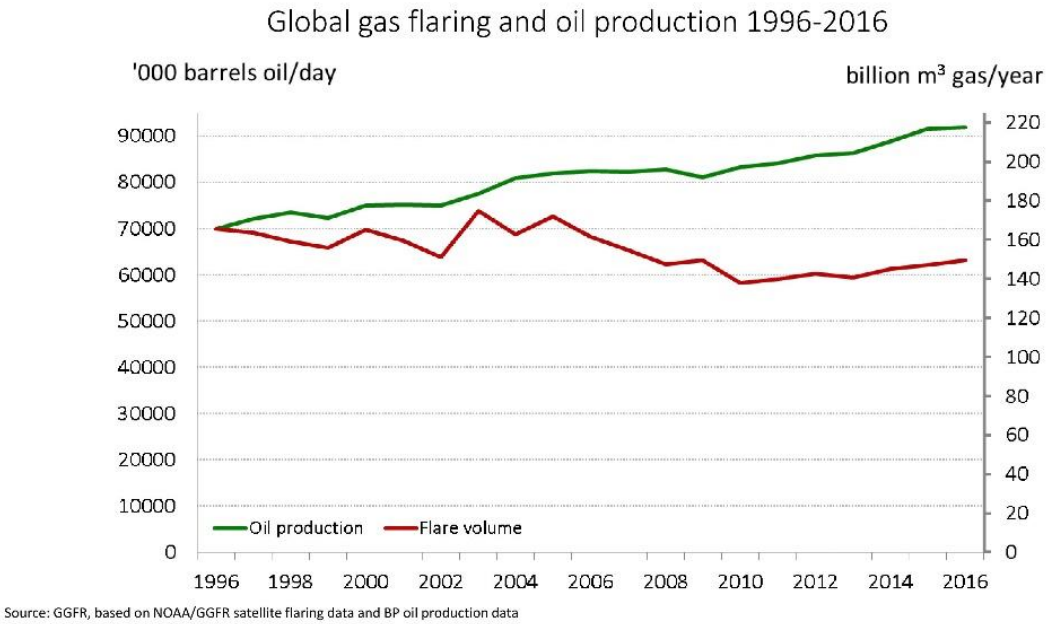

Figure 2-1: Global gas flaring and oil production [1].

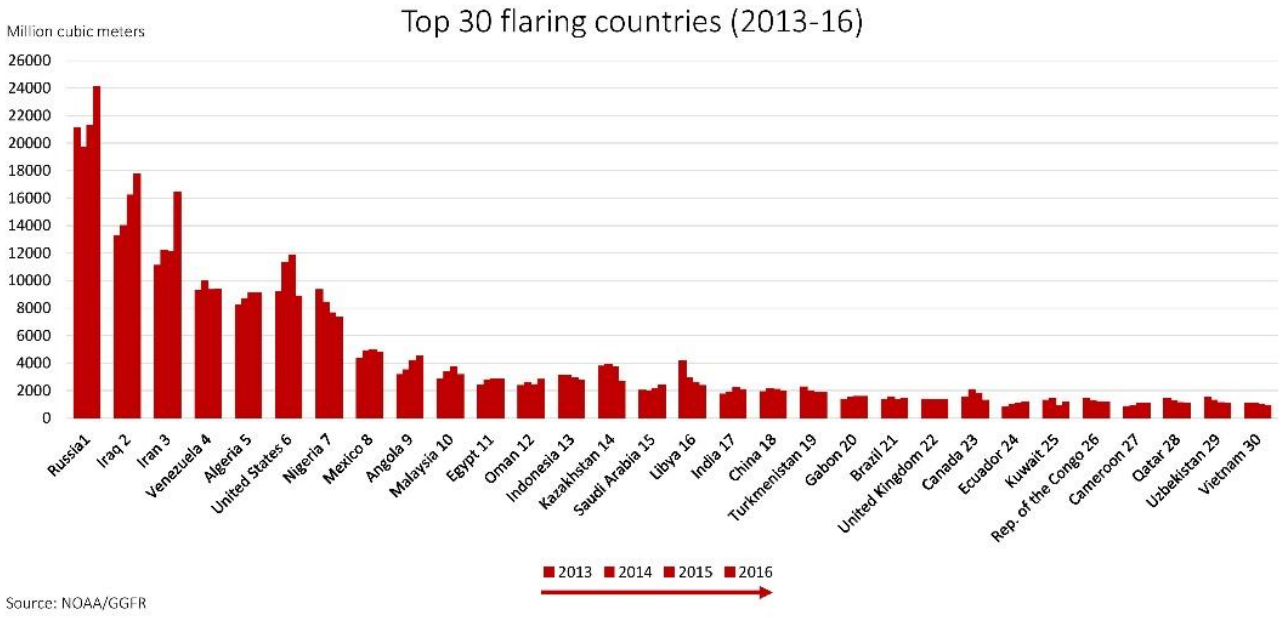

Figure 2-2: Top 30 gas flaring countries [1].

Even if environmental issues are ignored, the volume of burned gas in different countries of the world indicates that the gas flaring system is one of the most important sources of energy waste

in the oil and gas industries and imposes significant economic costs on countries. However, countries are faced with restrictions on the collection and utilization of associated gases [21]. For example, several reasons for flaring the associated gas in collection facilities are reported at the National Iranian South Oil Company [22]. Some of these reasons are: limitations and problems such as power outages due to the dependence on global power network, repair problems, such that the associated gas compressor stations are generally equipped with a spare row, but due to lack of sufficient currency or lack of timely preparation of parts and repair problems, these rows are not ready for service in some cases and the incoming gas is burned compulsorily.

Also, operational issues caused by the displacement and recovery systems, changes in programs, oil production problems and lack of adequate training of staff in technical fields and timely failure to perform periodic repairs due to exchange problems and failure to timely perform periodic repairs due to currency problems and lack of timely supply of spare parts are other problems and reasons for associated gas burning and flaring [21]. It can be seen that this limitation is a cross-sectional one and can be overcome by changing laws and regulations and solving some problems.

Therefore, the associated gases and methods of use should be investigated more precisely.

The study of the literature on flare gases can be classified from two technical and economic perspectives. Various studies have been carried out on the method of collecting associated gases. In the following, the strategies for reducing the burning of these gases are presented at scientific conferences and international and domestic research studies. In Table (2-1), the studies that have been carried out in this field in the country are presented briefly.Rahimpour and Jokar (2012) investigated the technical feasibility of flare gas conversion and using it in the Farrashband gas refinery. They used a simulation model for this purpose and concluded that electricity generation from Aghar Dalan gas fields efficient are economical. Rahimpour et al. (2012) performed the same study for the South Pars gas field based on the above method. In this study, the best option

for the use of flare gases is the final consumption for GTL production due to lower capital costs and a higher internal rate of throughput.

Table 2-1: Summery of studies.

Title	Author/Authors	Reference
Feasibility of flare gas recovery in Farrashband gas refinery	Rahimpour & Jokar	[23]
Comparison of different flare gas recovery method	Rahimpour et. al	[24]
Investigating the effect of light gas in reduction of liquid accumulation in the transferring pipe line and preventing gas flaring in oil fields	Ariaei	[25]
Study of the method of recyclable gas flaring reduction in Iran	Ghasemieh et. al	[26]
Review of the materials and methods utilized for the analysis of the gas flare recovery project	Abdulrahman et.	[27]
They present the results obtained by a feasibility study of a flare gas recovery system in a real refinery; their work focused on: i) the choice and the design of the flare gas recovery system; ii) the gas treatment and reuse; iii) the economic feasibility, and the payback period	Comodi et al.	[28]
They presents the results of two case studies of reducing, recovering and reusing flare gases from the Tabriz Petroleum	Zadakbar et. al	[29]

Refinery and Shahid Hashemi-Nejad (Khangiran) Natural Gas Refinery, both in Iran

---

As an example, in a report from the research center, the strategy of exploiting flares gas was presented as opportunities for using these gases in small-scale projects in 2004, in which the exploitation of flare gases in countries such as Chad and Ecuador has been studied technically and economically [1].

Various studies have been done on the optimal allocation of natural gas resources in Iran such as Jafari Samimi and Dehghani (2007) and Renani et al. (2009), [21]. Abdulrahman et al. in 2014 implement flare gas recovery in Egypt [27]. They reported that the potential annual grenhous gase emission reductions yielding expected yearly revenue around USD 1.5 million. Comodi et. al in 2016 studied the feasibility of a flare gas recovery system in a real refinery [28]. Their focused on: i) the choice and the design of the flare gas recovery system; ii) the gas treatment and reuse; iii) the economic feasibility, and the payback period. These authors reported that the yearly energy recovery was estimated to be 6600 tons of carbon dioxide equivalent. Finally, an economic evaluation was carried out, showing a payback period of about 2.5 years. Hajizadeh et. al in 2017 evaluated feasibility of three methods for FGR in a giant gas refinery in Iran [30]. They studied liquefaction, LPG production and compression in their survey. They reported that rate of return for liquefaction unit and LPG production unit are more than 200% for different scenarios and are higher than compression.

In this project, also a review was carried out on PSA technology because of using this method to flare gas recovery. During the progress made in the PSA process, studies of zeolites have been continually being pursued for years to improve quality (capacity and selectivity). One of the advances made in this regard is the reduction of inert inorganic materials (which causes the

binding of zeolite crystalline network). More comprehensive information on the progress of zeolites can be found in the literature [31, 32].

Fernandez & Kenney [33], provide a theoretical analysis for separation of the oxygen and nitrogen present in the air by the single-bed pressure swing adsorption process. By comparing the partial concentration distributions resulting from the analytical solutions of the equations of the theoretical model of adsorption bed and the results of the experiments, an approximate analytical solution for short-cycle time regions could predict the dynamic behaviour of the adsorption bed. The authors also reported that, generally, and especially for long-time cycles, the precise numerical resolution is an efficient method for numerical modelling and simulation of adsorption bed dynamic. Hassan et al. [34] presented a simple dynamic model for the PSA process of separating air components based on the linear-mass transfer rate relations and Langmuir equilibrium equation. In their work, it was assumed that the pressure was constant during the adsorption and surface desorption steps. Farooq et al. [35] presented a kinetic dynamics model for the process of separating oxygen from the air using zeolite adsorbent-which the equilibrium is governed on the adsorption action compared to the kinetics by the PSA technique. Their testing system was a Skarstrom cycle [14]. The advantage of the presented kinetic model for PSA systems to the equilibrium theory is that the effects of mass transfer resistance and axial diffusion on the system function can be more easily examined. The studied system is a simple two bed PSA Skarstrom system, but this is not a reason for limiting the application of this model to multi-bed systems commonly used in large-scale units. Farooq and Ruthven [36] presented a linear driving force model with the assumption of solid-constant concentration during the pressurization and purge steps in order to simulate the process of separating the components of air by pressure swing adsorption method for the production of nitrogen using a carbon molecular sieve. For experiments, a fixed bed was used for a four-step PSA cycle. The step of this cycle were the same step of the Skarstrom cycle: 1- high-pressure product, 2- purge, 3- purge with the

product, 4. pressurization with the feed. In their theoretical-laboratory study, the authors concluded that the simple model of linear driving force is consistent with the experimental results, as well as with more complex pore-diffusion model. Ruthven & Farooq [36] investigated the modelling of the dynamic behaviour of PSA systems for nitrogen recovery using 5A zeolite, 13X zeolite, and molecular sieve carbon by theoretical equations and experiments. Also, two models of linear driving force and pore-diffusion were used to compare the mass transfer rate in adsorption beds. The experiments were carried out in a two-bed system with two configuration: 1- Skarstrom cycle, and modified self-purging cycle. A comparison between the simulation and the results of the experiment showed that in general, the simple linear driving force model predicts the effects of process variables, but the complex model of pore-diffusion has a better match with the experimental results. Farooq & Ruthven [37] presented a pore-diffusion model for modelling the separation of the two-component gaseous bulk process by pressure swing adsorption based on Langmuir equilibrium and also consider the concentration dependence for diffusion coefficients. The PSA system tested by these authors was studied in two forms: the Skarstrom cycle and the modified Skarstrom cycle along with the step of pressure equalization and self-purging. In their study, the concentration dependence was investigated for the diffusion coefficient of the pore. Concentration dependence in the diffusion coefficient has a great influence on the steady state mode. Budner et al. [38] developed a non-equilibrium isothermal model for the multi-component adsorption process. The also provided a computer software for calculating and simulating the air separation process based on vacuum swing adsorption (VSA) technique using a molecular sieve zeolite adsorbent. They claimed that the expanded and researched mathematical model, along with computer software, was able to design VSA units for the production of oxygen and optimizing their operation. Shin et al. [39] determined the optimum conditions for efficiency and recovery of the product by conducting experiments on a two-bed PSA system along with incomplete equalization steps for oxygen

production from the air. According to the results, using the incomplete equalization step for the PSA cycle leads to improved efficiency at pressurization with feed steps. In the case of pressurization with the product, the maximum efficiency is achieved by using an incomplete equalization step, but its value is less than the pressurization with feed. On the other hand, the maximum recovery in any pressurization mode is created by the full equalization step. Mendes et al. [40] studied a pressure swing adsorption system based on the zeolite 5A absorbent and Skarstrom cycle by simulating and performing experiments. They showed that the speed of pressure increase during the pressurization stage increases the rate of diffusion in the PSA beds and ultimately and product recovery, reducing the time of pressurization at the purge stage for up to 4 seconds does not have any effect on product purity and recovery, and the existence of a pressure equalization step in the Skarstrom cycle improves the purity and recovery of the product. Mendes et al. [41], investigated the PSA separation of oxygen from the air using zeolite 5A adsorbent by performing simulations and experiments. The mentioned pressure swing adsorption system was studied in two modes: the Skarstrom cycle and the Skarstrom cycle along with the co-current pressure equalization step. They showed that product purity and recovery were reduced by increasing product pressure, increasing the product flow rate reduces the purity of the product and increase its recovery, by increasing the duration of the product stage, the product purity decreases, but its recovery increases ,by increasing the ratio of purge flow to the feed, product purity and recovery decreases. Cruz et al. [42] designed an innovative method for optimizing cyclic adsorption separation processes (PSA / VSA), which operates on the basis of the Skarstrom cycle along with the pressure equivalent step. They studied the formulation of the equalization step and concluded that bottom-to-bottom configuration is efficient only for low values of the absorbent productivity coefficient and in the Skarstrom cycle. Top-to-top is the most efficient configuration in all cases in terms of recovery and power consumption. Moghadaszadeh et al. [43], according to a study that carried out on the four-bed seven-steps

pressure swing adsorption for the separation of oxygen from air by zeolite 13X adsorbent, investigated the effect of various process parameters such as product recovery, cycle time, product flow rate, and purge flow rate on the oxygen purity. According to experimental and simulation results they reported that the purity of the product increased by increasing the purge flow rate. Also, by increasing the cycle time, the power consumption decreases and by increasing the purge ratio, the required power increases. Mofarahi et al. [44] simulated and tested a four-bed seven-step pressure swing adsorption system for the separation of oxygen from air by zeolite 5A absorbent. The authors reported the following results according to the range of their experiments: by increasing the adsorption pressure from 4 bar to 6 bar, the purity and recovery of oxygen will also increase, PSA unit performance will be better at higher cycle time, with increasing product flow rate oxygen recovery and purity will increase and decrease, respectively.

Chapter 3

The theory and mathematical modelling of the pressure swing adsorption process

3.1 Introduction

During the last two decades, there have been many advances in the field of pressure swing adsorption (PSA) process. By developing the industrial applications, a great demand arises for an appropriate strategy for modelling, simulation, and optimization. The PSA system is inherently a dynamical system and its operational behaviour is shown by partial differential equations. The PSA process consists of a series of steps that each of these steps occurs continuously during the implementation of the unit for each bed.

At the onset of operation, system characteristics (pressure swing behaviour, temperature swing behaviour, product purity, and product recovery) are not uniform, but over time, the process will come close to a cyclic steady state (CSS) condition. In this case, the conditions at the beginning and the end of each cycle and in each bed are known and its value is fixed in successive cycles and ultimately leads to the production of a normal product. CSS conditions are the most

important point in designing PSA processes. Determining this state of the system can be done by a detailed mathematical modelling. PSA systems can be represented by a series of equations in mathematical language. These models can evaluate and compare the product composition changes and feed intake by changing parameters such as bed length, flow rate, cycle time, operating pressure ratio, the ratio of purge flow to feed, and process performance [45]. The optimal performance of a PSA unit involves achieving a proper combination of process variables such as the cleaning flow intensity and the feed/product flow rate, operating pressure, cycle time, and bed length. Therefore, in order to establish the proper operating conditions and obtain the desired quality and quantity product, the mathematical simulation of the pressure swing adsorption process is first required.

3.2 Adsorption isotherms

The adsorption isotherm from the thermodynamic point of view is a thermodynamic equation for the adsorbed phase and is expressed as follows [46]:

For single-component systems:

$$m = m\left(p, T, m^{s}\right) \tag{3-1}$$

Or a set of functions for multi-component systems:

$$m_i = m_i\left(p_1, ..., p_N, T, m^{s}\right), i = 1, ..., N \tag{3-2}$$

Where, (m) and (m1,…,m_N) represent the mass (s) of adsorbent components (i=1,…,N), $p_i=y_iP$ represents the partial pressure of i^{th} component in gas phase with the molar concentration (yi), T is temperature of system, and finally (m^s) represents the mass of the absorbent material. Equilibrium adsorption data are generally presented in three forms:

1- Isotherms: m and p diagrams at a constant temperature.

2. Isobars: m and T Diagram in constant pressure.

3. Isosteres: ln(p/p0) and T diagrams in constant m.

Various examples of these graphs for the micro-pore material are shown in Figure (3-1).

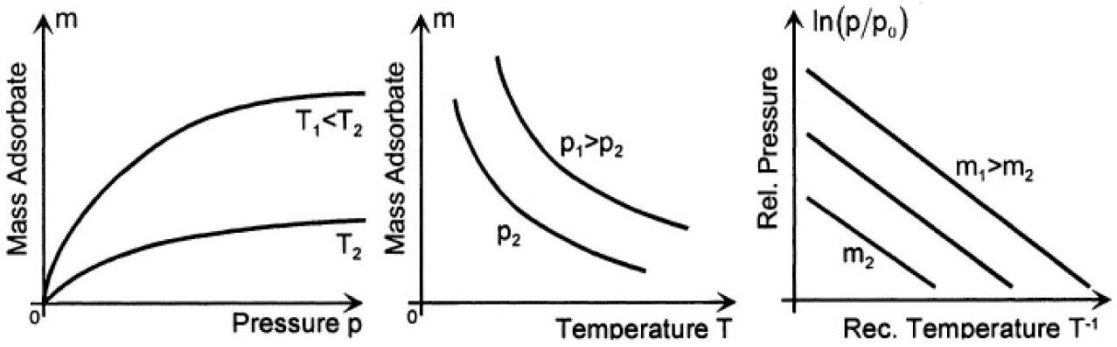

Figure 3-1: Equilibrium adsorption graph for constant temperature (T= cte.), constant pressure (p= cte.), and isosteres states (m= cte.) [46].

The driving force for all separation processes is a part of the equilibrium. Therefore, it is necessary to have information about adsorption isotherm for process design.

3.2.1 Investigation of different models of adsorption isotherms

The adsorption isotherms obtained experimentally can be classified into six different categories according to the IUPAC classification [46]. This category is shown in Figure (3-2).

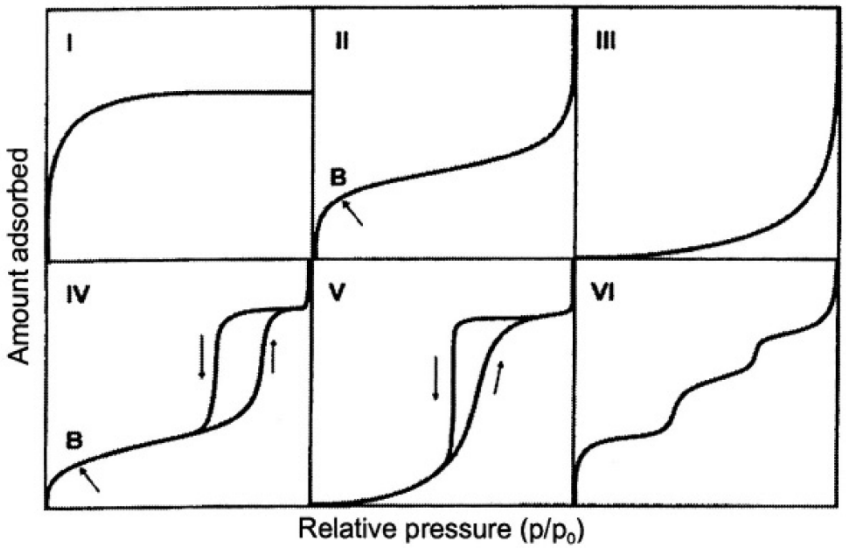

Figure 3-2: The main types of physical absorption isotherms (IUPAC, 1985).

The type I isotherm can be expressed by the Langmuir equation. These types of adsorption isotherms occur for micro-pore materials. An example of this type of isotherms is water on

zeolite or inorganic molecular sieves (polar) and organic vapour ($C_nH_{2n}+_2$) on zeolites and molecular sieves. Chemical adsorption systems also often exhibit the type I adsorption isotherm.

Type II isotherms diversity express adsorption in the cases of meso-pore adsorbents which show monolayer adsorption in lower pressures, multi-layer saturated adsorption in higher pressure and so pore density without hysteresis.

Also, these isotherms can be seen in the pore-free adsorbents or only macro- pore solids (50 nm in diameter). This kind of isotherm is also known as BET[1] isotherm. An example of this type of isotherm is the vapour of polar components (H_2O, $CCl_iF_kH_{4-i-k}$) on molecular sieves, as well as the vapour of non-polar organic material on moderate micro-pores, especially on activated carbons in the pore.

Type III isotherms occur in systems that adsorbate -absorbent interactions are small compared to the adsorbate-adsorbate interactions (associating admolecules). Water on activated carbon and hydrophilic zeolites is an example of this kind of isotherm.

Type IV isotherms show the adsorption behaviour of the material in a specific meso-pore, which shows the pore condensation along with the Hysteresis behaviour between the adsorption and desorption branches. Water vapour in the humid weather on a variety of activated carbons and hydrophilic zeolites is an example of this type of isotherm.

Type V isotherms differ from IV type by hysteresis loop in the range of $p(T)/ps\approx 0.5$ gas pressures.

These isotherms express meso-pore material which pore condensation can be occurs.

Water on activated carbons and carbon molecular sieves is an example of this type of isotherm.

Type VI isotherms represent stepwise multi-layer adsorbates. The layers shown in the figure for this type of isotherm will be much larger at lower temperatures. Non-polar spherical molecules

[1] Brunauer-Emmette-Teller Isotherm

(Noble gases) on smooth graphite surfaces, as well as butanol (C_4H_9OH) on aluminium silicate, is an example of this type of isotherm.

Among the above-mentioned isotherms, type I and II are the most common isotherms in separation processes. So far, several models have been developed to interpret different types of isotherms. The different isotherms models are most often based on one of the three following models [9]:

1- Langmuir Model

2- Gibbs Model

3- Potential Theorem

The Langmuir model has the most application in our subject. Therefore, this model is described.

3.2.2 Langmuir isotherm for single-component gases

The simplest and most useful single-layer adsorption theory model in separation processes was proposed by Langmuir in 1923. In this model, it is assumed that the adsorption system is in dynamic equilibrium. Langmuir type isotherms are used in a wide area for common applications.

The basic assumptions of this model are [18, 47]:

1- Molecules or atoms are absorbed on certain active sites.

2. Any active site can only absorb one molecule or atom.

3. The adsorption energy is the same for all the active sites.

4. There is no interaction between adsorbed molecules on adjacent active sites.

According to the above assumptions, the equation of obtained isotherm is based on the concept of dynamic equilibrium between absorption and desorption rates:

This type of isotherm for the surface adsorption of a pure species is [48]:

$$\theta\left(=\frac{q}{q_m}\right)=\frac{B.P}{1+B.P} \qquad (3\text{-}3)$$

$$B = \frac{\alpha'}{\beta'(2\pi.m.K.T)^{\frac{1}{2}}} e^{Q/RT} \quad (3\text{-}4)$$

In the above equation, the parameter 'α' is the probability of adhesion of the molecule to the surface or the stagnation coefficient of the molecule on the surface for adsorption (due to a collision on the surface), and β is the speed constant for desorption. At low pressures, the Langmuir isotherm is converted into a linear form or Henry Law:

$$q = K.P, K = B.q_m \quad (3\text{-}5)$$

Where K is Henry's constant. All isotherms must be converted into Henry Law in the infinite dilution. Henry's constant is an important factor for separation. This law is valid for physical adsorption that there is no change in the molecular state during adsorption [18]. According to this law, the equilibrium relationship between the fluid phase and the adsorbate phase concentration is linear for adsorption at a uniform surface at low concentrations (so that all molecules are isolated from their closest molecules adjacent to them). Henry's constant may be depended on pressure or concentration.

According to equation 3-4, B is proportional to Q (heat of adsorption). Q for physical adsorption is equal to the energy of adsorbate and adsorbent intermolecular bonding. Therefore, the bond energy is a critical issue for purification.

So far, many improvements have been made on Langmuir isotherm model, such as:

3.2.2.1 Langmuir isotherm, taking into account the interaction of molecules

One of the corrections made on Langmuir isotherm is to consider the interaction of adjacent adsorbed molecules. This effect is related to the van der Waals forces and therefore increases with physical absorption [18].

3.2.2.2 Freundlich Isotherm

In the Langmuir equation, amorphous surfaces adsorption was considered, and the absorbed amount is basically a sum of adsorbed masses in all types of active centres. Each of these centres has its own B-value and the amount of heat is also been averaged.

Zeldowistch [49], assumed an exponential decay function for the density of active centres in terms of q, and ultimately obtained a classic experimental isotherm in the form below:

$$q = K.P^{\frac{1}{n}} \tag{3-6}$$

The above isotherm is also known as the Freundlich isotherm. In this case, the Langmuir relation for sites with absorption energy between q and q+dq is:

$$\theta(q) = \frac{B.P.\exp\,(q/RT)}{1 + B.P.\exp(q/RT)} \tag{3-7}$$

In this relation, B is assumed to be constant despite weak dependence on temperature.

3.2.2.3 Langmuir-Freundlich isotherm equation

The following isotherm was introduced based on the Freundlich equation [50]:

$$\theta\left(=\frac{q}{q_m}\right) = \frac{B.P^{\frac{1}{n}}}{1 + B.P^{\frac{1}{n}}} \tag{3-8}$$

The above equation is known as Langmuir-Freundlich isotherm. This isotherm can be obtained from the Langmuir isotherm, assuming that each n adsorbate molecule occupy the center of the active surface of the adsorbent. It is also considered as Langmuir isotherm for non-uniform surfaces.

3.2.3 Equilibrium adsorption of multi-constituent gas mixtures

Equilibrium models or equations should be able to predict the amount of equilibrium absorbed from pure gas isotherms for each component in the mixture at the range of temperature and the total operating pressure. In the last decades, significant advancements have been made in theoretical issues and in parallel with this, absorption separation processes have grown abundantly. For adsorption of gas mixtures, models such as mono-constituent gas adsorption isotherms are divided into three categories, which Langmuir type models have developed more than other models.

3.2.3.1 Extended Langmuir and Langmuir- Freundlich equations

Langmuir isotherm can simply be expanded to an n-component mixture for pure component adsorption, in which case it is called extended Langmuir isotherm:

$$q_i = \frac{q_{m,i}.B_i.p_i}{1+\sum_{j=1}^{n} B_j.p_j} \tag{3-9}$$

In the above equation, the amount of single-layer adsorption for i^{th} species in the adsorption phase of the mixture is similar to that of single-layer adsorption for pure composition.

Similarly to the extended Langmuir equation for mixtures, the derivative Langmuir-Freundlich equation can also be extended to an n-component mixture [51]:

$$q_i = \frac{q_{m,i}.B_i.p_i^{\frac{1}{n}}}{1+\sum_{j=1}^{n} B_j.p_j^{\frac{1}{n}}} \tag{3-10}$$

The above relation is known as the loading ratio correlation (LRC) and is very useful for designing and simulating adsorption process.

3.3 Mathematical model for predicting the dynamic behaviour of the PSA process

We consider a section of the two-phase region consist of fluid (gas) and solid (adsorbent) within the adsorption bed as an element containing mass, energy, and momentum (Figure 3-3). Then, by using the material balances for the element, we examine the behaviour of the transfer phenomena (mass, energy, momentum) in the fluid phase.

The main assumptions for the mathematical modelling of this system are listed below:

1. The ideal gas law applies to the gas phase.

2. The total pressure during the absorption and purge steps remains constant over time.

3. Total pressure during stages of pressurization, pressure equalization and blow down are changed in a non-linear manner with time.

4. The flow pattern is assumed as an axially dispersed plug flow model.

5. The equilibrium equations for gas compounds are expressed by the multi-component Langmuir- Freundlich isotherms.

6. The mass transfer velocity is expressed by the linear driving force (LDF).

According to these assumptions, the dynamic behaviour of the system is expressed in the parts of the mass, energy and momentum balance.

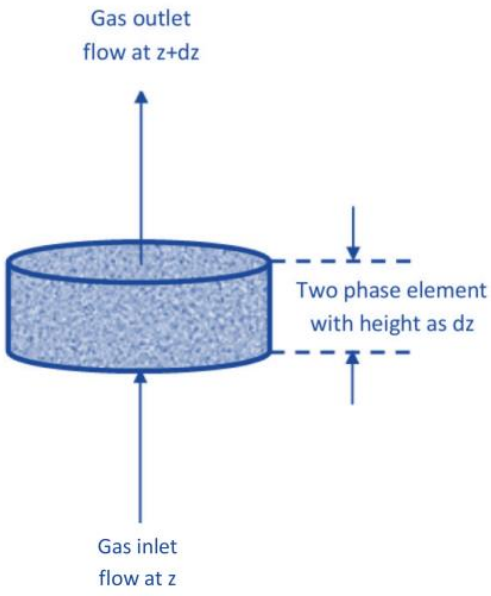

Figure 3-3: the Hypothetical element of two-phase solid-fluid for mathematical modelling of absorption bed.

3.3.1. Component mass balance

The mass balance of i[th] component of gas phase will be written as follows:

$$\left(A.N_i\big|_z - A.N_i\big|_{z+\Delta z}\right).\varepsilon - \rho_p.(1-\varepsilon).A.dz.\frac{\partial \overline{q}_i}{\partial t} = A.dz.\varepsilon.\frac{\partial C_i}{\partial t} \qquad (3\text{-}11)$$

By placing the definition of the mass flux of the i[th] component and dividing the sides of the equation by the volume of the element in the fraction of free space of the bed (A.dz.ε), the following relation is obtained which is consistent with the literatures [17,18,31].

$$-D_L\frac{\partial^2 C_i}{\partial z^2} + \frac{\partial(u.C_i)}{\partial z} + \frac{\partial C_i}{\partial t} + \rho_p.\left(\frac{1-\varepsilon}{\varepsilon}\right).\frac{\partial \overline{q}_i}{\partial t} = 0 \qquad (3\text{-}12)$$

The expression $\frac{\partial \overline{q}_i}{\partial t}$ in the above equations is expressed by the LDF relation as follows:

$$\frac{\partial \overline{q}_i}{\partial t} = \omega_i.(\dot{q}_i - \overline{q}_i) \qquad (3\text{-}13)$$

In the above equation:

ω_i: The coefficient of LDF equation for the i[th] gas component

q_i: The concentration of i component of gas in the solid phase when the equilibrium state between the concentration in the adsorbed phase and the concentration in the gas phase is established.

Here, q_i is defined by the LRC equation in the following form:

$$\dot{q}_i = \frac{q_{m,i}.B_i.P_i^{ni}}{1+\sum_{j=1}^{N} B_j.P_j^{nj}} \tag{3-14}$$

$q_{m,i}$ is the equilibrium parameter of the LRC equation and is defined as follow:

$$q_{m,i} = k_{1,i} + k_{2,i}.T \tag{3-15}$$

$k_{1,i}$ and $k_{2,i}$ are other parameters of the LRC equation and T is the system temperature. The parameters B_i and n_i are also determined by the following relations:

$$B_i = k_{3,i}.\exp(k_{4,i}/T) \tag{3-16}$$

$$n_i = k_{5,i} + \frac{k_{6,i}}{T} \tag{3-17}$$

3.3.2 Energy balance

The energy balance will be written as follows:

$$\begin{aligned} &\left(A.W\big|_z - A.W\big|_{z+\Delta z}\right) - \frac{2h_i.A.dz}{R_{B,i}}\left(T - T_w\right) - \\ &\rho_B.A.dz.\sum_{i=1}^{N}\left(\frac{\partial \bar{q}_i}{\partial t}.\left(-\Delta \bar{H}_i\right)\right) \\ &= \left(\varepsilon_t.\rho_g.c_{p,g} + \rho_B.c_{p,s}\right).A.dz.\frac{\partial T}{\partial t} \end{aligned} \tag{3-18}$$

Paying attention to all the tips will create a delicate dynamic modelling. In contrast to the diffusional mass transfer that occurs only in the empty space of the bed, energy can be directed to all bed spaces (empty and full). On the other hand, the convection transfer for both mass and energy phenomena occurs only in the empty spaces of the bed. By placing the definition of heat

flux (W) and dividing the sides of the equation by the volume of the element (A.dz), the following relation is obtained which is associated with the literature [17,18,31].

$$-K_L \frac{\partial^2 T}{\partial z^2} + \varepsilon.\rho_g.c_{p,g}.\left(u\frac{\partial T}{\partial z} + T\frac{\partial u}{\partial z}\right) + \left(\varepsilon_t.\rho_g.c_{p,g} + \rho_B.c_{p,s}\right).\frac{\partial T}{\partial t}$$
$$-\rho_B.\sum_{i=1}^{N}\left(\frac{\partial \overline{q}_i}{\partial t}.\left(-\Delta\overline{H}_i\right)\right) + \frac{2h_i}{R_{B,i}}\left(T - T_w\right) = 0 \qquad (3\text{-}19)$$

3.3.2.1 Equation of the bed wall heat transfer

Here, there is an extra energy equation for heat transferring from the bed wall to the surrounding area (conductor wall). The following main assumptions have been used to write this equation:

1- Due to the high thermal conductivity of the wall, it can be modelled as a lumped system.

2. The heat capacity of the wall remains constant with temperature changes.

According to the above assumptions, the equation of the wall temperature of the adsorption bed will be written as follows:

$$\frac{\partial T_w}{\partial t} = \left[\frac{2\pi.R_{B,i}.h_i}{\rho_w.c_{p,w}.A_w}\right].\left(T - T_w\right) - \left[\frac{2\pi.R_{B,o}.h_o}{\rho_w.c_{p,w}.A_w}\right].\left(T_w - T_{atm}\right) \qquad (3\text{-}20)$$

3.3.3 Momentum balance

In general, the momentum balance is used to achieve the distribution of pressure and velocity. In mathematical modelling of adsorption beds, researchers used two methods to estimate the velocity and pressure throughout the bed.

1- Writing the balance of momentum and solving it simultaneously with the equations of mass and energy conservation. As a result, the relation of speed and pressure distribution theory is obtained.

2- Use of experimental relationships such as Ergun's relation for pressure variations according to location and other semi-experimental relationships existing for pressure changes relative to time and simultaneous solving of the continuity equation along with the mass and energy conservation

equations that will result in a relation of speed theory. (It should be noted that the Ergun's relation is obtained from the balance of momentum).

In the mathematical modelling of pressure-vacuum swing adsorption beds, the second way have more generality than the first one. Therefore, here in order to predict the velocity distribution within the adsorption bed, we solve the continuity equation and mass and energy conservation equations at the same time.

By placing the definition of total mass flux and the dividing the sides of the continuity equation by the volume of the element in the fraction of free space of the bed (A.dz.ε), the following relation is obtained, which is consistent with the literature [17,18,31].

$$-D_L \frac{\partial^2 C}{\partial z^2} + \frac{\partial (u.C)}{\partial z} + \frac{\partial C}{\partial t} + \rho_p . \left(\frac{1-\varepsilon}{\varepsilon} \right) . \left(\frac{\partial \overline{q}_A}{\partial t} + \frac{\partial \overline{q}_B}{\partial t} + \frac{\partial \overline{q}_C}{\partial t} \right) = 0 \tag{3-21}$$

Here, the total pressure changes in terms of place are estimated using the Ergun's equation and total pressure variations relative to time based on a quadratic relation [38-41].

$$-\frac{dP}{dz} = a.\mu.u + b.\rho.u.|u| \tag{3-22}$$

$$a = \frac{150}{4R_p^2} . \frac{(1-\varepsilon)^2}{\varepsilon^2} ; b = 1.75 \frac{(1-\varepsilon)}{2R_p \varepsilon} \tag{3-23}$$

$$P(t) = A.t^2 + B.t + C \tag{3-24}$$

Where,

A, B, and C in equation (3-24) are obtained in terms of the initial and final time and pressures of each steps of the process.

3.3.4 Boundary and initial conditions

In order to solve the partial differential equations in each step, the appropriate boundary and initial conditions are needed for the same step. According to the nature of the PSA process, the boundary and initial conditions for each step are written as follows:

3.3.4.1 Pressurization with feed

- Boundary conditions

$$-D_L\left(\frac{\partial y_i}{\partial z}\right)\Big|_{z=0} = u.\left(y_i\big|_{z=0^-} - y_i\big|_{z=0^+}\right); \frac{\partial y_i}{\partial z}\Big|_{z=L} = 0 \tag{3-25}$$

$$-K_L\left(\frac{\partial T}{\partial z}\right)\Big|_{z=0} = \rho_g.c_{p,g}.u.\left(T\big|_{z=0^-} - T\big|_{z=0^+}\right); \frac{\partial T}{\partial z}\Big|_{z=L} = 0 \tag{3-26}$$

$$u\big|_{z=0} = u\big|_{feed}; u\big|_{z=L} = 0 \tag{3-27}$$

In Equation (3-25), the expression $y_i\big|_{z=0^-}$ represents the concentration of the component in the input feed, and also in equation (3-26) the expression $T\big|_{z=0^-}$ indicates the temperature of the feed.

- Initial conditions

$$y_i(z,0) = 0; \bar{q}_i(z,0) = 0; u(z,0) = 0 \tag{3-28}$$

$$T(z,0) = T_{atm}; T_w(0) = T_{atm} \tag{3-29}$$

3.3.4.2 High-pressure adsorption (AD)

- Boundary conditions

Like the pressurization with feed but with the difference that:

$$\frac{\partial u}{\partial z}\Big|_{z=L} = 0 \tag{3-30}$$

- Initial conditions

$$y_i(z,0) = y_i(z,t_{end}^{PR}); \bar{q}_i(z,0) = \bar{q}_i(z,t_{end}^{PR}); u(z,0) = u(z,t_{end}^{PR}) \quad (3\text{-}31)$$

$$T(z,0) = T(z,t_{end}^{PR}); T_w(0) = T_w(t_{end}^{PR}) \quad (3\text{-}32)$$

3.3.4.3 Counter-current pressure equalization to depressurization step (ED)

- Boundary conditions

$$\left.\frac{\partial y_i}{\partial z}\right|_{z=0} = \left.\frac{\partial y_i}{\partial z}\right|_{z=L} = 0 \quad (3\text{-}33)$$

$$\left.\frac{\partial T}{\partial z}\right|_{z=0} = \left.\frac{\partial T}{\partial z}\right|_{z=L} = 0 \quad (3\text{-}34)$$

$$\left.\frac{\partial u}{\partial z}\right|_{z=0} = 0; u\big|_{z=L} = 0 \quad (3\text{-}35)$$

- Initial conditions

$$y_i(z,0) = y_i(z,t_{end}^{AD}); \bar{q}_i(z,0) = \bar{q}_i(z,t_{end}^{AD}); u(z,0) = -u(z,t_{end}^{AD}) \quad (3\text{-}36)$$

$$T(z,0) = T(z,t_{end}^{AD}); T_w(0) = T_w(t_{end}^{AD}) \quad (3\text{-}37)$$

3.3.4.4 Counter-current blow down step (BD)

- Boundary conditions

Like the equalization to depressurization step.

- Initial conditions

$$y_i(z,0) = y_i(z,t_{end}^{ED}); \bar{q}_i(z,0) = \bar{q}_i(z,t_{end}^{ED}); u(z,0) = u(z,t_{end}^{ED}) \quad (3\text{-}38)$$

$$T(z,0) = T(z,t_{end}^{ED}); T_w(0) = T_w(t_{end}^{ED}) \quad (3\text{-}39)$$

3.3.4.5 Counter-current purge with the product (PG)

- Boundary conditions

$$\left.\frac{\partial y_i}{\partial z}\right|_{z=0} = 0; -D_L\left(\left.\frac{\partial y_i}{\partial z}\right)\right|_{z=L} = u.\left(y_i\big|_{z=L^+} - y_i\big|_{z=L^-}\right) \tag{3-40}$$

$$\left.\frac{\partial T}{\partial z}\right|_{z=0} = 0; -K_L\left(\left.\frac{\partial T}{\partial z}\right)\right|_{z=L} = \rho_g.c_{p,g}.u.\left(T\big|_{z=L^+} - T\big|_{z=L^-}\right) \tag{3-41}$$

$$\left.\frac{\partial u}{\partial z}\right|_{z=0} = 0; u\big|_{z=L} = -G.u_{feed} \tag{3-42}$$

Where G is the ratio of the purge to the feed.

$y_i\big|_{z=L^+}$ and $T\big|_{z=L^+}$ are component concentrations in the product of the AD step and the output flow temperature of the AD step, respectively.

- Initial condition

$$y_i(z,0) = y_i(z,t_{end}^{BD}); \bar{q}_i(z,0) = \bar{q}_i(z,t_{end}^{BD}); u(z,0) = u(z,t_{end}^{BD}) \tag{3-43}$$

$$T(z,0) = T(z,t_{end}^{BD}); T_w(0) = T_w(t_{end}^{BD}) \tag{3-44}$$

3.3.4.6 Co-current pressure equalization to pressurization (EP)

- Boundary conditions

$$-D_L\left(\left.\frac{\partial y_i}{\partial z}\right)\right|_{z=0} = u.\left(y_i\big|_{z=0^-} - y_i\big|_{z=0^+}\right); \left.\frac{\partial y_i}{\partial z}\right|_{z=L} = 0 \tag{3-45}$$

$$-K_L\left(\left.\frac{\partial T}{\partial z}\right)\right|_{z=0} = \rho_g.c_{p,g}.u.\left(T\big|_{z=0^-} - T\big|_{z=0^+}\right); \left.\frac{\partial T}{\partial z}\right|_{z=L} = 0 \tag{3-46}$$

$$u\big|_{z=0} = u\big|_{z=0}^{ED}; u\big|_{z=L} = 0 \tag{3-47}$$

In (3-46) and (3-47) equations, $y_i\big|_{z=0^-}$ represents the component concentration in the output flow from the equalization to depressurizing step (ED) and $T\big|_{z=0^-}$ is the output flow temperature from

the ED step. Also, the term $u|_{z=0}^{ED}$ in equation (3-47) means the output flow velocity of the ED step at any time.

- Initial conditions

$$y_i(z,0) = y_i(z,t_{end}^{PG}); \bar{q}_i(z,0) = \bar{q}_i(z,t_{end}^{PG}); u(z,0) = -u(z,t_{end}^{PG}) \quad (3\text{-}48)$$

$$T(z,0) = T(z,t_{end}^{PG}); T_w(0) = T_w(t_{end}^{PG}) \quad (3\text{-}49)$$

3.4 Preparation of partial differential equations for solving

Here, for solving partial differential equations, first, the equations are discretize by the implicit finite difference scheme and converted to algebraic equations, and then this set of algebraic equations will be solved by the Runge-Kutt Gill method for each specific time. If we consider m as the space node counter and n as time node counter, then the spatial and temporal derivatives discretization for the arbitrary variable $X(\hat{z},\tau)$ using the implicit finite difference scheme will be written as follows:

$$\frac{\partial X}{\partial \hat{z}} = \frac{X_{m+1,n+1} - X_{m-1,n+1}}{2\Delta\hat{z}} \quad (3\text{-}50)$$

$$\frac{\partial^2 X}{\partial \hat{z}^2} = \frac{X_{m+1,n+1} - 2X_{m,n+1} + X_{m-1,n+1}}{\Delta\hat{z}^2} \quad (3\text{-}51)$$

$$\frac{\partial X}{\partial \tau} = \frac{X_{m,n+1} - X_{m,n}}{\Delta\tau} \quad (3\text{-}52)$$

As well as the Runge-Kutt Gill method is used for the time terms as follow:

$$X_{m,n+1} = X_{m,n} + \frac{K_1 + K_4}{6} + \frac{b.K_2 + d.K_3}{3}$$

$$K_1 = \Delta t.f\left(t_n, X_{m,n}\right)$$

$$K_2 = \Delta t.f\left(t_n + \frac{\Delta t}{2}, X_{m,n} + \frac{K_1}{2}\right)$$

$$K_3 = \Delta t.f\left(t_n + \frac{\Delta t}{2}, X_{m,n} + a.K_1 + b.K_2\right) \qquad (3\text{-}53)$$

$$K_4 = \Delta t.f\left(t_n + \Delta t, X_{m,n} + c.K_2 + d.K_3\right)$$

$$f\left(t, X\right) = \frac{dX}{dt}$$

$$a = \frac{\sqrt{2}-1}{2}; b = \frac{2-\sqrt{2}}{2}; c = \frac{-\sqrt{2}}{2}; d = \frac{1+\sqrt{2}}{2}$$

Chapter 4

Experimental Section, Results and Discussion

4.1 Introduction

In the present chapter, a semi-industrial Pressure Swing Adsorption (PSA) unit was briefly described. In this laboratory pilot the mixed layer exclusive FAPKCO brand adsorbent was used for the first stage and the second stage used one layer adsorbent. The multi-leyar adsorbent is constructed in FAPKCO Engineering Group, which it passes the QC tests. In order to have accurate results, after performing each test, they were evaluated by system total mass balance

(through flow measurements and obtained results of each flow) and for error more than 5%, the test was repeated.

4.2 Description of the laboratory unit

In this laboratory unit, feed flow is compressed using a compressor (10 bars) and passes through the primary oil filter and enters in a primary water trap. Then, it enters a cooler for complete dehumidification. To ensure that the air is clean and free of any kind of contamination and moisture, output air is passed through a secondary dehumidifier. The process schematic is shown in Fig. (4-1). As seen, pure N_2 and pure C_1 were obtained at the top of the stages one and two, respectively. Further details on different parts of the pilot will be presented in detail. Fig. (4-2) shows a picture of experimental pilot plant.

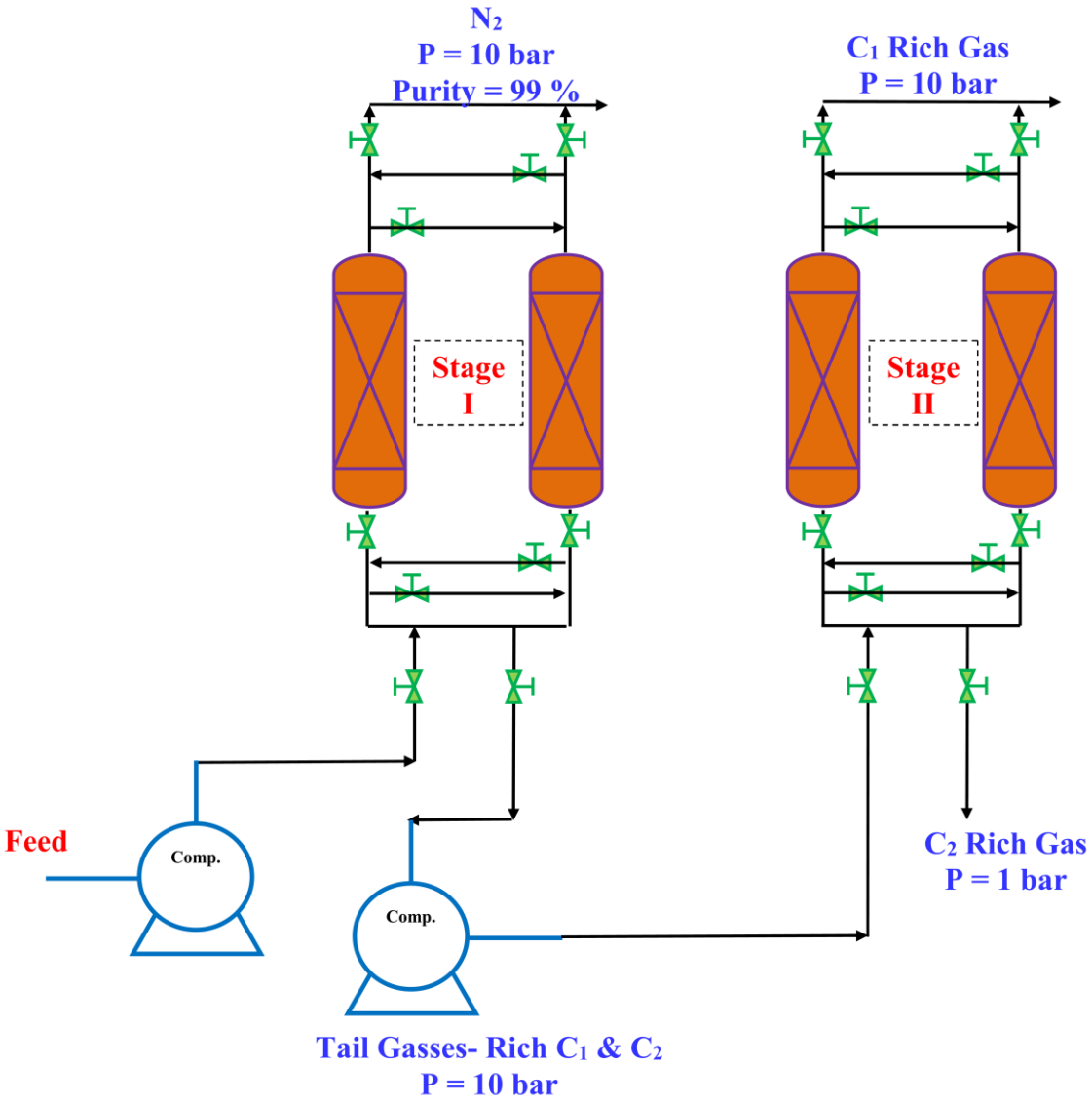

Figure 4-1: Schematic diagram of PSA laboratory unit.

Figure 4-2: A picture of full automated experimental pilot plant.

4.3 Simulation results

The fourth order Runge-Kutta Gill scheme was used to solve a mathematical model considered as coupled partial differential equations. Feed conditions of the industrial unit shown in table (4-1). The physical properties of the adsorption bed are listed in table (4-2).

Table 4-1: Feed conditions of the industrial plant [51].

Composition (%mole)	Design
Solid	**nil**
Water	**0.36**
Nitrogen-argon	**66.64**
Oxygen	**5.00**
Carbon monoxide(CO)	**0.88**
Methane(CH_4)	**16.17**
Ethylene(C_2H_4)	**0.51**
Ethane(C_2H_6)	**8.99**
Carbon dioxide(CO_2)	**1.41**
Ethylchloride (EDC)	**0.01**

Vinyl chloride	**0.00217**
1,2 Dichloroethane	**0.00595**
C_4,CH_3OH,H_2S	**0.154**
Chloroethane	**1.59**
Chloroform	**0.0311**
C-CL_4	**0.00281**
1,2-EDC	**0.595**
1,1,2-CL_3-C=C	**5.42×10^{-7}**
1,1,2,2-Cl_4-C-C	**0.00215**
Cl_5-C-C	**0.00494**
Dichlorobutenes	**2.52×10^{-7}**
2-Chloroethanol	**9.28×10^{-7}**
Chloral	**2.28×10^{-7}**
Solvent	**1.47×10^{-2}**
Pressure [bar]	**2.3**
Temperature [c]	**12.7**

Table 4-2: Physical properties of the adsorption bed.

Property	Quantity
Length (cm)	**70**
Inner radius (cm)	**2.25**
Outer radius (cm)	**2.75**
Tube body material	**High-density Polyethylene**

The experimental data obtained from literatures has been simulated in order to validate the PSA model in this study [41,54,55]. An experimental and simulation study of a PSA unit which is running a traditional Skarstrom cycle and a Skarstrom cycle with co-current equalization owing to separate oxygen from air using a 5A zeolite has been proposed by Mendes et al. in 2001.

The influences of production pressure, purge and product flow rates, and production step duration on the product purity and recovery are investigated for both cycles and compared.

Furthermore, a linear driving force representation of the dusty gas intra particle mass transport is considered in their model [41]. Moreover, a small-scale two-bed six-step PSA process using zeolite 13X was performed by Jee et al. in order to provide oxygen-enriched air. The effect of different operating parameters such as the P/F ratio, adsorption pressure, feed flow rate, and adsorption step time were investigated experimentally under the non-isothermal condition. They showed that there is a strong effect of feed flow rate on O_2 purity [54]. The effects of adsorption and desorption on zeolite 5A and CMS beds were investigated in a mixture of $N_2/O_2/Ar$ by Jee et al. in 2004. A non-isothermal mathematical model was applied in order to simulate the adsorption dynamics in their studies [55].

Figures 4-3(a) and (b) indicate the effect of product flow rate and P/F on the purity and recovery of oxygen during PSA process, respectively. The impact of temperature variations in gas phase during adsorption as a function of time is illustrated in Figure 4-3(c). It is obviously seen that there is a relatively high accuracy in the simulation of experimental data [56].

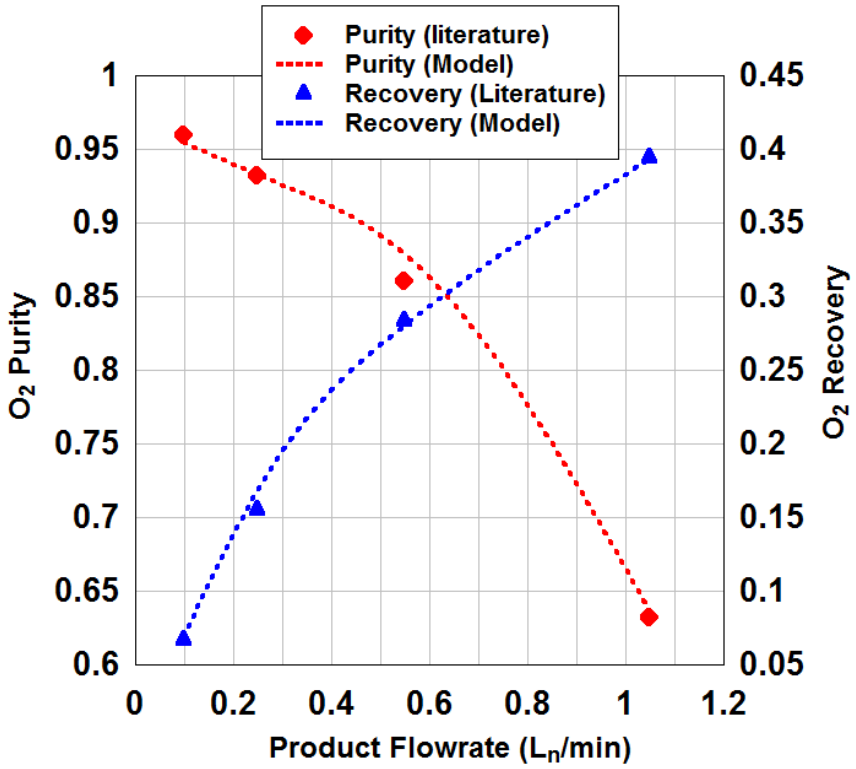

Figure 4-3(a): Numerical simulation of other experimental data in this work [41].

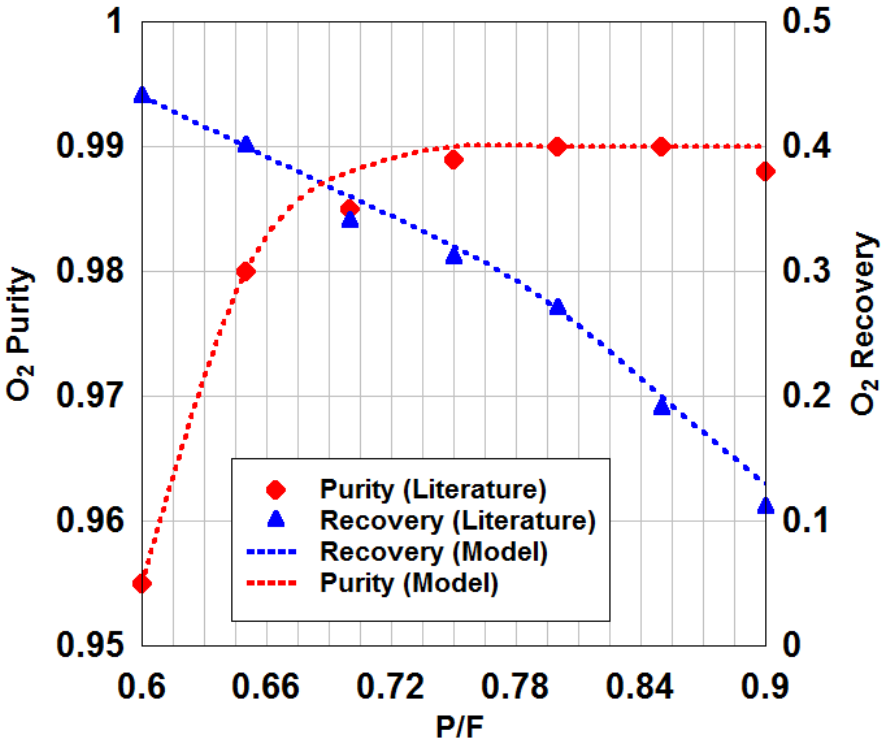

Figure 4-3(b): Numerical simulation of other experimental data in this work [54].

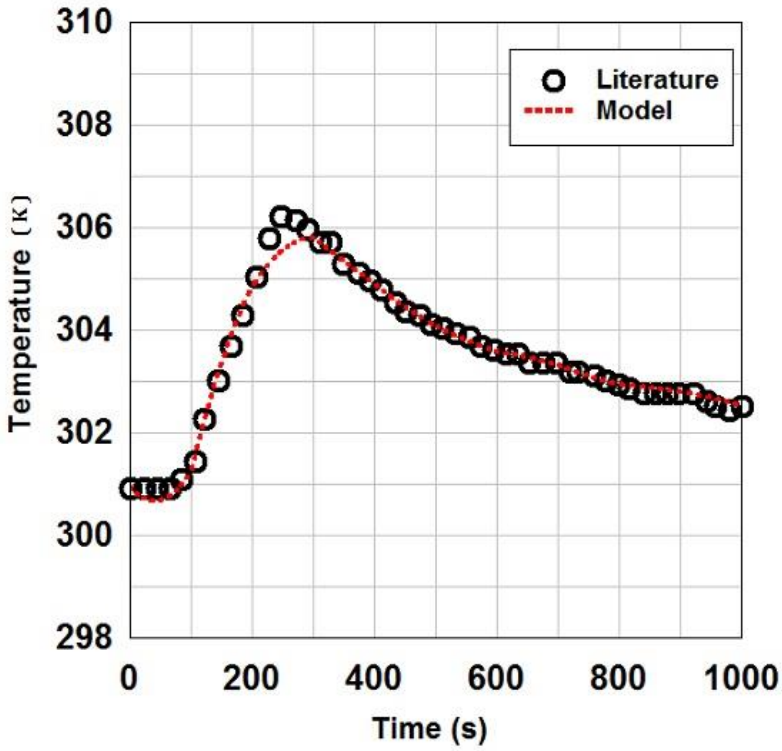

Figure 4-3(c): Numerical simulation of other experimental data in this work [55].

The PSA performances were studied in the range of cycle time of 65-85 s under various adsorption pressures of 9, 10, 11 atm., several feed flow rate and different purge-to-feed (P/F) ratios. More detailed operating conditions are shown in Tab. (4-3).

Table 4-3: Operating conditions for two-stage PSA experiments and their performances.

Experiment No.	Production pressure (bar)	Production time (s), [satge-1]	Feed flow rate (NL/min), [satge-1]	Purge flow rate (NL/min), [satge-1]	N_2 purity	N_2 recovery	N_2 productivity (mol/$kg_{ads.}$hr)	CH_4 purity	CH_4 recovery	CH_4 productivity (mol/$kg_{ads.}$hr)	C_2H_6 purity	C_2H_6 recovery	C_2H_6 productivity (mol/$kg_{ads.}$hr)
1	10	15	10	4	0.972	0.274	15.99	0.0931	0.3165	0.8289	0.0911	0.1503	0.2191
2	10	15	10	8	0.969	0.273	15.95	0.1252	0.3319	2.009	0.1716	0.2453	0.8258
3	10	15	10	9	0.992	0.251	17.80	0.1354	0.3345	2.4135	0.1962	0.2648	1.0623
4	10	15	8	9	0.765	0.216	10.07	0.1189	0.3059	1.6963	0.1605	0.2255	0.6951
5	10	15	12	9	0.967	0.273	19.09	0.1514	0.3643	3.2395	0.2283	0.2999	1.4829
6	10	15	16	9	0.965	0.272	25.42	0.1615	0.3746	4.6070	0.2995	0.3793	2.5939
7	10	20	16	9	0.966	0.272	25.45	0.1827	38.09	5.2104	0.3457	0.3937	2.9944
8	10	25	16	9	0.8368	0.236	22.03	0.1959	0.3769	5.5875	0.3852	0.4048	3.3359
9	9	20	16	9	0.902	0.283	26.42	0.1849	0.3015	6.5821	0.4074	0.3230	3.9203
10	11	20	16	9	0.969	0.248	23.20	0.1772	0.3569	4.1403	0.3212	0.3921	2.5289
11	13	20	16	9	0.976	0.212	19.78	0.1417	0.2742	2.3370	0.3104	0.4364	2.0678

Fig. (4-4) illustrates the experimental and fitted values for the pressure history during a cycle time of 70 seconds. As indicated, simulated pressure changes have a very good agreement with

the experimental data. According to this figure, purge step pressure (or final pressure of the blow down step) is a little less than atmospheric pressure which is due to the errors of RTDs.

N_2 mole fraction profile for a cycle time of 70 s and the pressure of 8 bar in the top and the first stage bed is given in Fig. (4-5). The mole fraction of N_2 in the column has the incremental trend in the pressurization and adsorption steps and it is decreased in the depressurization and blow-down steps. This figure shows that the mole fraction of N_2 variation in the top of the column is less than 0.01 during the whole cycle time under the cyclic steady state conditions (after 450 sec.). This also can be seen for CH_4 and C_2H_6 mole fractions in stage two (Figs. 4-6 and 4-7). These Figs., show that the cyclic steady state in current PSA system was reached at 13th cycle. In this state, the system output is constant through the time.

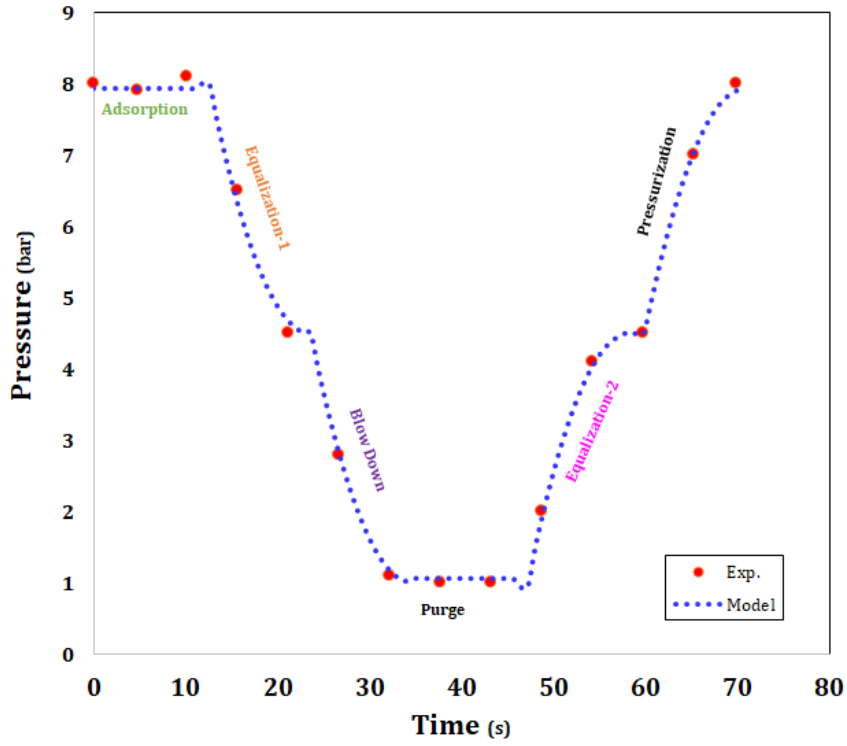

Figure 4-4: Simulation and experimental results of pressure changes for a cycle time of 70 sec.

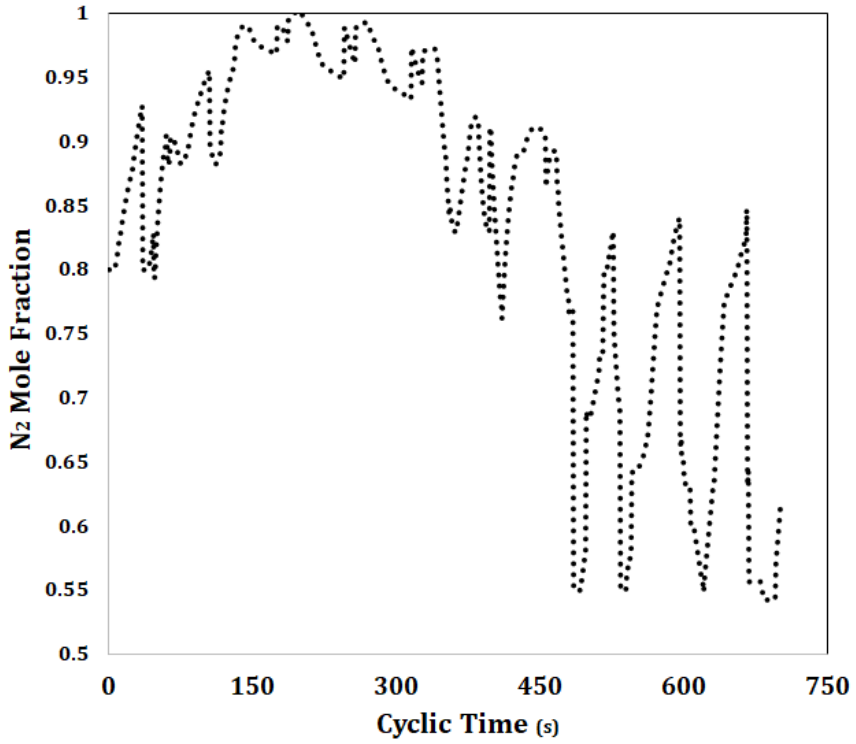

Figure 4-5: Experimental N_2 mole fraction at the top of the first stage column, (P_{AD}=8 bar, t_{AD}=20 sec.).

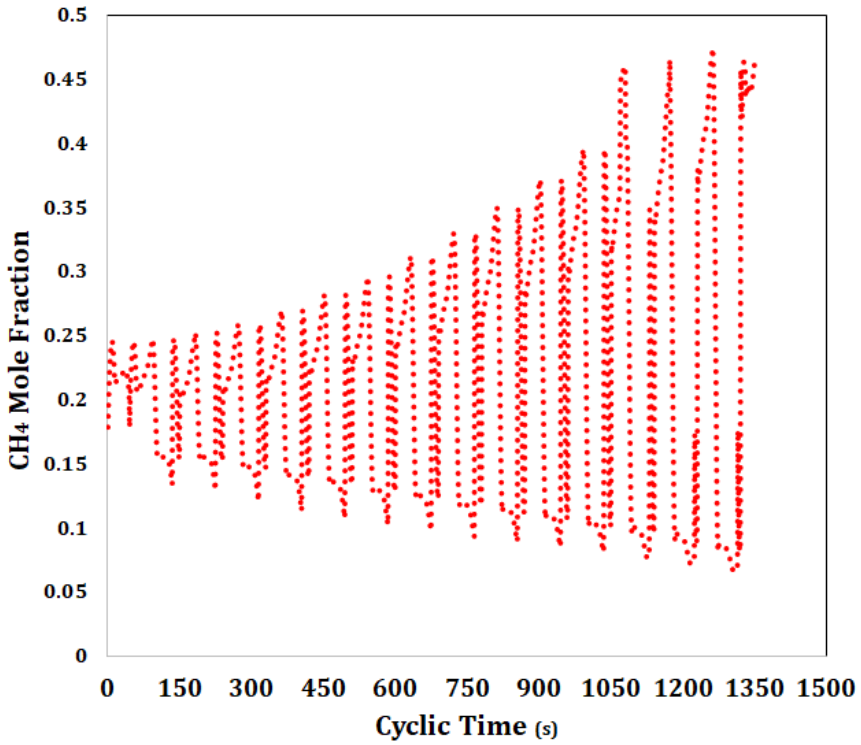

Figure 4-6: Experimental CH_4 mole fraction at the top of the second stage column, (P_{AD}=8 bar, t_{AD}=30 sec.).

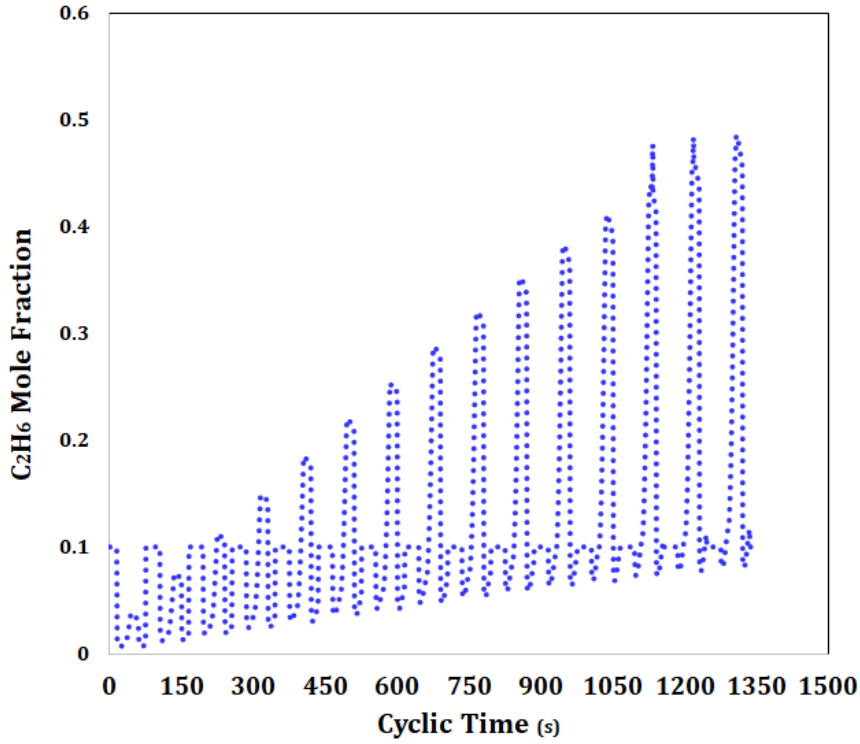

Figure 4-7: Experimental C_2H_6 mole fraction at the top of the second stage column, (P_{AD}=8 bar, t_{AD}=30 sec.).

Figure (4-8) shows N_2 purity and recovery as a function of first layer adsorbent in the first stage. By referring to this Fig., as the height of the first layer adsorbent increased in the column N_2 purity increases up to 99.2 % corresponding to layer fraction of 0.3 and, after that purity passes a minimum on the layer fraction of 0.5. On the other hand, N_2 recovery has a decrement mode up to the layer fraction of 0.5 and, so the recovery increases after that. The optimum performance in terms of the first layer adsorbent for nitrogen as a desired product is corresponded to first layer fraction of 0.3. First layer adsorbent tends to adsorb CH_4 and C_2H_6 and, the second layer has more trapped O_2 instead of N_2 but; it is important that the first layer height in the column be optimum because nitrogen adsorption increases compare to methane and ethane when the contact time on the first layer unduly increased. Accordingly, both CH_4 and C_2H_6 mole fractions increased in the column corresponding to the longer first layer height. In fact, the system mode shifted to methane production as the desired product in the first stage. So, it can be expected that feed of the second stage (blow down and purge streams of the first stage) will be more enriched with methane and ethane. Both of carbon dioxide and carbon monoxide are trapped on the both

adsorbent layers. In this point, the pilot plant experiments show that nitrogen has purified at the amount of 99.2 % with recovery of 25 %.

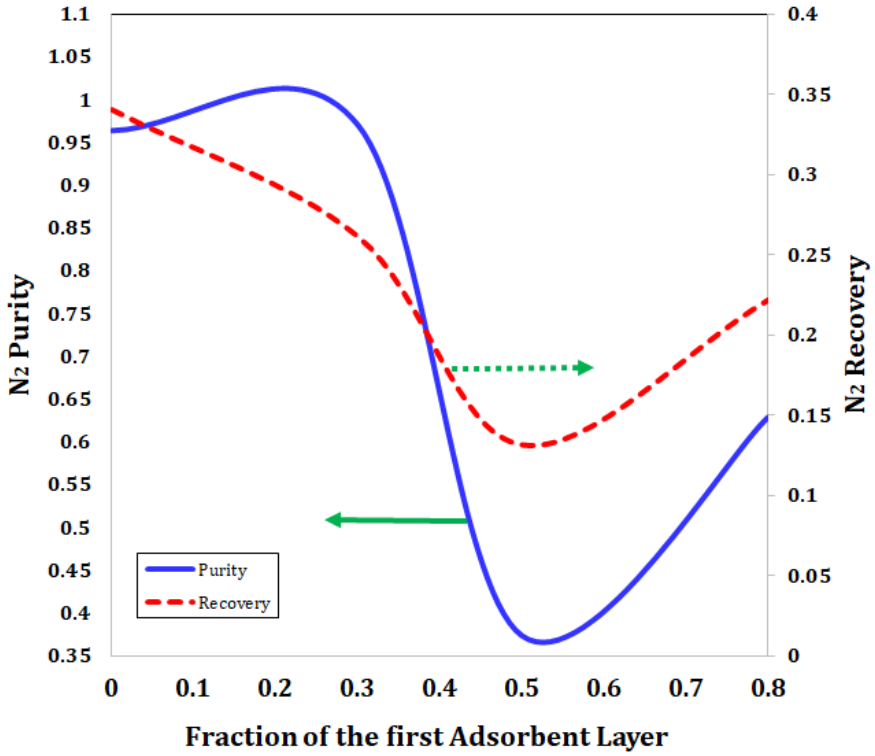

Figure 4-8: N_2 purity and recovery as a function of first layer adsorbent in the first stage.

The purity and recovery of CH_4 in the second stage as a function of the first layer adsorbent in the first stage were shown in Fig. (4-9). Referring to the last paragraph, first layer adsorbent specially tends to adsorb CH_4 and C_2H_6 comparing to N_2 up to height fraction of 0.3. So this is evident that methane purity increases when the feed gas of second stage more enriched with methane. This Fig. shows that the optimum height fraction of the first layer adsorbent in the first stage is 0.55 in terms of methane purity. In this point, methane has purity of 46 % and, its recovery is 35.1 %. This fact also can be seen for ethane in Fig. (4-10). The optimum point for ethane is the also height fraction of 0.55. Ethane purity is 49 % in the optimum point while ethane recovery in this point is 24 %.

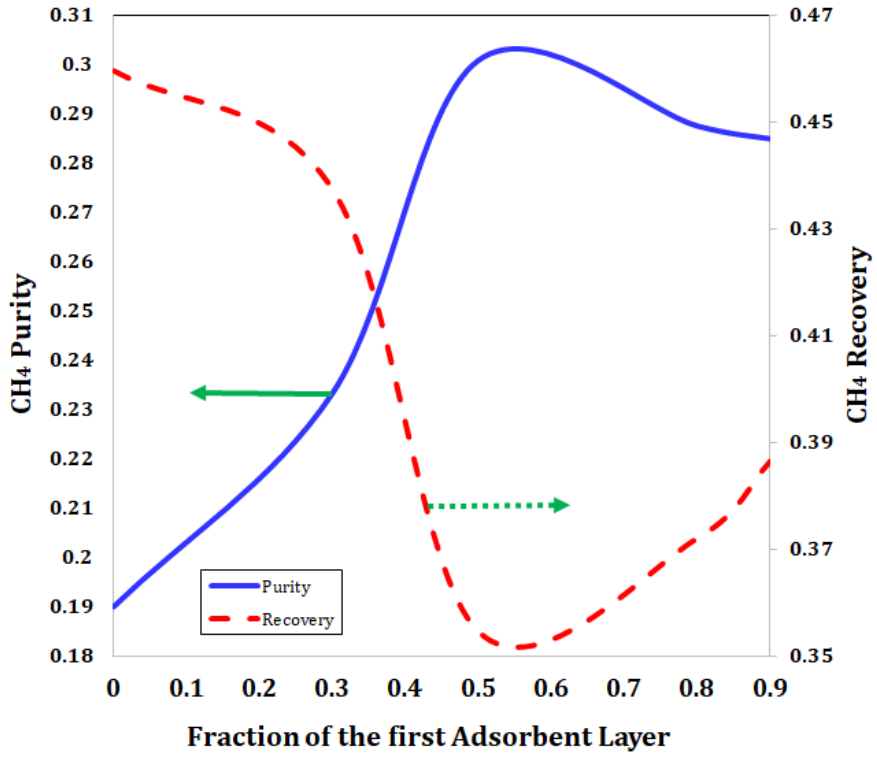

Figure 4-9: CH_4 purity and recovery in the second stage as a function of the first layer adsorbent in the first stage.

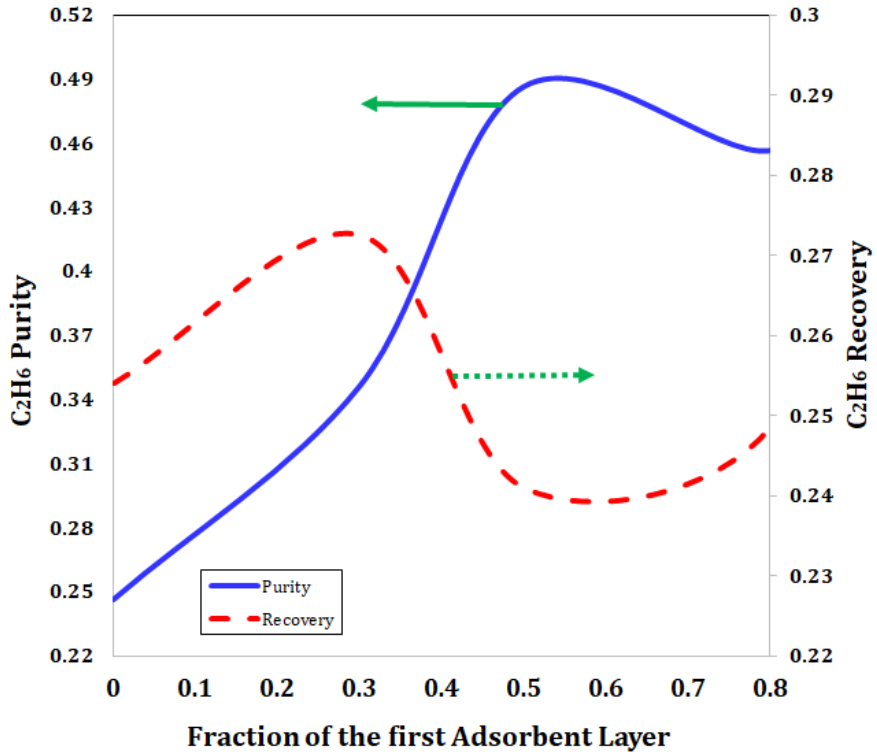

Figure 4-10: C_2H_6 purity and recovery in the second stage as a function of the first layer adsorbent in the first stage.

Referring to table (4-3) the system performances in terms of purities, recoveries and productivities were shown in green, blue and, orange colors, respectively. As can be seen, the

designed system can produces nitrogen with the purity of 99.2 %, recovery of 28.3 % and, productivity of 26.42 mol/($kg_{ads.}$ hr). These values are 19.59, 38.09, 6.5821 for methane and also; 40.74, 43.64, 3.9203 for ethane, respectively. The operating conditions should be set in terms of purity, recovery and, productivity of each desire product according to the table (4-3).

Chapter 5

Conclusion

In this project, nitrogen, methane, and ethane are simultaneously recovered from the flow of submitted gases to the oxychlorination unit flare by the PSA process and sent to the relevant units for reuse. For this purpose, an experimental pilot is constructed in the FAPKCO Industrial Engineering Group, and then the relevant tests are carried out in the oxychlorination unit of a domestic industrial Petrochemical Complex. This leads to providing quite realistic and reliable results for the proposed plan.

- In this work, the cyclic steady state in PSA system was reached at 13^{th} cycle, which the system output is constant through the time
- The optimum performance in terms of the first layer adsorbent for nitrogen as a desired product in the first stage is corresponded to height fraction of 0.3 for the first layer
- In the optimum point, the pilot plant experiments show that nitrogen has purified at the amount of 99.2 % with recovery of 25 %
- The optimum height fraction of the first layer adsorbent in the first stage is 0.55 in terms of methane purity. In this point, methane has purity of 46 % and, its recovery is 35.1 %
- The optimum point for ethane is the also height fraction of 0.55. Ethane purity is 49 % in the optimum point while ethane recovery in this point is 24 %

The designed system can produces nitrogen with the purity of 99.2 %, recovery of 28.3 % and, productivity of 26.42 mol/($kg_{ads.}$ hr). These values are 19.59, 38.09, 6.5821 for methane and also; 40.74, 43.64, 3.9203 for ethane, respectively

References

[1] Global Gas Flaring Reduction Partnership (GGFR), "Estimated Flared Volumes from Satellite Data, Top 20 Flaring Countries," NOAA Satellite data, The World Bank, http://www.worldbank.org/en/programs/gasflaringreduction, 2016.

[2] LLC john zink company, "Flare Gas Recover y Systems," Reduce Recover Reuse, Tulsa, Oklahoma, USA, www.johnzink.com, 2000.

[3] Diana K. Stone, Susan K. Lynch, Richard F. Pandullo, Radian Corporation, Leslie B. Evans, and William M. Vatavuk, Chapter 7- FLARES, Research Triangle Park, NC 27711: Office of Air Quality Planning and Standards.

[4] EPA/452/B-02-001, Section 3.0: VOC Controls, Section 3.2: VOC Destruction Controls, Chapter 1: Flares. A U.S. Environmental Protection Agency report, 2000.

[5] Kayode Coker A., Ludwig's Applied Process Design for Chemical and Petrochemical Plants, Volume 1, 4th ed., Gulf Professional Publishing, 732–737. ISBN 0-7506-7766-X, 2007.

[6] Mannan Sam. Lee's Loss Prevention in the Process Industries: Hazard Identification, Assessment and Control, Volume 1, 3rd ed., Elsevier Butterworth-Heinemann, 12/67–12/71. ISBN 978-0-7506-7857-5, 2005.

[7] Shahini M., Flare gas management, 2nd ed., Jahan-e no Publications, 2010.

[8] Elsenbruch Thomas, Stop Flaring and Venting-Utilization of Associated Petroleum Gas with Gas Engines, GE Power & Water Jenbacher gas engines, Marketing, 2nd M2M Partnership Expo, New Delhi, India, 2-5, March 2010.

[9] Baradaran S., Shoja Moradi A., Asgharian F., Bastami A., Used technologies for reduction and recovery of flare gas conjugating case studies, Shiraz university, 2008.

[10] MTR Inc. Membrane Technology and Research, LPG Recovery from Associated Gas: LPG-Sep™, www.mtrinc.com.

[11] Nemati Shahab S., Omidkhah Nasrin M., Investigation of Waste Gas Disposal Methods and Improving the Performance of Flare Systems, 10th Iran national conference of Chemical Engineering, 2005.

[12] J. D. Miles, A Flare Gas Recovery System, Argo Environmental Engineering Limited, www.argoengineering.com, 2006.

[13] Flow Measurement for Air Monitoring Users Group NPL, December, 2003.

[14] Skarstrom, C. W., Method and Apparatus for Fractionating Gaseous Mixture by Adsorption, U. S. Patent, No. 2,944,627, 1960.

[15] Hasche, R. L; Dargan, W. N., Separation of Gaseous, U. S. Patent, No. 1,794,377, 1931.

[16] Skarstrom, C. W., Oxygen Concentration Process, U. S. Patent, No. 3,237,377, 1966.

[17] Ruthven, D. M.; Farooq, S.; Knaebel, K. S., Pressure Swing Adsorption. New York: VCH Publishers, Inc., 1994.

[18] Ruthven, D. M., Principle of Adsorption and Adsorption Processes. New York: John Wiley & Sons, Inc., 1984.

[19] Carlos, J., Study of New Adsorbents and Operation Cycles for Medical PSA Units, Dissertation Presented for the Degree of Doctor in Chemical Engineering, University of Porto, 2005.

[20] Shadivandi Gh., Iran, the burned gases and necessity to cooperate with World Bank, Energy economiy, 7-9, 2010.

[21] Faridzadeh A., Ghazizadeh M., Heydari K., The economic survey on optimal allocation of the burned associated gases in the country oil fields, Iran economic research, 63-92, 2004.

[22] Sahabi M., Vatani A., Farahani M, Zadakbar O., The solutions for reduction of associated gas burning in their collection units, 7th national conference on energy, Iran, 2009.

[23] Rahimpour M.R. and Jokar, S.M., Feasibility of Flare Gas Reformation to Practical Energy in Farashband Gas Refinery: No Gas Flaring, Journal of Hazardous Materials, No. 209-210, 204-217, 2012.

[24] Rahimpour M.R., Jamshidnejad Z., Jokar, S.M. Karimi G., Ghorbani S. and Mohammadi, A.H., A Comparative Study of Three Different Methods for Flare Gas Recovery of Asalooye Gas Refinery, Journal of Natural Gas Science and, Engineering, 4, 17-28, 2012.

[25] Ariaei F., Investigating the mixing of light gas with the associated gas effects on reduction of liquid accumulation inside the transferring tube lines and preventing associated gas burning in the oil fields, exploration and production, No. 73, 57-59, 2010.

[26] Ghasemieh A., Rostami Sh., MohammadiRad R., Bour H., Hamlehdar O., Study of solutions for reduction in burning of recoverable gases in Iran, National conference on energy, Tehran, Iran, 2010.

[27] Abdulrahman A. O., Huisingh D., Hafkamp W., Sustainability Improvements in Egypt's Oil & Gas Industry by Implementation of Flare Gas Recovery, Journal of Cleaner Production, 10.1016/j.jclepro.2014.11.086, 2014.

[28] Comodi G., Renzi M., Rossi M., Energy efficiency improvement in oil refineries through flare gas recovery technique to meet the emission trading targets, Energy, 109, 1-12, 2016.

[29] Zadakbar O., Vatani A. and Karimpour K., Flare Gas Recovery in Oil and Gas Refineries, Oil & Gas Science and Technology – Rev. IFP, Vol. 63, No. 6, 705-711, 2008.

[30] Hajizadeh A., Mohamadi-Baghmolaei M., Azin R., Osfouri Sh., Heydari I., Technical and Economic Evaluation of Flare Gas Recovery in a Giant Gas Refinery, Chemical Engineering Research and Design https://doi.org/10.1016/j.cherd.2017.11.026.

[31] Yang R. T., Air Separation by Pressure Swing Adsorption Using Superior Adsorbents, Final Technical Report, Department of Chemical Engineering, University of Michigan, 2001.

[32] Santos J. C., Magalhaes F. D., Mendens, A., Contamination of Zeolites Used in Oxygen Production by PSA: Effects of Water and Carbon Dioxide, Ind. Eng. Chem. Res., Vol. 47, pp. 6197–6203, 2008.

[33] Fernandez G., Kenney C. N., Modeling of The Pressure Swing Air Separation Process, Chem. Eng. Sci., Vol. 38, No. 6, pp. 827-834, 1983.

[34] Hassan M. M., Ruthven D. M., Raghavan N. S., Air Separation by Pressure Swing Adsorption on a Carbon Molecular Sieve, Chem. Eng. Sci., Vol. 41, No. 5, pp. 1333-1343, 1986.

[35] Farooq S., Ruthven D. M., Boniface H. A., Numerical Simulation of a Pressure Swing Adsorption Oxygen Unit, Chem. Eng. Sci., Vol. 44, No. 12, pp. 2809-2816, 1989.

[36] Farooq S., Ruthven D. M., A Comparison of Linear Driving Force and Pore Diffusion Models for a Pressure Swing Adsorption Bulk Separation Process, Chem. Eng. Sci., Vol. 45, pp. 107-115, 1990.

[37] Farooq S., Ruthven D. M., Numerical simulation of a Kinetically Controlled Pressure Swing Adsorption Bulk Separation Process Based on a Diffusion Model, Chem. Eng. Sci., Vol. 46, No. 9, pp. 2213-2224, 1991.

[38] Budner Z, Dula J., Podstawa W., Gawdzik A., Study and Modeling of The Vacuum Swing Adsorption (VSA) Process Employed in The Production of Oxygen, Ins. Chem. Eng., Vol. 77, Part A, pp. 405-412, 1999.

[39] Shin H. S, Kim D. H., Koo K. K., Lee T. S., Performance of a Two-Bed Pressure Swing Adsorption Process with Incomplete Pressure Equalization, Adsorption, Vol. 6, pp. 233-240, 2003.

[40] Mendes A. M. M., Costa C. A. V., Rodrigues A. E., Analysis of Nonisobaric Steps in Nonlinear Bicomponent Pressure Swing Adsorption Systems: Application to Air Separation, Ind. Eng. Chem. Res., vol. 39, pp. 138-145, 2000.

[41] Mendes A. M. M., Costa C. A. V., Rodrigues, A. E., Oxygen Separation from Air by PSA: Modeling and Experimental Results Part I: Isothermal Operation, Sep. Purif. Tech., Vol. 24, pp. 173-188, 2001.

[42] Cruz P., Magalhaes F. D., Mendes A., On the Optimization of Cyclic Adsorption Separation Processes, AIChE Journal, Vol. 51, pp. 1377–1395, 2005.

[43] Moghadaszadeh Z., Towfighi J., Mofarahi M., Study of a Four-Bed Pressure Swing Adsorption for Oxygen Separation from Air, Int. J. Chem. Bio. Eng., Vol. 1, No. 3, pp. 140-144, 2008.

[44] Mofarahi M., Towfighi J., Fathi L., Oxygen Separation from Air by Four-Bed Pressure Swing Adsorption, Ind. Eng. Chem. Res., Vol. 48, pp. 5439-5444, 2009.

[45] Jiang L., Biegler L. T., Simulation and Optimization of Pressure-Swing Adsorption Systems for Air Separation, AIChE Journal, Vol. 49, No. 5, pp. 1140-1156, 2003.

[46] Keller J, Staudt R., Gas Adsorption Equilibria: Experimental Methods and Adsorption Isotherms. Boston: Springer Science + Business Media, Inc., 2005.

[47] Suzuki M., Adsorption Engineering. Tokyo: Kodansha Ltd., 1989.

[48] Yang R. T., Adsorbents: Fundamentals and Applications. New Jersey: John Wiley & Sons, Inc., 2003.

[49] Zeldowitsch J., Acta Physicochim. U.R.S.S. 1, 961, 1934.

[50] Yang R. T., Gas Separation by Adsorption Processes. London: Butterworth, Reprinted by Imperial College Press., 1987.

[51] Yon C. M., Turnock P. H., AIChE Symp. Ser., Vol. 67, No. 117, 1971.

[52] Research & Development Department, FAPKCO Engineering Group (*PART-SHIMI Co.*), URL:<< http://www.fapkco.ir/ >> ,Shiraz, Iran.

[53] Rege S. U., Yang R. T., Qian K., Buzanowski M. A., Air-Prepurifcation by Pressure Swing Adsorption Using Single/Layered Beds, Chem. Eng. Sci., Vol. 56, pp. 2745-2759, 2001.

[54] Jee J. G., Lee J. S., Lee C. H., Air Separation by Small-Scale Two-Bed Medical O2 Pressure Swing Adsorption, Ind. Eng. Chem. Res., Vol. 40, pp. 3647-3658, 2001.

[55] Jee J. G., Lee S. J., Lee C., H., Comparison of the Adsorption Dynamics of Air on Zeolite 5A and Carbon Molecular Sieve Beds, Korean J. Chem. Eng., Vol. 21, pp. 1183-1192, 2004.

[56] Mofarahi M., Javadi Shokroo E., Comparison of two pressure swing adsorption processes for air separation using zeolite 5A and zeolite 13X, Petroleum Coal, 55(3), 216 2013.